Universidade do Minho
Escola de Engenharia

Diogo Albano Cavaleiro Ventura de Carvalho

The importance of Ag content for optimizing the machining performance of Ti-Si-(Ag)-N coatings

The importance of Ag content for optimizing the machining performance of Ti-Si-(Ag)-N coatings

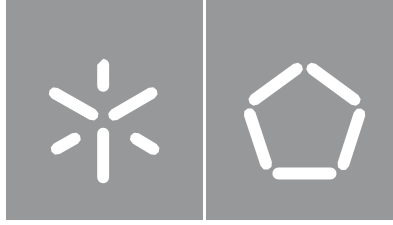Diogo Albano Cavaleiro Ventura de Carvalho

UMinho | 2021

June 2021

Universidade do Minho
Escola de Engenharia

Diogo Albano Cavaleiro Ventura de Carvalho

The importance of Ag content for optimizing the machining performance of Ti-Si–(Ag)-N coatings

Tese de Doutoramento Programa
Doutoral em Engenharia de Materiais

Trabalho efetuado sob a orientação da
**Professora Doutora Sandra Carvalho e do
Doutor Filipe Fernandes**

Junho de 2021

STATEMENT OF INTEGRITY

I hereby declare having conducted this academic work with integrity. I confirm that I have not used plagiarism or any form of undue use of information or falsification of results along the process leading to its elaboration.

I further declare that I have fully acknowledged the Code of Ethical Conduct of the University of Minho.

ACKNOWLEDGEMENTS

RESUMO

Nesta tese, foram depositados revestimentos do sistema TiSiN com incorporação de prata como agente lubrificante utilizando a técnica de *high power impulse magnetron sputtering* (HiPIMS) a trabalhar em *deep oscillations magnetron sputtering* (DOMS), de forma a avaliar o seu comportamento químico, estrutural, morfológico, mecânico, térmico e tribológico. A sua performance numa operação de maquinagem foi também estudada de forma a determinar a potencial aplicação destes revestimentos em ferramentas de corte para maquinar a liga aeroespacial TiAl6V4, considerada "difícil de maquinar". A matriz de TiSiN foi escolhida pelas sua bem conhecida elevada dureza e resistência à oxidação e também pela barreira de difusão proporcionada pela fase SiN que poderá ajudar a travar a rápida difusão da prata.

O conteúdo de prata presente nos revestimentos foi de 0 a 29 at.%, sendo que um filme de TiSiN, sem qualquer prata, foi também depositado que serviu de referência ao longo desta tese. Durante as deposições, a introdução de pellets de prata no alvo foi aumentando, progressivamente, o teor de prata nos revestimentos levando a que influenciasse a taxa de deposição, a estrutura e a morfologia dos filmes. Todos os revestimentos apresentaram picos cristalinos na análise de difração de raios X, atribuídos à estrutura cfc TiN tipo NaCl. A adição de prata contribuiu significativamente para o alargamento desses mesmos picos e para o decréscimo abrupto do tamanho de grão das cristalites de TiN. A adição de prata levou também a um decréscimo da dureza e do módulo de Young dos revestimentos devido ao crescente aumento da fase macia na microestrutura.

O recozimento dos filmes em atmosfera protetora não promoveu quaisquer mudanças significativas na estrutura/composição fásica ou nas propriedades mecânicas. A prata nos filmes continuou homogeneamente distribuída na matriz. O recozimento em atmosfera oxidante permitiu anotar, através da difração de raios X in-situ a alta temperatura, os primeiros sinais de oxidação aos 850 °C com o aparecimento dos picos de rutilo TiO_2. Nas partes que ficaram por oxidar dos revestimentos, a prata continuou homogeneamente distribuída na matriz. A análise termogravimétrica confirmou que a adição de prata não teve qualquer influência no ponto de inicio de oxidação. No entanto, mostrou que a velocidade com que a oxidação ocorre se deteriora, claramente, com a introdução de prata. Uma incomum perda de massa foi também descoberta na análise dos revestimentos com 6 e 10 at.% de prata, explicado pela evaporação/sublimação da prata.

RESUMO

O comportamento tribológico dos revestimentos foi aferido a altas temperaturas e com dois tipos diferentes de contra corpos (bolas de alumina e TiAl6V4). Os testes conduzidos à temperatura ambiente contra as bolas de alumina mostrou um ligeiro decréscimo no coeficiente de atrito mas, ao mesmo tempo, uma deterioração da resistência ao desgaste. Esta resistência é melhorada á temperatura acrescida de 600 °C, quando comparado com os seus equivalentes à temperatura ambiente. Os testes contra as bolas de TiAl6V4 mostraram a prata a apresentar um efeito benéfico na redução do atrito e do desgaste. Foi ainda observado que a prata diminui e/ou atrasa a adesão de material à superfície de desgaste. Estes resultados começaram a indiciar a promissora aplicação destes revestimentos em ferramentas de corte para a maquinagem de ligas de titânio.

Finalmente, dois tipos diferentes de insertos foram testados no torneameanto, a seco, da liga aerospacial TiAl6V4. Um dos tipos de insertos foi testado em ambiente laboratorial com um torno mecânico, enquanto que o outro tipo foi testado numa máquina CNC. Estes últimos foram testados para serem comparados e referenciados em relação a um revestimento comercial de AlTiN. Em ambos os casos, o comportamento foi semelhante com a adição de prata a mostrar uma clara melhoria no tempo de vida dos insertos, especialmente para as velocidades de corte mais altas. A prata mostrou ainda o seu efeito como lubrificante sólido ao reduzir o desgaste e a formação de built-up edges (BUE). No geral, esta tese atingiu e mostrou o potencial da aplicação dos revestimentos TiSiN(Ag) em ferramentas de corte para usar na maquinagem da liga aerospacial TiAl6V4, sem a aplicação de qualquer lubrificante líquido.

Palavras chave: TiSiN(Ag); Estrutura; Tribologia; Maquinagem; Lubrificante sólido

ABSTRACT

TiSiN coatings with incorporation of silver serving as the lubrication agent, were deposited by high power impulse magnetron sputtering (HiPIMS) working in deep oscillation magnetron sputtering (DOMS) mode in order to evaluate the chemical, structural, morphological, mechanical and thermal behaviour. The tribological and machining performance was also assessed to determine the potential application of these coatings in cutting tools to machine the hard-to-cut TiAl6V4 aerospace alloy. TiSiN matrix was selected owing to its well-known high hardness and oxidation resistance and due to reported diffusion barrier property of the SiN phase that could help hindering the fast diffusion of the silver.

Silver content on the coatings ranged from 0 to 29 at.% with a TiSiN film also being deposited to serve as the reference throughout the whole characterization. During the depositions, the introduction of silver pellets on the target progressively increased the Ag concentration on the films, influencing the deposition rate, structure and morphology of the films. All the coatings displayed crystalline peaks assigned to a TiN fcc NaCl type structure. Ag additions significantly broadened these TiN diffraction peaks and abruptly decreased the grain size of the TiN crystallites. Hardness and Young's modulus of the coatings decreased with increasing Ag additions mainly due to the increase of this soft phase on the microstructure.

Annealing treatment in protective atmosphere didn't promote any significant changes in the structure/phase composition or mechanical properties of the coatings. The silver signal kept being homogeneously distributed on the coatings. When oxidative atmosphere was present, in-situ high-temperature X-ray diffractograms allowed to observe the first signs of oxidation occurring at about 850 °C with the appearance of the rutile TiO_2 peaks. Observation of even distribution of silver was still possible on the un-oxidized part of the films. TGA analysis showed that silver addition did not change the onset point of oxidation of the coatings. However, the oxidation rate deteriorated with the presence of Ag. An unusual mass loss could be observed for the coatings with 6 and 10 at.% of Ag, as a result of silver evaporation/sublimation process.

The tribological behaviour of the coatings was assessed at high temperatures and by using two different types of counterbodies (alumina and TiAl6V4 balls). Room temperature (RT) tests conducted against alumina balls showed that silver slightly decreases the friction but deteriorates the wear resistance. Wear resistance is improved when the temperature is increased to 600 °C, when compared to RT tests. The tests against TiAl6V4 balls showed that silver has a beneficial effect in the reduction of friction and wear. Additionally, silver hinders the adhesion of material to the wear track. Temperature also plays an

important role in propelling the effects of silver. These results started to show the promising application of these coatings in cutting tools to machine titanium alloys.

Finally, two type of cutting inserts were tested in the dry turning of the TiAl6V4 aerospace alloy. First type of cutting inserts were tested in laboratorial environment using a conventional lathe, whilst, second types of inserts were tested in an CNC machine. Tests in the CNC machine were performed to assess their performance benchmarked in relation to a commercial insert coated with AlTiN coating. In both of these tests, the same behaviour was found with the addition of silver clearly displaying an improvement in the tool life of the inserts, especially for higher cutting speeds. Addition of silver also showed its solid lubricant effect by reducing either the wear or the formation of built-up edges (BUE) during the tests. Ultimately, this thesis achieved and showed the potential application of TiSiN(Ag) coatings in cutting tools for the machining of the TiAl6V4 aerospace alloy under dry conditions.

Keywords: TiSiN(Ag); Structure; Tribology; Machining; Solid lubricant

TABLE OF CONTENTS

LIST OF FIGURES

LIST OF TABLES

CHAPTER I - Introduction

The importance of Ag content for optimizing the machining

performance of Ti-Si-(Ag)-N coatings

1 Introduction

This work focuses on the production and characterization of novel Ti-Si-(Ag)-N coatings to be applied in cutting tools. The main objective is to improve their lifetime and performance in dry machining of the so called "difficult-to-cut" materials, often used in components for automotive and aerospace industries. This new system is proposed due to its well-known enhanced mechanical, oxidation and tribological properties. The novelty is based on the introduction of silver, to the TiSiN hard system, as a lubricant agent which could potentially reduce friction and wear, especially at high temperature environments which occur in the aforementioned industries. With this in mind, due to the new demands of the automotive and aerospace industries to reduce their environmental footprint (by eliminating the use of liquid lubricants) and their economic burden (by increasing the cutting speed), new functional coatings must be developed to process the "hard-to-machine" materials used in these industries. Additionally, this chapter will show some of the main functionalities, requirements, problems and materials used in the mobility industry as well as an explanation of the project proposal for this thesis.
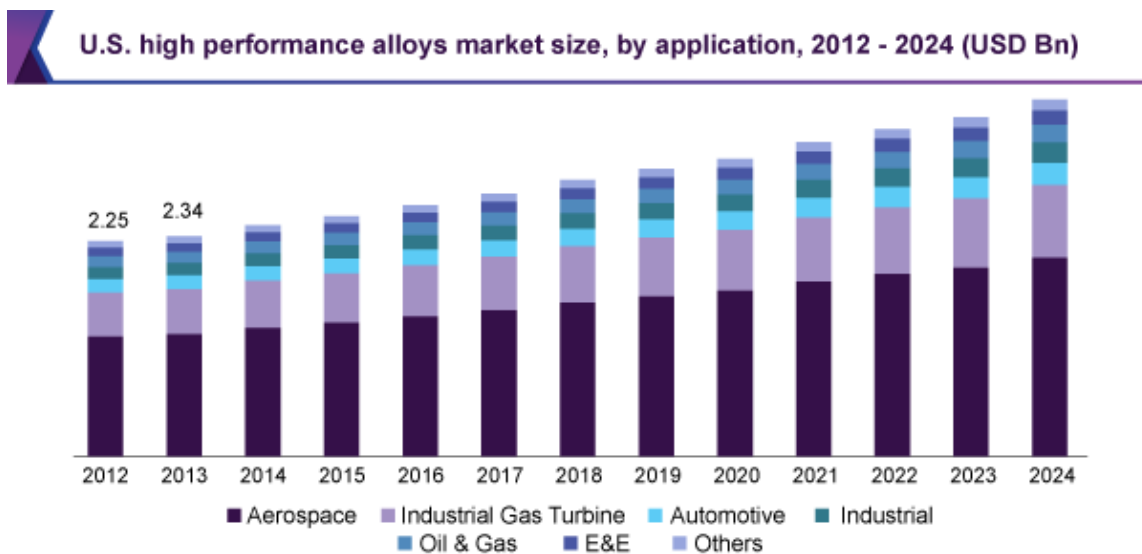
Figure I-1 Past, present and future global market size of high performance alloys (period of 2012 – 2024) [1]

Market analysis report from 2012 to 2024 [1] shows a continuous incremental increase in the use of these alloys in the various markets but most noticeable for the aerospace industry, as displayed in Figure I-1. The same report shows how, in 2016, the non-ferrous metals (where the titanium and aluminium alloys are included) were the largest product segment mostly due to their ability to reduce weight, increase fuel efficiency and most important, their superior recycling capability (Figure I-2).

Figure I-2 Global market share, by product, of high performance alloys in 2016 [1]

1.1 Machining of advanced aerospace alloys

The continuous growth in transportation has placed an increasing demand on the mobility industry to manufacture efficient vehicles at lower cost, more friendly to the environment while meeting the safety requirements [2]. This requires an enhancement in fuel economy and in the aerodynamic performance with stricter accuracies and reduced errors in the reproducibility of the machined parts [3]. This can be achieved through the use of lightweight metallic alloys and composite materials [4, 5]. Table I-1 shows the percentage of materials used in the construction of various aircrafts, by weight percentage, displaying the relevance of these materials in aerospace crafting. However, most of the parts involved in the building of an aircraft (as seen on Figure I-3), can have incredibly complex shapes and geometries. Therefore, these parts must be machined which leads to the search for cost effective and high performance machining solutions required for these advanced aerospace alloys.

Table I-1 Weight percentage of alloys used on the fabrication of parts for various aircrafts (adapted from [3])

	COMPOSITES	ALUMINIUM	TITANIUM	STEEL	OTHERS
AIRBUS A350	52	20	14	7	7
BOEING B787	50	20	15	10	5
BOMBARDIER CS300	46	24	8	1	21
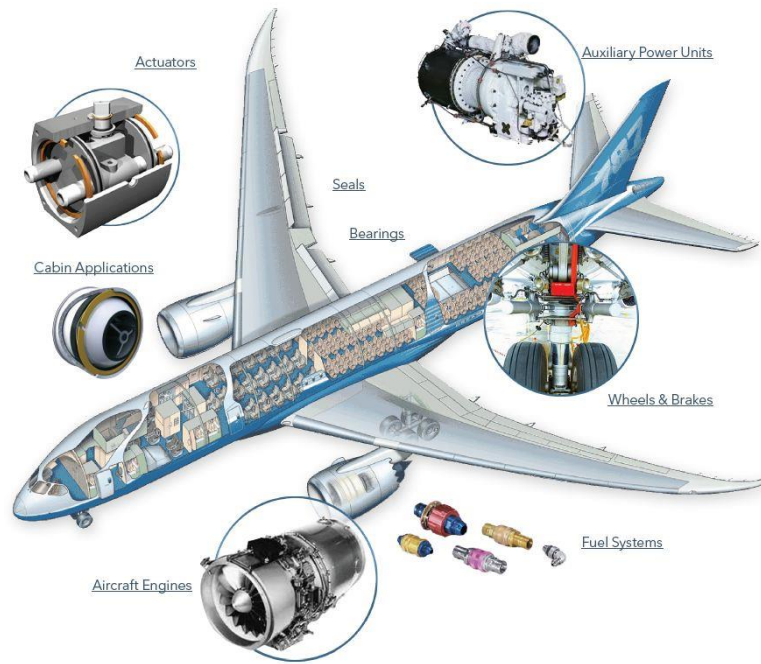
Figure I-3 Different types of parts within an aircraft

1.1.1 Requirements for aerospace components

Nowadays, the main requirement for aerospace is tied to its environmental impact with fuel economy being one of the main driving forces in modern aircraft design [3]. This is why the Advisory Council for Aviation Research, in its "Flightpath 2050 Europe's Vision for Aviation" [6], established as goals for 2050 the reduction of CO_2 emissions per passenger kilometre by 75%, the reduction of NO_x emissions by 90% and the reduction of noise emission by 65% while also keeping aircraft movements emission-free during taxiing. In order to achieve this, improvements in the airframes and engines of the aircrafts are required by a proper selection of materials with adequate characteristics.

Due to the requirement of mass producing of some components, aluminium alloys are some of the most common materials used in modern aerostructure parts mainly because of it being one of the most abundant metals present in planet earth. Add to this, its easy machinability, light weight and its own anticorrosion mechanism (formation of a protective oxide when exposed to air) [7] and there's a material that allows its usage in most of aircraft parts with safety factors and reduced costs. Typically, some of the commercial aircrafts from Boeing (747, 757 or 767) or Airbus (A380) can have up to 80% of its weight composed of aluminium alloys [8].

When higher performance, reduced life cycles, reduced maintenance and production costs are required, composite materials become an interesting solution for the design of modern aerostructures. Usually,

their rising use in the industry comes from some of these composites having higher specific strength and corrosion and fatigue resistance than most of metals [9]. Nowadays, as much as 55% of the weight of an aircraft, such as the Boeing B787 or the Airbus A350, can be constituted by composite materials [10].

The introduction of titanium alloys not only allow for the building of structural parts, due to their exceptional high specific strength and excellent corrosion resistance, but also for its application in the engines due to its high temperature performance for temperatures up to 600°C [11]. Another advantage of these alloys is their high compatibility with composite materials which reduces thermally induced loads and removes the risk of galvanic corrosion at the interfaces of the materials [3, 11]. Usage of titanium alloys, in weight percentage, in aircrafts went from 1% back in the 60's to up to 18% in most modern airplanes [12], quite far from the values aluminium and composites can reach. Despite its fantastic properties, the drawbacks of the titanium alloys beyond the much higher cost, is its poor machinability efficiency when compared with aluminium alloys [11].

Lastly, when the temperatures involved in modern aero engines exceed the 600°C and higher strength levels at elevated temperatures are required to support higher compression rates, the so-called superalloys (nickel-base and cobalt-base alloys) are the only materials capable of meeting such criteria [13]. In fact, in the combustor and turbine sections of the aircraft engine the temperatures can reach very high temperatures in the order of 1500°C, being these alloys the only ones able to possess such incredible resistance to creep, oxidation and corrosion [14-16]. Despite the increase usage of superalloys in most industries (as seen on Figure I-2) they are, just as titanium alloys, extremely expensive and difficult to machine while also having the disadvantage of being heavy alloys with lower specific strength, contrarily to titanium alloys [13].

This panoply of materials allowed for continuous improvement in the capabilities of modern aero structures and engines, granting levels of noise and emissions considerably lower than ever seen before. The still on-going development in materials, methods and processes, all combined, favour the progress towards the goals aforementioned for the project "Flightpath 2050".

1.1.2 Materials used for aerospace components

As referred previously, the most common materials used in the production of components for aerospace industry are aluminium alloys, composite materials, titanium alloys and superalloys. What started as a wooden structure, started changing with the introduction of aluminium alloys as aircraft materials way

back in 1927 with the development of some important processing technologies [8] and which would then dominate the aerospace materials for over 80 years [17]. In the last years however, the rest of the referred materials were introduced to aircrafts to further improve and develop the aerospace industry. Nonetheless and despite the different usages for all these materials, they all present advantages and drawbacks, and are only applied to build specific components/parts, as summarized in Table I-2.

Table I-2 Advantages, disadvantages and applications of the different materials used in the aerospace industry

	ADVANTAGES	DISADVANTAGES	APPLICATIONS
ALUMINIUM ALLOYS	Low cost Lightweight Easy processing	Low operating temperatures Susceptible to empennage Low compatibility with composites	Fuselage skin [8] Wing skin [17] External fuel tanks [18] Landing gear [19]
COMPOSITES	Lightweight Great formability Good corrosion and fatigue resistance	Operating limited to medium temperatures Susceptible to moisture	Nose and wing skin [13] Brakes [9] Empennage, bulkheads and engine cowlings [20]
TITANIUM ALLOYS	High specific strength High temperature performance (up to 600°C) High compatibility with composites	High cost Excepcionally poor machininability	Landing gears [11] Compressor blades and rotors [21] Springs, bulkheads and wing boxes [10] Compressor sections of engines [13]
SUPERALLOYS	Exceptional high temperature strength Fantastic creep resistance	Extremely costly Excepcionally hard to process Heavyweight (low specific strength)	Entire combustion and turbine sections of engines [22]

Adding to the mentioned materials and with even higher turbine efficiencies in mind (where temperatures can go higher than 1600°C), molybdenum-based alloys were proposed as a solution material due to their extremely high melting temperatures (> 2500°C) [23].

1.2 Project proposal for increasing cutting speed

As it has been shown so far, titanium alloys can be considered one of the most important materials in the construction of modern aircrafts, either for structural or engine parts, for increasing the efficiency with lower economic and environmental burdens all the while keeping the safety requirements in check [2].

Despite the demonstrated amazing properties of these alloys, one of the modern problems ties itself with their poor machinability which increase tool wear and lower the production rates, effectively increasing the cost [24, 25]. Therefore, the most important drive force for the increase in productivity capacity relies on the increase of the material removal rate, through the increasing of cutting speed [26-28].
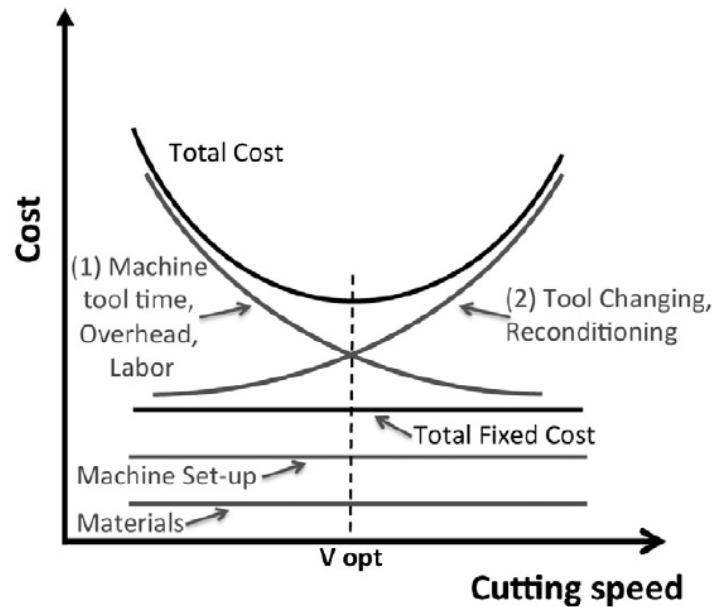
Figure I-4 Effect of cutting speed on the machining costs [26]

The effect of the cutting speed in the machining cost (cost per part) is plotted in Figure I-4. The "total fixed cost" line represents the sum of the costs that are independent of the cutting speed. The two curves labelled "1" and "2" depict the costs dependent on the cutting speed. The costs represented in curve "1", like manpower, water and energy consumption and so on, usually decrease with the cutting speed since more parts are produced for the same period of time. Curve "2" shows the costs that raise with the cutting speed, considering tools that wear faster and have to be replaced and, most importantly, the cost of time and of the lost productivity when the machine is stopped to replace the worn tool. The actual machining cost is given by the sum of the fixed costs and the cutting speed dependant costs. If better performing tools could be produced, curve "2" in the graph would raise slower. Thus, the minimum in the total cost curve would occur for higher cutting speeds and, therefore, at lower values of the total cost per part.

As seen, the increase in the cutting speed comprises an important parameter to take into consideration when machining aerospace titanium alloys however, this will come with a burden on the cutting tools as higher cutting speeds will produce tougher contact conditions leading to an increase of the cutting/contact temperature and increase of the wear, ultimately, conducting to the earlier degradation of the cutting tool.

As such, self-lubricant coating systems with release of the lubricious species [29] have enormous potential to be used in the protection of surfaces of components working in extreme conditions of wear. This thesis therefore, foresees the application of a self-lubricant coating on cutting tools to improve the machining performance of titanium alloys, mainly by increasing the cutting speed. To accomplish this goal, TiSiN films deposited as nanocomposite structure, with silver (Ag) dispersed on the microstructure were developed and characterized. The TiSiN coating system was selected due to its well-known excellent mechanical properties and thermal stability at high temperatures, especially if deposited as a nanocomposite structure [30, 31]. Moreover, this structure is comprised of a SiN_x phase that has been reported to be an efficient diffusion barrier [32] that could help solve one of the main problems of self-lubricant coatings that is the quick diffusion of the lubricious material. As for the lubricious agent, the silver is selected for its multitude of functional characteristics [33] but mainly, because of its low shear strength and friction coefficient over a wide range of temperatures while also having a relatively high melting temperature point of 960°C [34, 35].

To achieve the main objective of this thesis, the development of a self-lubricant coating for cutting tools to improve the machining of titanium alloys, through the increasing the cutting speed, the following sub-objectives should be fulfilled:

- **Develop** Ti-Si-(Ag)-N films with nanocomposite structure with variable TiN grain sizes and different Si-N phase thicknesses, together with the variable distribution and content of silver on the films to ensure both high mechanical strength and good anti-diffusion properties required for a proper self-lubricant behaviour at high temperatures;
- **Correlate** the morphology and the developed structure with mechanical properties, thermal stability and oxidation resistance in order to select the good candidates for self-lubricant coatings at high temperatures;
- **Evaluate** the silver effect on the tribological performance of the films at high temperature to select the coatings which could have potential to be used on the machining of Ti alloys.
- **Study and compare**, respectively, the effect of silver on the machining behaviour for increasing cutting speeds and the performance of the Ti-Si-(Ag)-N coatings with the state of the art market coatings.

1.3 References

[1] G.V. Research, High Performance Alloys Market Size, Share & Trend Analysis Report By Product (Non-ferrous, Platinum group, Refractory, Super alloys), By Material, By Application, And Segment Forecasts, 2018 - 2024, in, 2018, pp. 80.

[2] M. Kuttolamadom, J. Jones, L. Mears, T. Kurfess, A. Choragudi, Investigation of the Machining of Titanium Components for Lightweight Vehicles, in, SAE International, 2010.

[3] R. M'Saoubi, D. Axinte, S.L. Soo, C. Nobel, H. Attia, G. Kappmeyer, S. Engin, W.-M. Sim, High performance cutting of advanced aerospace alloys and composite materials, CIRP Annals, 64 (2015) 557-580.

[4] N. Khanna, J.P. Davim, Design-of-experiments application in machining titanium alloys for aerospace structural components, Measurement, 61 (2015) 280-290.

[5] P.J. Arrazola, A. Garay, L.M. Iriarte, M. Armendia, S. Marya, F. Le Maître, Machinability of titanium alloys (Ti6Al4V and Ti555.3), Journal of Materials Processing Technology, 209 (2009) 2223-2230.

[6] Flightpath 2050: Europe's Vision for Aviation: Report of the High Level Group on Aviation Research, European Union, (2011).

[7] Aluminum, in: F.C. Campbell (Ed.) Elements of Metallurgy and Engineering Alloys, ASM International, 2008, pp. 0.

[8] E.A. Starke, J.T. Staley, 24 - Application of modern aluminium alloys to aircraft, in: R. Lumley (Ed.) Fundamentals of Aluminium Metallurgy, Woodhead Publishing, 2011, pp. 747-783.

[9] L.A. Pilato, M.J. Michno, Advanced composite materials, Springer Science & Business Media, 1994.

[10] X. Zhang, Y. Chen, J. Hu, Recent advances in the development of aerospace materials, Progress in Aerospace Sciences, 97 (2018) 22-34.

[11] R.R. Boyer, Attributes, characteristics, and applications of titanium and its alloys, JOM, 62 (2010) 21-24.

[12] M.J. Krane, A. Jardy, R.L. Williamson, J.J. Beaman, Proceedings of the 2013 International Symposium on Liquid Metal Processing and Casting (LMPC), John Wiley & Sons, 2013.

[13] Z. Huda, P. Edi, Materials selection in design of structures and engines of supersonic aircrafts: A review, Materials & Design, 46 (2013) 552-560.

[14] Z. Huda, Development of design principles for a creep-limited alloy for turbine blades, Journal of Materials Engineering and Performance, 4 (1995) 48-53.

[15] R.C. Reed, T. Tao, N. Warnken, Alloys-By-Design: Application to nickel-based single crystal superalloys, Acta Materialia, 57 (2009) 5898-5913.

[16] Z. Huda, Development of heat-treatment process for a P/M superalloy for turbine blades, Materials & Design, 28 (2007) 1664-1667.

[17] T. Dursun, C. Soutis, Recent developments in advanced aircraft aluminium alloys, Materials & Design (1980-2015), 56 (2014) 862-871.

[18] B. Smye, Aluminum alloys for aerospace, in, 2018.

[19] C.S.T. Company, A Guide to Aluminum Use in the Aerospace Industry, in, 2016.

[20] M. Bellonte, Composite Materials in the Airbus A380 - From History to Future, in, 2001.

[21] C.T.S. Company, All About Titanium from Continental Steel & Tube: Properties, Forms, and Applications, in, 2020.

[22] J.C. Williams, E.A. Starke, Progress in structural materials for aerospace systems11The Golden Jubilee Issue—Selected topics in Materials Science and Engineering: Past, Present and Future, edited by S. Suresh, Acta Materialia, 51 (2003) 5775-5799.

[23] J.H. Perepezko, The Hotter the Engine, the Better, Science, 326 (2009) 1068.

[24] A. Pramanik, Problems and solutions in machining of titanium alloys, The International Journal of Advanced Manufacturing Technology, 70 (2014) 919-928.

[25] C.R. Dandekar, Y.C. Shin, J. Barnes, Machinability improvement of titanium alloy (Ti–6Al–4V) via LAM and hybrid machining, International Journal of Machine Tools and Manufacture, 50 (2010) 174-182.

[26] E.M. Trent, Metal Cutting, 3rd ed., Butterworth-Heinemann, London, 1991.

[27] W.W. Gilbert, Economics of Machining, ASM, Cleveland, 1950.

[28] A. Niazi, J.S. Dai, S. Balabani, L. Seneviratne, Product Cost Estimation: Technique Classification and Methodology Review, Journal of Manufacturing Science and Engineering, 128 (2005) 563-575.

[29] A.A. Voevodin, C. Muratore, S.M. Aouadi, Hard coatings with high temperature adaptive lubrication and contact thermal management: review, Surface and Coatings Technology, 257 (2014) 247-265.

[30] S. Vepřek, S. Reiprich, A concept for the design of novel superhard coatings, Thin Solid Films, 268 (1995) 64-71.

[31] J. Musil, Hard nanocomposite coatings: Thermal stability, oxidation resistance and toughness, Surface and Coatings Technology, 207 (2012) 50-65.

[32] G. Bilger, T. Voss, T. Schlenker, A. Strohm, High-temperature diffusion barriers from Si-rich silicon-nitride, Surface and Interface Analysis, 38 (2006) 1687-1691.

[33] S. Calderon Velasco, A. Cavaleiro, S. Carvalho, Functional properties of ceramic-Ag nanocomposite coatings produced by magnetron sputtering, Progress in Materials Science, 84 (2016) 158-191.

[34] F.P. Bowden, F.P. Bowden, D. Tabor, The friction and lubrication of solids, Oxford university press, 2001.

[35] H.E. Sliney, Solid lubricant materials for high temperatures—a review, Tribology International, 15 (1982) 303-315.

CHAPTER II - State of the Art

The importance of Ag content for optimizing the machining

performance of Ti-Si-(Ag)-N coatings

2 Introduction

To have a better understanding of the solution proposed in the previous chapter, it is important to perceive the problems with the machining of titanium alloys while keeping in mind the promising approach of surface modification to solve said problems. Thus, in order to develop a self-lubricant coating that can improve the machining of titanium alloys, it is imperative to: i) grasp the concepts of coatings and its requirements for appliance in cutting tools for high cutting speeds and ii) research about the solid lubrication concepts as a way to eliminate environmental harmful fluids. Therefore, this chapter will provide a critical perception of the state of the art of the problems associated with the machining of titanium alloys, the most common proposed solutions for said problems and meanwhile, a brief focus on coatings as one of the most promising solution to improve the machinability of aerospace titanium alloys.

Lately, self-lubricant coatings reached a leading role on green machining, due to the reduction/removal of liquid lubrication at the same time that the tool lifetime is extended with improvement of the surface finishing of the parts. Those coatings combine a highly oxidant resistant coating matrix with a lubricant element providing enhanced high temperature strength as well as reduced friction. One of the most interesting features of these coatings is the potentiality to adapt their final functional properties by changing the chemical composition (base matrix and/or the lubricant agent) or by tailoring the different phases distribution, size or lattice parameter. One way to do this, and the one used in this thesis, is by using a different deposition technique called high power impulse magnetron sputtering (HiPIMS) that is very useful in tailoring the structure of the self-lubricant coating system. The challenge of these coatings reside, however, in achieving an adequate control of the diffusion rate of the lubricious metal in order to obtain low friction and high wear resistance in the long-term allowing these coatings to be used as a viable solution in the cutting tool industry for a wide range of operation conditions.

2.1 Titanium alloys

Titanium is an industrial metal which happens to be the fourth most abundant in planet earth's crust [1] and although, when unalloyed, it's considered a relatively soft metal with low strength, its alloys actually show exceptional mechanical properties with high strength, good wear resistance and a fantastic strength-to-weight ratio which makes it a remarkable material for use in the aerospace industry [2-5]. Beyond this sector, these alloys are gaining popularity in the automotive, navy, biomedical and food processing industries [6]. From an overall perspective, titanium alloys can be divided into three categories, based on

their structure: the alpha titanium alloys, the beta titanium alloys and the alpha-beta titanium alloys [1], as shown on Figure II-1.
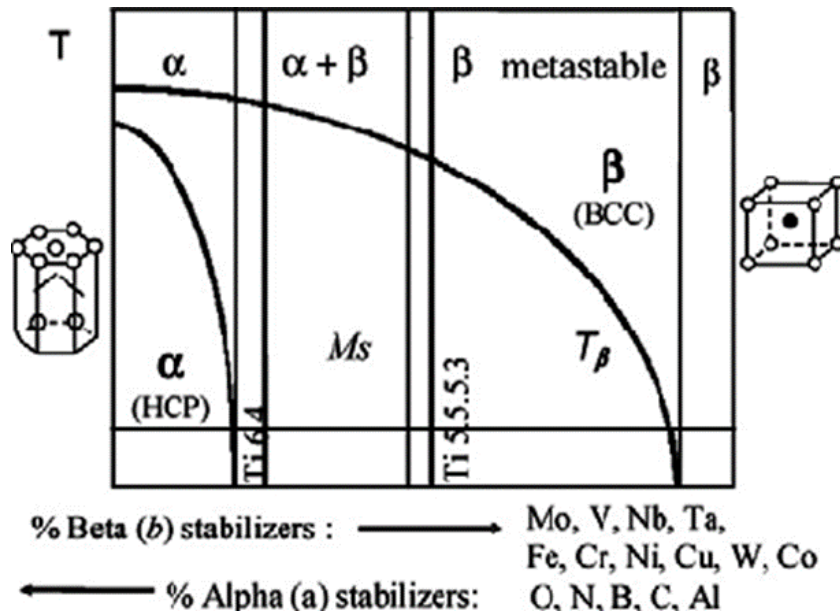
Figure II-1 Phase diagram of the different structures of titanium alloys

Alpha titanium alloys are consisted of the all α phase (like commercially pure titanium) or with some alloying α stabilizers [7], usually showing lower densities, high creep resistances and normally, usually better corrosion resistance than the beta titanium alloys [7]. Although these alloys seem to show some potentialities, they are hugely hindered by the poor high temperature properties of the alpha phase [8] which is what the alpha stabilizers addition aimed to solve by increasing the service temperature to up to 600°C [9, 10].

Beta titanium alloys consist in its entirety of the β phase or β phase with stabilizers [7]. These alloys usually display higher tensile and fatigue strengths than those of alpha titanium alloys while also being much easier to process [11]. The use of the β stabilizers serve as a way to reduce the binding energy of the Ti atomic clusters so that stronger bonds can be formed between the alloying atoms and the titanium atoms, effectively increasing the strength of the beta titanium alloys [12]. Nonetheless and despite their common use in some high stress regions of aircrafts [11], these alloys usually have the problem of possessing a low tensile ductility [13].

The alpha-beta titanium alloys, take the best of the two worlds by comprising the properties of both phases, exhibiting an excellent combination of ductility, tensile strength, fracture toughness and high temperature strength [7]. Of all the alpha-beta titanium alloys available, the most famous one is the

TiAl6V4, as it accounts for almost 80% of all the titanium consumption [14]. This alloy is heat treatable and possesses a really high yield and ultimate tensile strength [15] being produced with variable distributions of the alpha and beta phases, allowing for a larger spectrum of properties that can be achieved [2].

2.2 Problems during the machining of titanium alloys

Despite the outstanding properties of the Ti alloys presented so far, they present a really poor machinability (difficult-to-machine material), due to their extremely complex deformation mechanisms [16], their high chemical reactivity with most elements [17], their low Young's modulus [18] and poor thermal conductivity [19].

One of the problems associated with poor machinability, is the variation in the chip thickness which can lead to rougher machined surfaces, chatter, vibration and eventually to tool tip breakage [18, 20, 21]. When machining titanium alloys, typically chip segmentation occurs [22, 23] (also known as saw-tooth chip), as seen on Figure II-2, which is believed to be formed due to the formation of an adiabatic shear band [24, 25] and the growth of cracks [26]. Due to intense shear concentration and low thermal conductivity of titanium alloys, the temperature reached in the shear band can reach very high values which leads to increase strain rates and thermal softening, increasing the tendency for saw-tooth chip formation. On the same page, it's the springback of the tool [27] that can happen due to the low Young's modulus of the titanium alloys which cause excessive workpiece deflection creating a bouncing action and thus, a spring back of the tool.
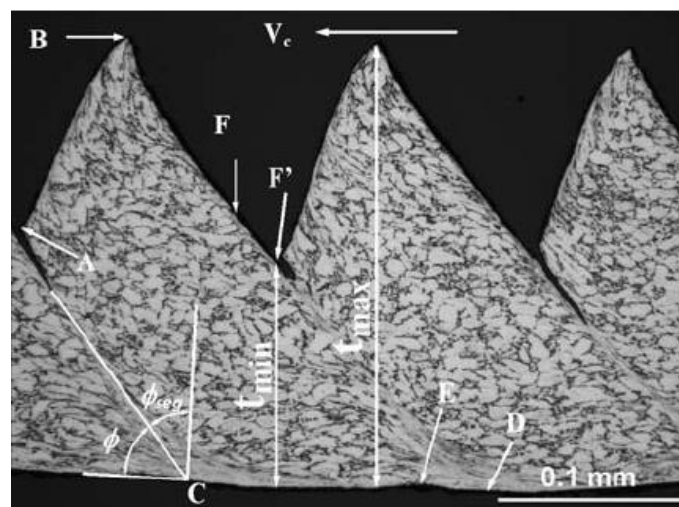
Figure II-2 Typical geometric shape of a saw-tooth type chip [22]

However, one of the main problems in the machining of titanium alloys is the high temperatures that can be generated in the cutting edge, mostly due to the poor thermal conductivity of titanium alloys [28]. Reportedly, the cutting temperatures during the machining of titanium alloys can reach temperatures as high as 1000°C even for relatively low cutting speeds (60 m/min) [29]. Therefore, diffusion and adhesion processes are enhanced, deteriorating tool life, cutting accuracy and subsequent surface quality [30]. Furthermore, the inherently high chemical reactivity of titanium with most elements, is aggravated for higher temperatures, leading to chemical wear and promoting the welding of the chips to the cutting edge forming the built-up edges (BUE) [30]. Naturally, the most relevant cutting parameters for dealing with the temperature seem to be the cutting speed and the feed rate [31], which are also some of the most important parameters to take into account when dealing with cost efficiency in the machining of titanium alloys, as shown before (see Figure I-4). Figure II-3 shows the effect of the cutting speed and feed rate on the tool wear rate, based on temperature, for the turning of TiAl6V4 aerospace alloy. The map clearly shows that even for relatively low cutting speeds and feed rates (55 - 80 m/min and 0.15 - 0.19 mm/rev), the tool can easily land on the "high tool wear" region of the map.

In the last few decades, researchers have been trying to improve the machinability of these alloys for their industrial applicability. The following section will detail some of the main solutions found useful to deal with the aforementioned problems.
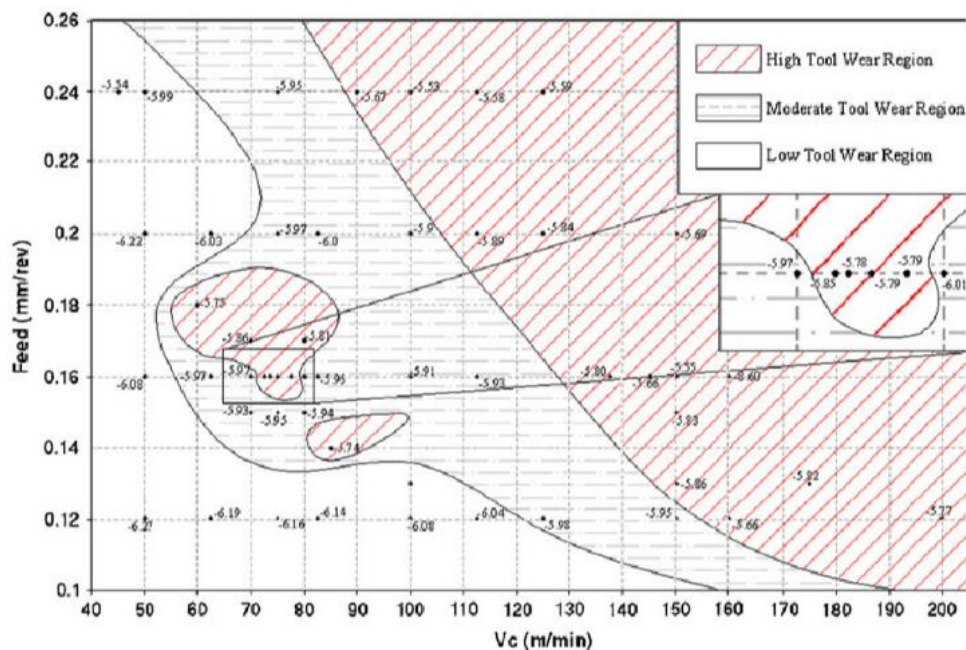
Figure II-3 Tool wear rate map for turning TiAl6V4 alloy [31]

2.3 Solutions to improve the machinability of titanium alloys

The first and the most traditional approach to solve the problem was based on the careful selection of cutting parameters by using low feed and cutting speeds and by keeping the machine tool as vibration free as possible while also replacing the cutting edge as soon as the minimum sign of wear was detected [32]. Obviously, this approach was everything but efficient in terms of the economic cost and time spent machining and as such, many other methods tried to be implemented to improve the productivity of titanium alloys machining. Some of those methods are described in the following sub sections.

2.3.1 Liquid cooling

Application of a liquid that could serve as a coolant was undoubtedly the next solution to be found and still one of the most commonly used solutions [33]. The coolant effectiveness comes from the tool-chip and tool-workpiece interface which can drop the temperature as much as almost 30% while also having some lubricant effect, effectively increasing tool life [34, 35]. However, the conventional low pressure cooling used sometimes doesn't have enough efficiency in the heat removal [36] and thus, high-pressure lubricoolant supply became the main way to introduce coolant, especially for the cutting of nickel based and titanium alloys [37]. For example, Sharman et al. [38] was able to reduce the temperature of the tool by almost 40% by using high-pressure lubricoolant supply instead of normal conventional flood cooling. Nowadays, tool holder systems to apply this type of supply are already commercially available on the market for multiple type of applications, just as the ones shown on Figure II-4. Nonetheless, this solution comes with a heavy economic and ecologic burden due to the high share of the coolant in the total cost of a machined part [39], the difficulty in the disposal [40] and most importantly, their fast degradation when operating with high temperatures [41].
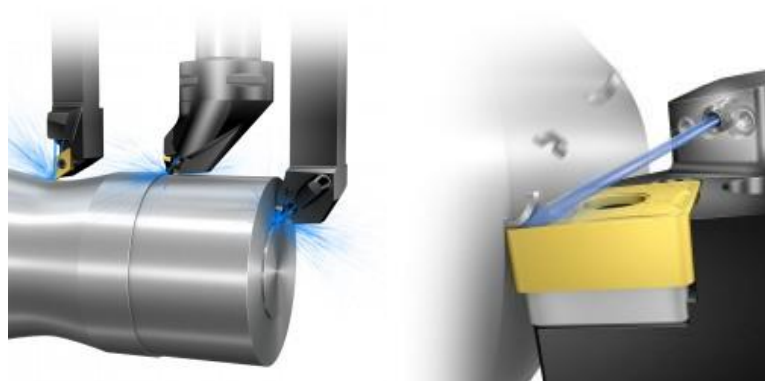
Figure II-4 High-pressure coolant supply on tools for different applications (Source: Sandvik Coromant)

2.3.2 Cryogenic cooling

Another solution similar to liquid coolants, is cryogenically freezing the workpiece with liquid nitrogen or carbon dioxide which can greatly reduce the temperature even for high cutting speeds, effectively improving the machinability of titanium alloys [42, 43]. Liquid nitrogen is, generally, a relatively safe, clean and non-toxic fluid with an inexpensive disposal that can easily be supplied in a liquid state at extreme low temperatures (almost negative 200°C) and low pressures [33]. Similarly to liquid coolants supply, cryogenic cooling supply can also be done using a different strategy by changing the zone where the liquid nitrogen is applied: by pre-cooling the workpiece, by directly cooling the cutting zone or by internal cooling of the tool [44]. Cryogenic cooling increases the tool lives up to five times comparing with conventional cooling [43, 45, 46], just as observed in Figure II-5. Despite this, cryogenic fluids pose some of the same problems as the conventional cooling, as the liquid nitrogen is a relatively costly fluid and there's the possibility of the building up of ice in the tool and/or tool holders. Additionally, it's also considerably tricky to keep a constant supply of the fluid during the machining process [47].
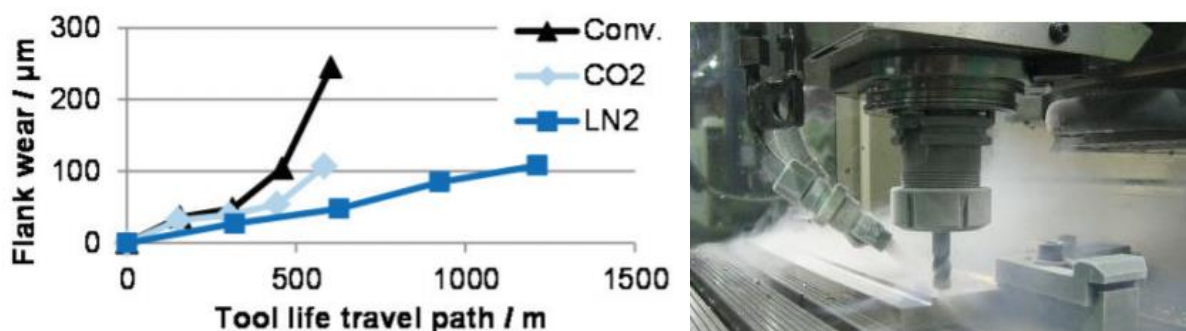
Figure II-5 Evolution of flank wear as function of the type of coolant used during machining of TiAl6V4 aerospace alloy (adapted from [46])

2.3.3 Dry machining and minimum quantity lubrication (MQL)

Eventually, a paradigm shift in lubrication, termed as "Dry machining", started to appear, to avoid the use of hazards liquids to decrease the temperature and friction on the contact tool/workpiece during the machining process [48]. In modern industries, this solution represents a huge possibility in terms of cost savings, as the cutting fluid is completely eliminated [49]. Another close solution is through the use of the so called minimum quantity lubrication (MQL), whenever total elimination of the cutting fluid is not possible, by applying a miniscule quantity of lubricant [49]. Although, these solutions effectively remove the health and ecologic hazards, they also come with heavy burdens, especially in terms of the excessive temperatures that can be reached on the cutting edge [50], that makes the tool heat up, lose its hardness,

deforming and becoming blunt, eventually leading to its failure. Adding to this, the high temperatures reached also affect the workpiece by making it lose its dimensional accuracy, completely altering subsurface properties and surface integrity [51]. Figure II-6 shows the difference in the temperature reached when using the different cooling techniques for varying cutting speeds and feed rates. Clearly, MQL seems to be able to decrease the temperature to values even lower than that of conventional flood cooling while dry condition shows much higher cutting temperatures, almost doubling the temperature reached for the MQL condition. All of this combined can lead to extremely severe shear stresses which leads to increased tool wear consequently lowering production rates and increasing the fabrication costs [18, 52].

The major aim in dry machining then ties itself to the development of suitable coatings with exceptional properties for high temperature performance [33, 48] that can help achieve the goals of keeping the desired surface and geometrical accuracies while also improving productivity at lower impact for cost and the environment. This connects with the coming sub-section where a major relevance is given to the one of the most promising ways of extending the service life of machining tools through the application of coatings.
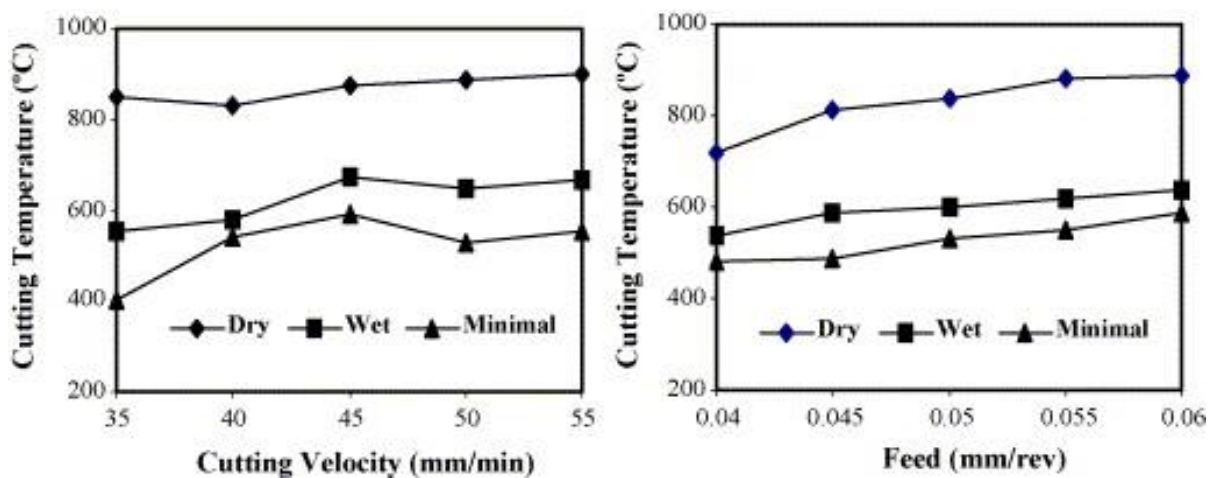
Figure II-6 Variation of the cutting temperature with the cutting speed and feed rate for the different cooling techniques [53]

2.3.4 Coatings for cutting tools

For successful application in cutting tools for the machining of titanium alloys, coatings should try to serve as a barrier that comprises a range of properties like high hot hardness to resist the stresses and further reduce abrasion wear, some chemical inertness to titanium and they should help with reducing friction at the cutting interface [48, 54]. Practically all developed coatings were deposited by either Physical

Vapour Deposition (PVD) or Chemical Vapour Deposition (CVD) techniques, with special focus on PVD technologies. PVD coatings can have a multitude of architectures [55] that lead to a higher range of possible properties, as schematized on Figure II-7.
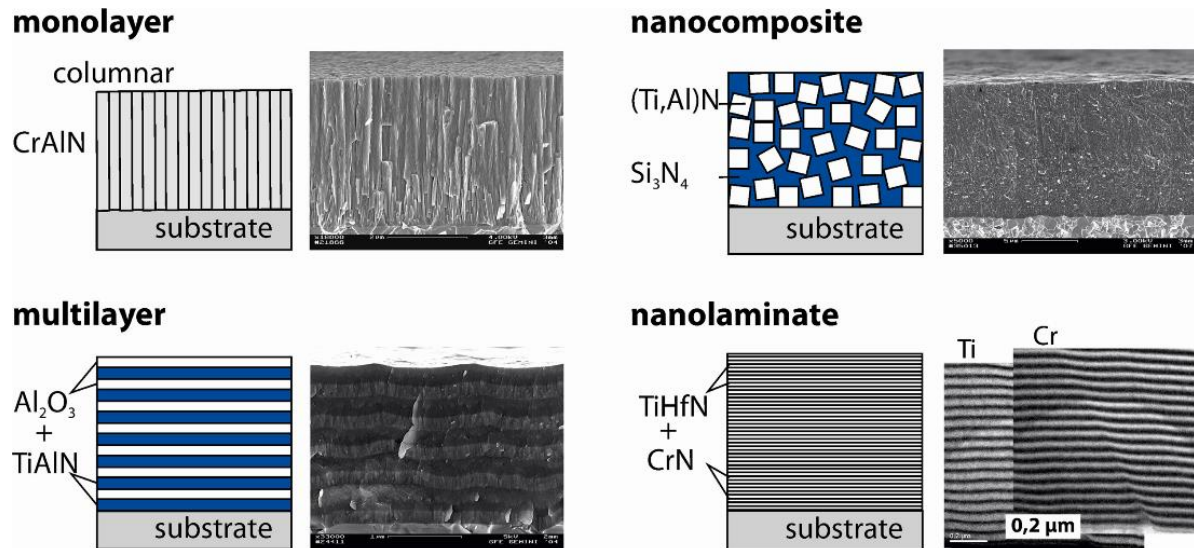
Figure II-7 Schematic of the different PVD coating architectures (adapted from [55])

All the PVD coatings initially used in the protection of the cutting tools were produced as monolithic single layer which, as the name suggests, are comprised of a single layer of a specific material. The first generation of protective commercial PVD coatings was the single layer, monolithic TiN system, initially used on carbide inserts for milling applications [56]. This was quickly followed by the introduction of other coating systems such as TiC, Ti(CN) and ZrN [57]. However, for higher cutting speeds, the thermal load that the tools were exposed to, promoted a decrease on the hardness and an increase on the oxidation kinetics mechanisms, ultimately leading to the premature tool failure [58]. To overcome this short coming, harder coatings with higher oxidation resistance were developed. Thus, ternary and quaternary coatings based on carbides and nitrides of transition metals appeared, with special attention being given to the TiAlN and AlCrN systems due to their good mechanical, tribological and oxidation properties at high temperature.

Specifically, the development of the TiAlN coating had a big impact in the functionalization of coatings for machining applications [59]. The introduction of smaller aluminium atoms in the TiN-NaCl type structure promotes a decrease in the lattice parameter, resulting in an increase in the hardness of the coating [60-62], with the additional potential advantage of high oxidation resistance due to aluminium's ability to form a protective oxide layer at high temperatures.
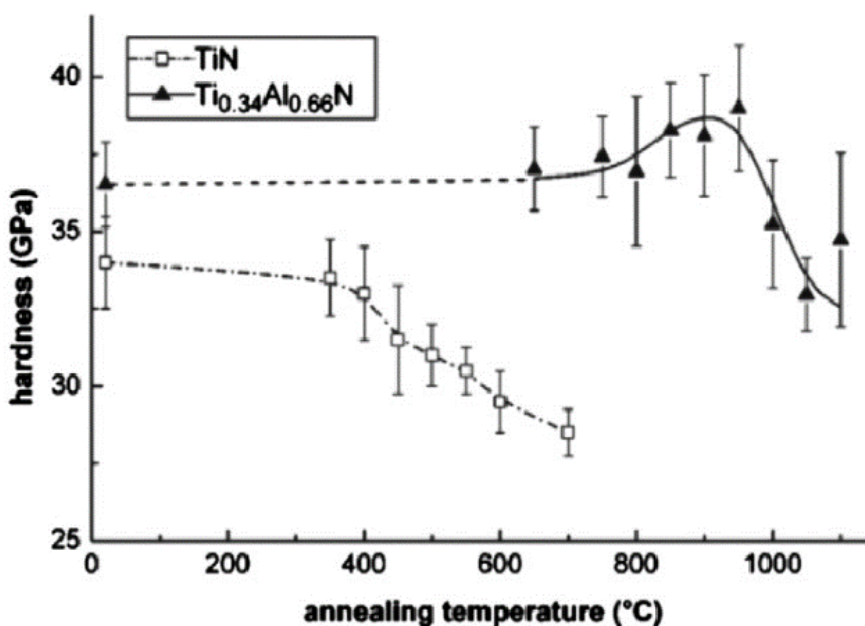
Figure II-8 Hardness as a function of the exposure temperature for the TiAlN and TiN coatings [63]

Figure II-8 also clearly shows the superior hardness stability of the TiAlN coating for higher temperatures when compared to the simple TiN system. Indeed, the hardness of reference TiN steadily decreases above 400°C, while for the TiAlN an increase in hardness is observed in the temperature ranges of 800°C to 900°C followed by a drop in the hardness due to the transformation of the fcc-AlN phase into the hcp-AlN phase [63]. This is an important thing to take into account since this temperature range is often reached during the machining of titanium alloys [64], making it a potential coating system used in machining of materials that require high mechanical strength at elevated temperatures [65, 66]. Later, the machining performance of these coatings was found to be enhanced by adding certain functional elements such as Cr [67-69], Y [70, 71], Si [70], B [72] and V [73, 74]. Bouzakis et al. [75], showed how addition of silicon on TiAlN can display improvements in the tool life for concentrations higher than 8 at.%. Boron and vanadium additions have been reported to improve the hardness and tribological behaviour of TiAlVN and CrAlN films [72, 76, 77]. The effect of adding chromium and small amounts of yttrium to TiAlN is seen by increasing the oxidation resistance to 900°C compared to the 600°C of TiN and by increasing the thermal stability even when compared to simple TiAlN or TiAlCrN [78]. Other type of coatings also used are the superhard coatings with high hardness and high resistance to thermal deformation such as the cubic boron nitride (cBN) and the tetrahedral amorphous diamond like carbon (ta-C DLC) [79-81]. The main problem with these type of coatings tie itself to the elevated level of stresses present on the films and consequent poor adhesion to the substrate. In the case of DLC's, their application is even limited due to their low oxidation resistance and poor thermal stability.
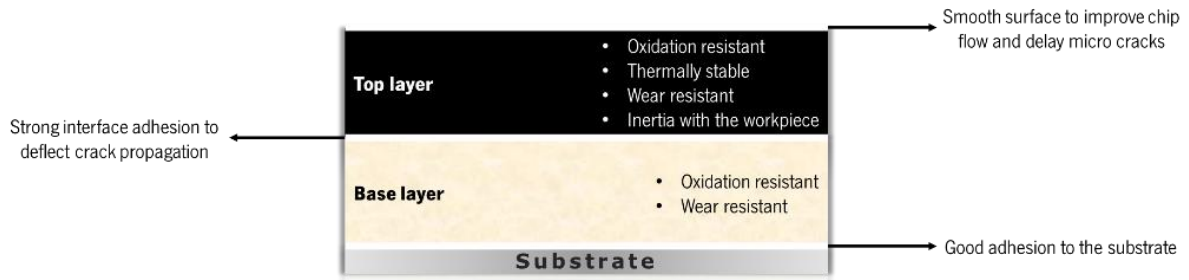
Figure II-9 Conceptual multilayer design with improved performance to resist mechanical and thermal loads

As shown before on Figure II-7, another possible architecture to improve the machining performance of coatings is by using a multilayer configuration consisting of two or more monolithic coatings where each layer can serve a different purpose, be it granting the film additional toughness, hardness, oxidation resistance, etc. The final structure usually presents superior mechanical and thermal performance comparing with that of the individual layers. An example of this can be seen in Figure II-9, where a multilayer coating comprised of different materials is shown, with each layer contributing with its own functional property be it, increasing the adhesion to the substrate, decreasing crater wear, increasing the chip flow smoothness or delay and/or deflect micro cracks. PVD multilayer coatings with larger periods for each layer composed of TiC, TiN, Ti(CN) and TiAlN [82] or with smaller layer periods of TiN, TiC and TiB$_2$ [83, 84] were the first generation of multilayer coatings developed. Inspektor et al. [66] prepared a double layer coating composed of a base layer of monolithic TiAlN and an outer layer of TiSiAlN and compared it with a simple monolithic TiAlN coating which showed a significant increase in tool life for the multi-layer coating when compared to the monolithic coating.
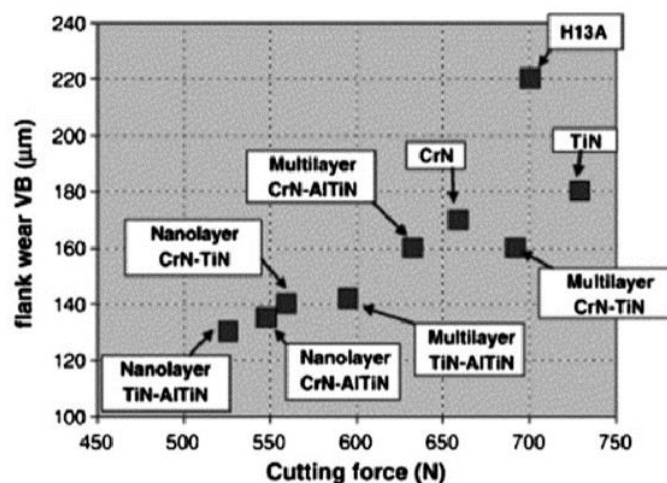
Figure II-10 Comparison of the flank wear and cutting force for various coatings with different architectures [85]

On a similar configuration are the nanolaminates (Figure II-7) or nanolayered films which consist on the same as a normal multilayer coating but the period of the layers is reduced to nanometre scale and the elastic modulus of the different composing materials are significantly different. The concept for these type of coatings was originally proposed by Koehler [86] defining that multilayers composed by different layers at nanoscale level with different elastic moduli may give rise to new and improved properties, including high hardness and high thermal stability. This may be observed in Figure II-10 where flank wear and cutting force of tools coated with nanolayers and multilayers of the same main material are compared. The harder nanolayered coated tools present much lower values of flank wear and cutting force than their sibling multilayers. However, as previously mentioned, the high hardness alone is not enough to assure protection of the tool. Thermal stability is required to protect it from thermal damage and have a wider functionality range. This can be achieved by a careful selection of the base materials and by using combinations of ceramic and metals including TiN/Ni [87] or ZrN/Cu [88] that combine high hardness with good toughness, or even CrN/Ag [89] that makes use of the soft and lubricious properties of the Ag.
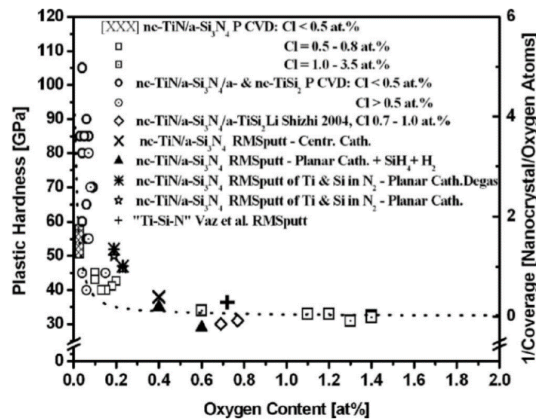
Figure II-11 Hardness of nanocomposite TiSiN films deposited by CVD and PVD as a function of oxygen content [90]
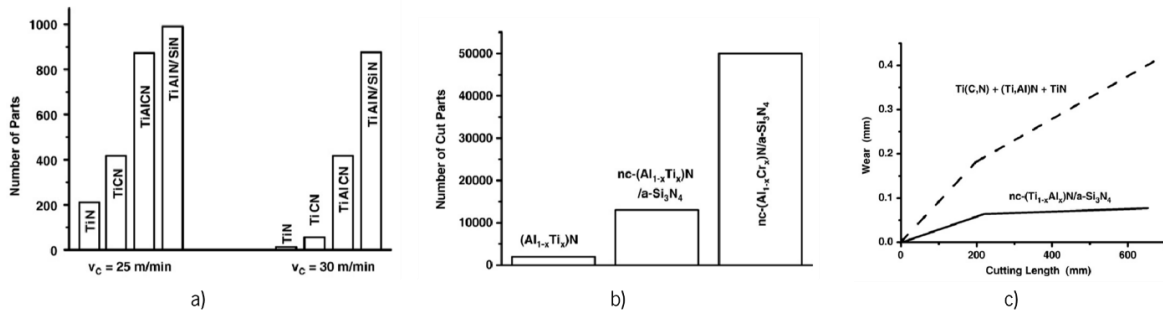
Figure II-12 Machining performance comparison of nanocomposite coatings for: a) dry tapping [91], b) circular saw cutting [92] and c) milling of a jet turbine part [93]

The last architecture that opened a range of new designs for coatings with tailor made properties were the nanocomposite coatings. Firstly described for nanocomposite TiSiN films by Veprek et al. [94, 95], the properties of these coatings depends on the coatings chemical composition and on the coatings structure (relation between the size of TiN grains and Si_3N_4 phase thickness). Either deposited by CVD or PVD and related to their dependence on the oxygen content, their hardness always displays high values of hardness, as shown on Figure II-11. Without surprise, the tooling industry quickly applied this type of coatings on the protection of the surface of the machining tools due to their extremely high hardness > 40 GPa, good oxidation resistance and their capacity to deflect cracking propagation [96, 97]. Several other coatings systems developed as nanocomposite have been developed to protect the surface of the cutting tools such as: nc-W_2N/a-SiN [98, 99], TiAlCN [100, 101] and TiAlSiN [102]. The machining performance of these nanocomposites coating can be observed in Figure II-12, where it is clearly seen the improvement in tool life when using nanocomposites for different machining operations.

To summarize, this section presented a series of coatings with different configurations, all with serious potential to be used in the machining of titanium alloys. Table II-1 displays a summary of the different coatings systems presently used to protect the surface of machining tools, the type and parameters of machining and the tool life. The success of these type of coatings stimulated further interest and adaptation by the machining industry and sector leading to a continuous effort to develop new and improved coating systems with lubricious properties that can sustain their capabilities at extremely harsh machining conditions. Taking this into account, nowadays solid-lubrication and self-lubricant coatings are a promising challenge.

Table II-1 Machining performance of titanium alloys for different coatings and cutting operations (nc for referring to nanocomposite architecture)

COATING	CONDITION	OPERATION	DEPTH OF CUT [MM]	FEED RATE [MM/REV]	CUTTING SPEED [M/MIN]	TOOL LIFE [MIN]	REFERENCE
Uncoated	Dry	Turning	1	0.1	80	4	[103]
Uncoated	Dry	Turning	1	0.28	150 / 220	1 / 1	[104]
TiN	Dry	Turning	0.5	0.15	60 / 120	6 / 6	[105]
TiN	Dry	Turning	0.5	0.25	60 / 120	10 / 5	[105]

TiN	Dry	Drilling	NA	0.07	50	7	[106]
AlTiN	Dry	Turning	1	0.1	80	>7	[103]
AlTiN	Wet	Milling	1.25	0.4	100	11	[107]
AlTiN	Wet	Turning	0.25	0.125	150	17	[108]
TiB$_2$	Wet	Turning	2	0.15	45	130	[109]
TiAlN	Wet	Turning	2	0.15	45	60	[109]
TiAlN	Wet	Drilling	NA	0.06	25 35 45 55	8 6 3 <1	[110]
TiAlCrN	Wet	Milling	1.25	0.4	100	9	[107]
AlTiN/VN	Wet	Turning	0.25	0.125	150	24	[108]
TiAlN/TiN	Dry	Milling	2	0.15	40	30	[111]
TiAlN/TiN	Dry	Milling	1	0.06	150 300	21 7	[112]
TiN/TiCN/TiAlN	MQL	Milling	2	0.1	120 135	<1 <1	[113]
TiC/TiCN/TiN	Dry	Turning	1	0.25	75	11	[114]
AlTiSiN (nc)	Dry MQL	Turning	1.2	0.1	120	14 32	[115]
AlCrSiN (nc)	Dry MQL	Turning	1.2	0.1	120	9 14	[115]

2.4 Solid lubrication as a way to increase cutting speed

With all the different type of architectures and coatings presented so far, their use became standard in machining applications due to the achievable improvement on machining and reduction of production costs. However, to this day, surface friction and wear remain a technological challenge, especially for high cutting speeds where high temperatures are involved [64]. Opposite to this relatively young approach of modifying the working tools surface, the use of lubricants to reduce the friction between the tool and

the material prevailed for over a thousand years but, just as it was shown on section 2.3.1, their usage comes with severe burdens to the environment [40] and their use is limited at high temperatures [41]. This led to a lubrication paradigm shift from liquid to solid lubrication, first by introducing dry machining (section 2.3.3) and then into coatings that could have optimized mechanical properties [116, 117] while keeping in mind the high temperature oxidation resistance required, which gave rise to the so-called "chameleon" or "self-adapting" coatings [118] which make use of a lubricious element that due to its own intrinsic properties and/or when combined with other elements can lead to the formation of a protective tribolayer, effectively reducing the friction and temperature in the contact zone. For example, by making use of elements that can form high temperature lubricant Magnéli phase oxides [119], such as vanadium or molybdenum, it is possible to reduce friction in the cutting zone [74, 120, 121]. Erdemir et al. [122] summarized the key advantages of using solid lubrication over liquid lubrication for friction applications, showing the potential for solid lubrication cutting tools as a way to increase cutting speed, increasing the effectiveness of machining titanium alloys.

2.4.1 Self-lubricant coatings

The name "chameleon" given to those type of coatings come from their ability to "adapt" to different environments and temperatures through self-guided complex adaptive behaviours, just as depicted on Figure II-13. The most common solid lubrication adaptive strategies, mechanisms, and their main benefits and challenges are summarized on Table II-2. None of the mechanisms shown can cover the entire temperature range from room temperature to the order of 1000 °C, which creates a challenge for their use as solid lubricants in machining components.
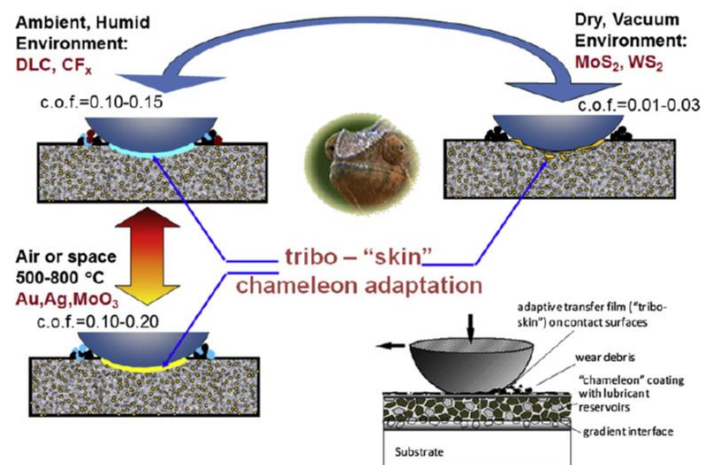
Figure II-13 Schematic representation of a "chameleon" coating functionality [118]

Table II-2 Typically used solid lubrication adaptive mechanisms (adapted from [118])

ADAPTIVE MECHANISM	TEMPERATURE RANGE	MATERIAL	BENEFITS	CHALLENGES
BASAL PLANE FORMATION	<300°C	MoS_2 WS_2 DLC	Lowest friction and wear rates Low cost option	Oxidizes at high temperatures
LUBRICIOUS OXIDE FORMATION	500 to 1000°C	Magnéli phase oxides Silver double oxides Silicate glass	Provides low friction Wear track self-healing	Abrasive at low temperatures Removal of lubricant by the load
NOBLE METAL DIFFUSION	300 to 500°C	Ag and Au encapsulated in ceramic matrixes	Oxidation stable Temperature self-regulated	Fast noble metal diffusion

The sliding contacts between surfaces are used for modifying the structural surface through the re-orientation of randomly-oriented polycrystalline planes into parallel oriented and easily shearable hexagonal basal planes that greatly reduce the shear strength providing a low friction surface leading to a considerable reduction in the friction and wear [123-126]. These type of coatings provide extremely low friction and in some cases are considered as almost "frictionless" with COF values below 0.02 [127, 128]. Nevertheless, their behaviour was highly dependent on the temperature used and on the environment. Another type of approach explored was the incorporation of these very "soft" lamellar solids into hard nanocomposite coatings where they could be combined to present high hardness and reduced friction [129, 130]. An example of this was shown by Stuber et al. [131] with TiC-DLC coatings deposited by magnetron sputtering displaying values of hardness close to 40 GPa while maintaining a substantially low COF of 0.1, at room temperature. Nonetheless, these coatings have the drawback of being limited in the range of temperatures at which they can efficiently operate, due to their sensitivity to oxidation at temperatures as low as 300°C [132, 133], consequently not being the mostly preferred solution to be used in the protection of machining tools.
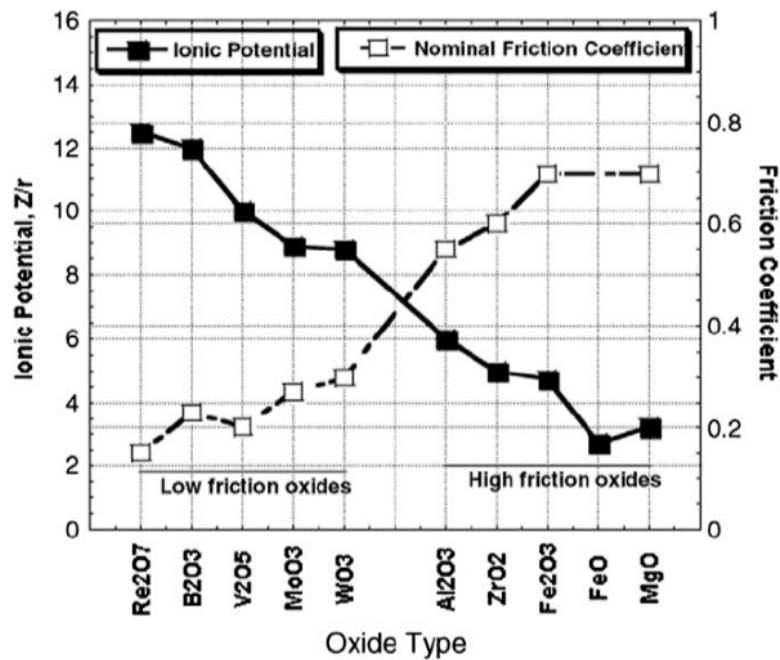
Figure II-14 Coefficient of friction of different type of oxides [134]

The use of metal oxides that plastically deform and form low shear strength layers are a common solution for applications where extreme temperatures are expected [135, 136]. They are, however, abrasive at lower temperatures which made researchers exploring "chameleon" coatings that could adapt their surface and keep the lubricious properties at all temperature ranges [137, 138]. At higher temperatures, the mechanism that guides the formation of the lubricious oxide is very important, with the challenge being the reversibility of the surface to its "original" state after temperature cycling. The majority of the oxides possess thermodynamic stability for temperatures of 1000ºC and greater but require higher surface shearing strengths due to strong ionic bonding. Furthermore, large coefficients of friction and high tensile stresses in ceramic oxides consequently results in the production of surface cracks and wear debris particles [139]. Figure II-14 shows a comparison of coefficients of friction between different types of oxides with different ionic potentials. Despite this, the coefficient of friction of oxides usually varies inversely with increasing temperature, thereby achieving lubrication under high temperature conditions. In 1954, a homologous series of compounds were discovered to be formed through sub-stoichiometric compositions of various transition metals by Magnéli [140] with planar lattice defects that resulted in compounds with greater crystallographic shear planes possessing lower binding strengths. Among the most common of these oxide phases, special attention has been given to vanadium based Magnéli oxides [121]. For example, the tribological characteristics of VO_x were researched as a component of temperature by Fateh et al. [141] where it was reported a reduction in the COF value from room temperature to 600°C. As an alternative to the Magnéli phase oxide approach, another promising strategy is through the use of

the so-called ternary oxides which combine a transition metal and a noble metal to spawn lubricious materials at high temperatures [119]. The concept of forming a ternary oxide to protect the surface was firstly reported by Zabinski et al. [142] with a PbO-MoS$_2$ composite coating that formed a PbMoO$_4$ lubricious layer at high temperature. More recently, the focus has shifted towards the formation of ternary oxides by adding silver to binary oxides [143]. Three different silver molybdate phases (Ag$_2$MoO$_4$, Ag$_2$Mo$_2$O$_7$ and Ag$_6$Mo$_{10}$O$_{33}$) were examined by Muratore et al. [144] which saw low COF values when sliding at high temperatures, due to the weaker bond of Ag-O when compared to Mg-O bond that makes it easily shearable. Despite this, this type of mechanism presents the challenge of being extremely abrasive at low temperatures and due to the easily shearable planes, the lubricant can easily be removed by the applied load, leading to the quick loss of its lubricious properties.
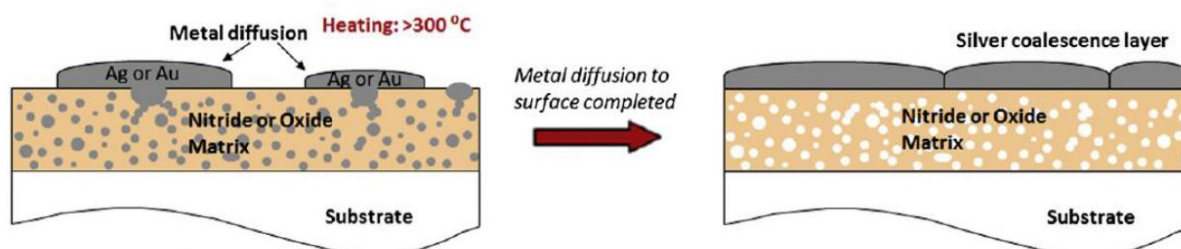
Figure II-15 Schematic illustration of metal out-diffusion on a self-lubricant film (adapted from [118])

As an alternative solution, self-lubricant coatings started being developed by combining the intrinsic properties of a high oxidation resistant coating doped with a noble metal which due to their own properties or due to the combination of other elements forms a tribolayer on the sliding contact which protects the coating from wear [118]. A schematic representation of this self-adapting mechanism is shown on Figure II-15. Silver and gold are reliable noble metals to be used in solid lubrication due to their low shear strength over a wide range of temperatures and by the fact of having relatively high melting points [145]. Due to the coalescence of the noble metal layer on the contact, it is normal that the thickness of said layer will influence the COF values, as a too thin layer might not be able to completely fill the surface of the wear zone and an over exceeding thickness might lead to a significant increase in the "plowing force", increasing the total tangential force [146]. To maintain the exceptional mechanical properties and wear resistance, the noble metal is commonly introduced in a hard nanocomposite coating. As such, even with relatively high values of gold added (up to 20 at.%) to a yttrium stabilized zirconia (YSZ) coating, the hardness value was kept relatively high (close to 15 GPa) while also keeping high ductility and fracture resistance [147]. Further studies of those films at high temperatures, revealed the appearance of small volumes of Au coalesced at the coating surface, allowing for a lubrication effect [148]. The main challenge

nowadays with the noble metals however, resides in the fast migration of the lubricious element to the surface, leading to its complete depletion from the volume of the coating and consequent loss of lubricious properties [149, 150]. Section 2.5 will further extend and present some of the solutions proposed for this problem.

2.4.2 Silver as a solid lubricant element

As already mentioned, silver is one of the most common noble metals used in conjunction with ceramic matrices as a self-adaptive mechanism to reduce friction and wear. These type of coatings are really promising due to their immense range of applications conferred by their multitude of functional properties. Velasco et al. [151] summarizes the panoply of functional properties of silver and its effect when applied with ceramic matrices.

Before releasing the stress   After releasing the stress
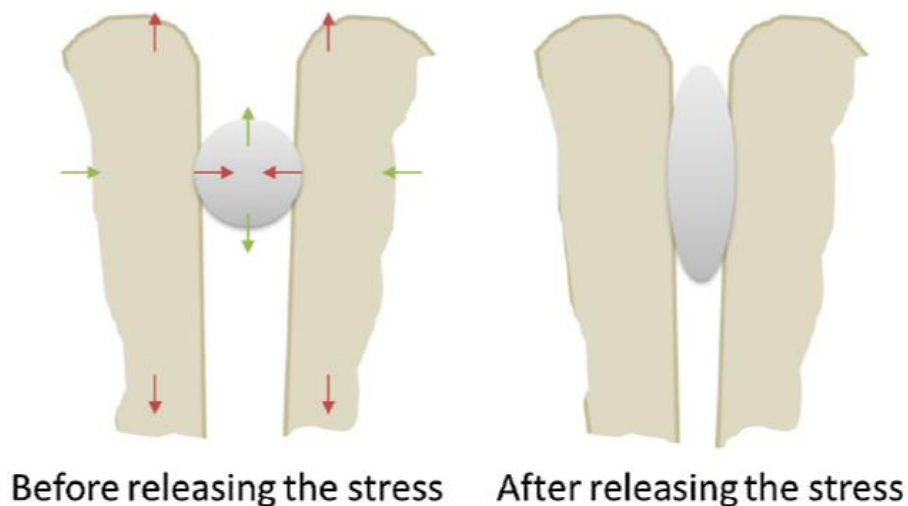
Figure II-16 Schematic representation of the silver effect on the residual stresses of Ag-containing coatings [151]

Of most importance in the context of machining are the mechanical and tribological properties of silver due to those properties being directly related to the machining behaviour when it comes to temperature, friction and wear. Due to silver being a soft metallic phase, adhesion too the substrates is a concern when designing new coating systems with Ag integration. Residual stresses left from the deposition of the coatings can have a significant impact on their adhesion, not to mention their mechanical properties [152, 153], making it an important parameter when considering the introduction of silver. Residual stresses in films deposited by PVD are generally under compressive residual stresses [154] due to a series of induced growth effects that cause lattice distortions in a phenomenon originally called as "atomic peening" [155]. Due to being a soft metallic phase, the incorporated silver will easily plastic deform and

help release the compressive stresses [156], just as schematized in Figure II-16. The release of the compressive stresses then helps with increasing the adhesion properties of some of the coatings [157, 158].
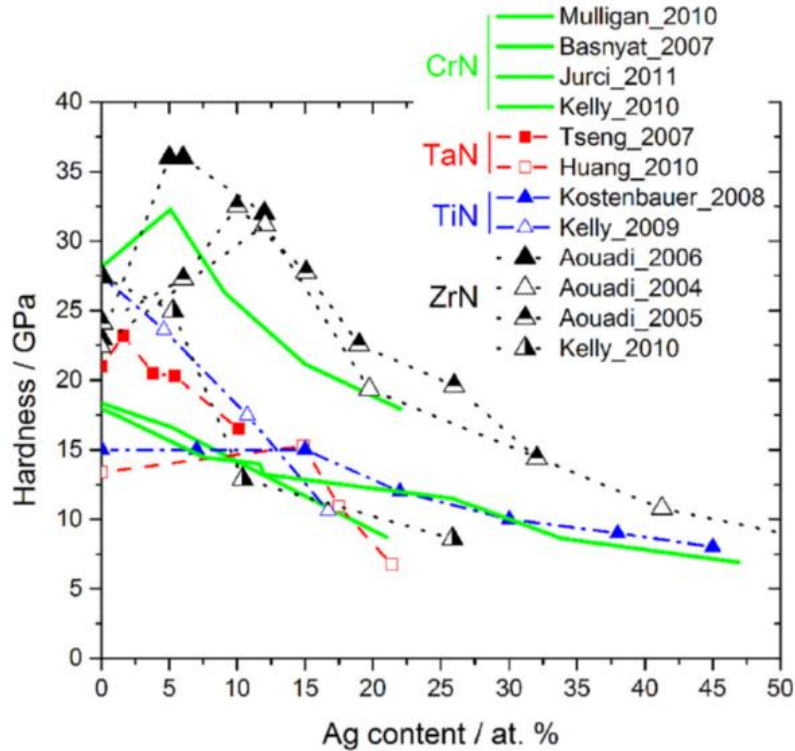
Figure II-17 Hardness of various coating systems as a function of silver content [151]

As mentioned, hardness is another important mechanical property to take into account, especially when Ag, as a soft phase, is to be incorporated as it, generally, shows a detrimental effect on the hardness and Young's modulus of the coatings, just as observed on Figure II-17 for different coating systems. An improvement of hardness is normally observed for low Ag concentration additions [159, 160] due to grain refinement, hindering dislocation motion and avoiding cracking at the interfaces. After this silver content threshold is surpassed, silver segregates to the grain boundaries facilitating grain boundary sliding which combined with the release of the residual stresses all lead to the quick deterioration of the hardness of the coatings. Another factor that have been reported to impact the hardness of such coatings was the deposition temperature, as it was reported that its increase gave rise to higher values of hardness due to the segregation of silver to the surface which gave rise to pure ceramic phases, free of Ag [161, 162]. Nonetheless, there seems to be reported issues when measuring the hardness of these systems, as the high deposition temperature, makes silver tendentiously segregate to the surface which makes the Ag-rich agglomerations lead to masking in the real measured values [163].
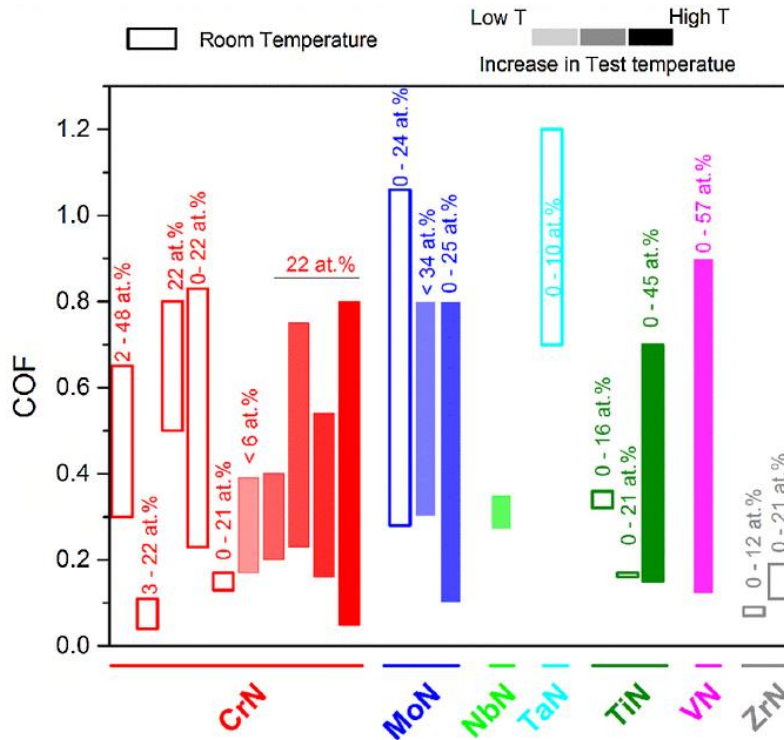
Figure II-18 Reported COF values for multiple different coating systems as a function of temperature and silver content [151]

Tribological properties are the other important functional characteristics when dealing with machining operations. As previously mentioned on section 2.4.1, silver segregation to the surface is one of the key parameters to consider for the adaptive mechanism in self-lubricant coatings. For higher temperatures, silver shows higher mobility which allows it to diffuse to the surface forming islands that can act as a lubricant due to its low shear strengths effectively reducing the COF [162, 164, 165].

In this context, deposition temperature should be also considered as trigger to silver self-lubricant properties. In fact, Mulligan et al. [164] proposed that the disparity between the deposition temperature and the testing temperature ($T_t - T_d$) can work as a way to assess the silver lubrication effect, by noticing that tests carried out at higher temperature than the deposition temperature ($T_t > T_d$) show a reduction of the COF, until the silver is depleted. When the opposite occurs ($T_t < T_d$), the COF is constant and it can be located within the range of normal values of ceramic matrices coatings, depending on the Ag content. When silver reach large concentrations, the diffusion and segregation might lead to the formation of pores left by the silver nanoparticles, making the topmost part of the coating an unstable porous matrix that due to the mechanical solicitation nature of the tribology tests can disintegrate the pores, collapsing the film and registering higher values of COF [159]. Figure II-18 shows a comparison of the range of COF values for multiple different coating systems for different temperatures and silver contents.

This noble metal is clearly an element to be used in self-lubricant coatings as a way to reduce friction and wear in the machining of titanium alloys. However, nowadays, the main challenge of these type of coatings resides on the controlled release of Ag to the sliding contact.

2.5 The diffusion problem of solid lubrication and solutions

As mentioned on section 2.4.1, one of the adaptive mechanisms is through the diffusion of a noble metal working as a lubricant agent in the contact zone. This phenomenon was first reported for the surface of YSZ-Au adaptive coatings where migration and coalescence of the gold to the surface was induced at sliding in air at 500°C for about 10 at. % of Au [148]. Then, an even faster metal migration was observed for a oxide and nitride coatings with incorporated silver [165, 166]. Independently of the films configurations, the friction coefficient was reduced and the wear resistance of films improved. However, such improvements were of short duration due to the rapid release of the metal, its quick depletion from the entire volume of the coating and the consequent loss of the low-friction tribolayer after few minutes [167]. As an example, YSZ coatings doped with gold were found to have depleted almost all of the 20 at.% of Au in less than 5 minutes, even for a relatively low temperature of 500°C [149, 150]. The metallic noble metal inclusions are embedded in the matrix during the deposition, increasing strain and interfacial energy, reducing the activation energy which is then further reduced by the high vacancy concentration of the matrix left by silver diffusion, resulting in the even quicker movement of the noble metal throughout the highly defective matrix, even for temperatures as low as 300°C [149, 168].

Thus, the challenge nowadays resides in an adequate control of the diffusion rate of the lubricious metal in order to obtain low friction and high wear resistance in the long-term allowing these coatings to be used as a viable solution in the cutting tool industry for a wide range of operation conditions [118]. A promising approach to control the release of the lubricious metal was demonstrated by Muratore et al. [161, 168, 169] by using diffusion barrier layers. By making use of YSZ–Ag–Mo multilayer coatings with a TiN cap barrier layer, the control release of the lubricious phase to the surface can be achieved. Tribological results revealed that wear rate was reduced and the coating lifetime increased from 4500 cycles to over 50000 cycles in relation to the reference monolithic coating of identical composition and total thickness. Also, MoS_2 has been reported to be an effective diffusion barrier for Ag transport to the wear track for a $Mo_2N/MoS_2/Ag$ coating system tested at 350 °C [170, 171]. Similarly, a dense CrN cap layer on CrN–Ag composite coating has been reported to be an effective diffusion barrier, limiting Ag transport to the surface to areas within the wear track, which resulted in lower cumulative wear rates [156]. Xiong et al. [172] who worked with the Ag/TiO_x also observed that silver diffusion can be avoided/delayed when an

excessively high total pressure is used in the sputtering process of the TiO cap layer. However, despite these results, the cap layers are of short-term efficiency, since they are easily removed due to their lower thickness when compared to the entire base coating which allows the total depletion of the lubricious metal after a critical time.

Thus, the metal out-diffusion, can be only achieved if a dense barrier layer, which initially encapsulates the solid lubricant within the matrix, can be established, preventing the fast depletion of the lubricant. Accordingly, matrix materials with excellent thermal and chemical stability at elevated temperatures, high mechanical strength and toughness should be good candidates to encapsulate the lubricious agent. The following section will discuss the use of a coating system that can maintain all the aforementioned properties while hindering the diffusion of the silver.

2.6 TiSiN coatings as a way to control the diffusion of the lubricious agent (Ag)

The development of a new and green coating system with controlled release of the lubricious phase could be the solution to achieving high-speed and high-performance machining of titanium alloys, which could have big influence on tool life, metal removal rate, surface quality and machining costs. One of the possible solutions to achieve this is through the use of a coating system formed by a dual phase structure, in which one of the phases could act as a diffusion barrier to the silver which should be responsible for the lubrication.
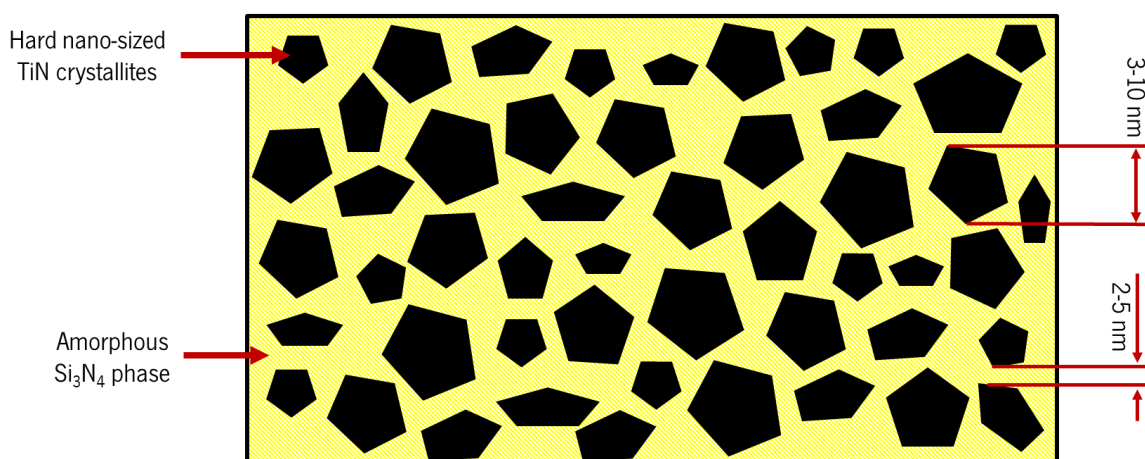
Figure II-19 Schematic representation of the proposed nanocomposite TiSiN(Ag) system

The coating system proposed is the well-known TiSiN. This system can be deposited as a nanocomposite structure [94, 95] which, as seen on section 2.3.4, can lead to fantastic mechanical properties such as high hardness, thermal stability and oxidation resistance. The silver addition will incorporate the

lubrication activity. The challenge remains: controlling the silver diffusion. In fact, when deposited as a nanocomposite structure (nano-sized TiN crystallites surrounded by an amorphous SiN matrix), the amorphous phase, in the grain boundaries or as a layer itself, will work as an diffusion barrier to the lubricious metal ions diffusion [173] while also increasing the oxidation resistance [174, 175]. A schematic of the proposed nanocomposite coating structure is shown on Figure II-19. Thus, by doping this coating system with a lubricious element and by playing with the nanocomposite structure (different TiN grain sizes and Si3N4 phase thickness), the control release of the lubricious phase may be achieved.

Given this concept, a new challenge arises: How is the nanocomposite structure achieved and its structure dimensions attained. This challenge can be overcome through the use of a relatively novel PVD magnetron sputtering technique called High Power Impulse Magnetron Sputtering (HiPIMS). The next section will provide a brief insight into this technique and how it allows for the deposition of nanocomposite structure.

2.6.1 HiPIMS as a way to deposit the nanocomposite structure

Initially, nanocomposite structures (nc-TiN/a-Si_3N_4) were only able to be achieved with extremely high deposition temperatures by CVD techniques [94, 95]. For PVD techniques, without pre-heating of the substrates, high energetic ion bombardments are required for the silicon to have enough mobility to segregate and form the amorphous phase [176, 177].
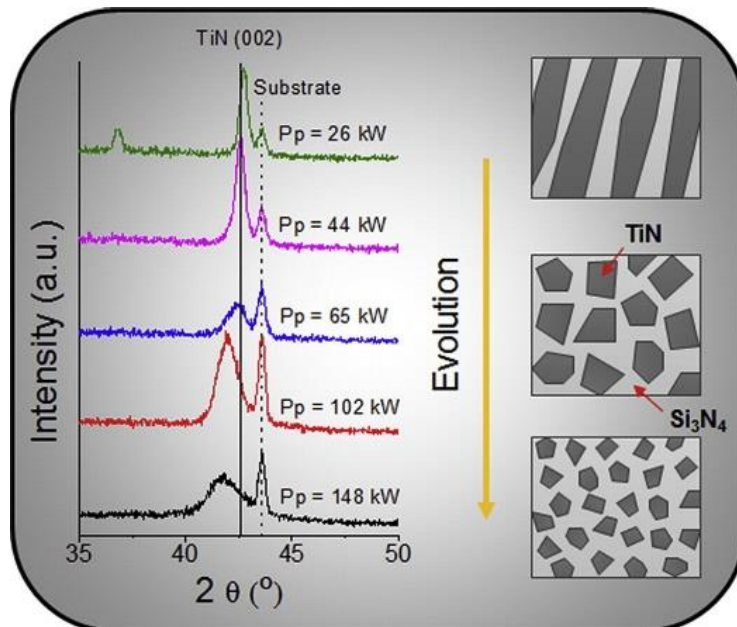
Figure II-20 Schematic representation of the structure evolution with the increase in the peak power parameter of the HiPIMS [178]

More recently, a novel PVD magnetron sputtering technique known as High Power Impulse Magnetron Sputtering (HiPIMS) has emerged that can produce highly ionized fluxes of sputtered material when compared to conventional magnetron sputtering techniques (DCMS or Rf-MS), allowing control over the energetic ion bombardment [179, 180]. HiPIMS is characterized by the application of very high target power densities to achieve higher plasma densities and subsequent ionization of the sputtered material. In typical DCMS techniques, depending on the power applied to the target, the percentage of species that are ionized is quite small by, typically, having only close to 1% of the sputtered species reaching the substrate in the form of ions, while with HiPIMS this is greatly increased to more than 50%, with some elements reaching almost 100% of ionized material [181]. With this in mind, Oliveira et al. [178] reported that, for the same silicon concentration and without any intentional substrate heating, the nanocomposite structure in TiSiN films was able to be attained and tailored by applying high peak powers to the targets by using the HiPIMS technology, as shown on Figure II-20.

Thus now, all the criteria required to deposit hard, thermally stable, highly oxidation resistance and self-lubricant TiSiN(Ag) films have been met, allowing for the design of a novel coating system that enables to reach the proposal of this thesis of increasing the cutting speed by applying the coating in cutting tools to be used for increasing the machining performance and efficiency of titanium alloys.

2.7 References

[1] G. Lütjering, J. Williams, Titanium Springer-Verlag Berlin Heidelberg, New York, 48 (2003).

[2] V. Weiss, J. Sessler, Aerospace structural metals handbook, Syracuse University Press, 1963.

[3] R.R. Boyer, Attributes, characteristics, and applications of titanium and its alloys, JOM, 62 (2010) 21-24.

[4] C.T.S. Company, All About Titanium from Continental Steel & Tube: Properties, Forms, and Applications, in, 2020.

[5] N. Khanna, J.P. Davim, Design-of-experiments application in machining titanium alloys for aerospace structural components, Measurement, 61 (2015) 280-290.

[6] J.R. Myers, H.B. Bomberger, F.H. Froes, Corrosion Behavior and Use of Titanium and Its Alloys, JOM, 36 (1984) 50-60.

[7] C. Veiga, J.P. Davim, A.J.R. Loureiro, Properties and applications of titanium alloys: A brief review, Reviews on Advanced Materials Science, 32 (2012) 133-148.

[8] C. Leyens, M. Peters, Titanium and titanium alloys: fundamentals and applications, John Wiley & Sons, 2003.

[9] W. Jia, W. Zeng, J. Liu, Y. Zhou, Q. Wang, On the influence of processing parameters on microstructural evolution of a near alpha titanium alloy, Materials Science and Engineering: A, 530 (2011) 135-143.

[10] X. Wang, M. Jahazi, S. Yue, Substructure of high temperature compressed titanium alloy IMI 834, Materials Science and Engineering: A, 434 (2006) 188-193.

[11] R.R. Boyer, R.D. Briggs, The use of β titanium alloys in the aerospace industry, Journal of Materials Engineering and Performance, 22 (2013) 2916-2920.

[12] Y. Song, D.S. Xu, R. Yang, D. Li, W.T. Wu, Z.X. Guo, Theoretical study of the effects of alloying elements on the strength and modulus of β-type bio-titanium alloys, Materials Science and Engineering: A, 260 (1999) 269-274.

[13] J.C. Williams, E.A. Starke, Progress in structural materials for aerospace systems11The Golden Jubilee Issue—Selected topics in Materials Science and Engineering: Past, Present and Future, edited by S. Suresh, Acta Materialia, 51 (2003) 5775-5799.

[14] C. Cui, B. Hu, L. Zhao, S. Liu, Titanium alloy production technology, market prospects and industry development, Materials & Design, 32 (2011) 1684-1691.

[15] S. Zherebtsov, G. Salishchev, R. Galeyev, K. Maekawa, Mechanical properties of Ti–6Al–4V titanium alloy with submicrocrystalline structure produced by severe plastic deformation, Materials Transactions, 46 (2005) 2020-2025.

[16] A. Pramanik, M.N. Islam, A. Basak, G. Littlefair, Machining and Tool Wear Mechanisms during Machining Titanium Alloys, Advanced Materials Research, 651 (2013) 338-343.

[17] B.M. Kramer, D. Viens, S. Chin, Theoretical Consideration of Rare Earth Metal Compounds as Tool Materials for Titanium Machining, CIRP Annals, 42 (1993) 111-114.

[18] E.O. Ezugwu, Z.M. Wang, Titanium alloys and their machinability—a review, Journal of Materials Processing Technology, 68 (1997) 262-274.

[19] A.K.M.N. Amin, A.F. Ismail, M.K. Nor Khairusshima, Effectiveness of uncoated WC–Co and PCD inserts in end milling of titanium alloy—Ti–6Al–4V, Journal of Materials Processing Technology, 192-193 (2007) 147-158.

[20] S. Sun, M. Brandt, M.S. Dargusch, Characteristics of cutting forces and chip formation in machining of titanium alloys, International Journal of Machine Tools and Manufacture, 49 (2009) 561-568.

[21] R. Komanduri, Z.-B. Hou, On thermoplastic shear instability in the machining of a titanium alloy (Ti-6Al-4V), Metallurgical and Materials Transactions A, 33 (2002) 2995.

[22] S. Sun, M. Brandt, M.S. Dargusch, Effect of tool wear on chip formation during dry machining of Ti-6Al-4V alloy, part 1: Effect of gradual tool wear evolution, Proceedings of the Institution of Mechanical Engineers, Part B: Journal of Engineering Manufacture, 231 (2015) 1559-1574.

[23] E.O. Ezugwu, J. Bonney, Y. Yamane, An overview of the machinability of aeroengine alloys, Journal of Materials Processing Technology, 134 (2003) 233-253.

[24] J. Barry, G. Byrne, D. Lennon, Observations on chip formation and acoustic emission in machining Ti–6Al–4V alloy, International Journal of Machine Tools and Manufacture, 41 (2001) 1055-1070.

[25] R. Komanduri, B.F. Von Turkovich, New observations on the mechanism of chip formation when machining titanium alloys, Wear, 69 (1981) 179-188.

[26] A. Vyas, M.C. Shaw, Mechanics of Saw-Tooth Chip Formation in Metal Cutting, Journal of Manufacturing Science and Engineering, 121 (1999) 163-172.

[27] C. Friedrich, V. Kulkarni, Effect of workpiece springback on micromilling forces, Microsystem technologies, 10 (2004) 472-477.

[28] M.C. Shaw, Metal cutting principles, 2nd ed., Oxford University Press, Oxford, 2005.

[29] N. Narutaki, A. Murakoshi, S. Motonishi, H. Takeyama, Study on Machining of Titanium Alloys, CIRP Annals, 32 (1983) 65-69.

[30] M. Kikuchi, The use of cutting temperature to evaluate the machinability of titanium alloys, Acta Biomaterialia, 5 (2009) 770-775.

[31] S. Jaffery, P. Mativenga, Assessment of the machinability of Ti-6Al-4V alloy using the wear map approach, The International Journal of Advanced Manufacturing Technology, 40 (2009) 687-696.

[32] F.C. Campbell Jr, Manufacturing technology for aerospace structural materials, Elsevier, 2011.

[33] R. M'Saoubi, D. Axinte, S.L. Soo, C. Nobel, H. Attia, G. Kappmeyer, S. Engin, W.-M. Sim, High performance cutting of advanced aerospace alloys and composite materials, CIRP Annals, 64 (2015) 557-580.

[34] T. Kitagawa, A. Kubo, K. Maekawa, Temperature and wear of cutting tools in high-speed machining of Inconel 718 and Ti・6Al・6V・2Sn, Wear, 202 (1997) 142-148.

[35] S. Palanisamy, S.D. McDonald, M.S. Dargusch, Effects of coolant pressure on chip formation while turning Ti6Al4V alloy, International Journal of Machine Tools and Manufacture, 49 (2009) 739-743.

[36] E.O. Ezugwu, J. Bonney, Effect of high-pressure coolant supply when machining nickel-base, Inconel 718, alloy with coated carbide tools, Journal of Materials Processing Technology, 153-154 (2004) 1045-1050.

[37] F. Klocke, H. Sangermann, A. Krämer, D. Lung, Influence of a High-Pressure Lubricoolant Supply on Thermo-Mechanical Tool Load and Tool Wear Behaviour in the Turning of Aerospace Materials, Proceedings of the Institution of Mechanical Engineers, Part B: Journal of Engineering Manufacture, 225 (2011) 52-61.

[38] A.R.C. Sharman, J.I. Hughes, K. Ridgway, Surface integrity and tool life when turning Inconel 718 using ultra-high pressure and flood coolant systems, Proceedings of the Institution of Mechanical Engineers, Part B: Journal of Engineering Manufacture, 222 (2008) 653-664.

[39] F. Klocke, G. Eisenblätter, Dry Cutting, CIRP Annals, 46 (1997) 519-526.

[40] J.C.J. Bart, E. Gucciardi, S. Cavallaro, Environmental life-cycle assessment (LCA) of lubricants, in, Woodhead Publishing Ltd, Cambridge, 2013, pp. 527-564.

[41] M.B. Peterson, S.F. Murray, J.J. Florek, Consideration of Lubricants for Temperatures above 1000 F, A S L E Transactions, 2 (1959) 225-234.

[42] S.Y. Hong, Y. Ding, Cooling approaches and cutting temperatures in cryogenic machining of Ti-6Al-4V, International Journal of Machine Tools and Manufacture, 41 (2001) 1417-1437.

[43] S.Y. Hong, I. Markus, W.-c. Jeong, New cooling approach and tool life improvement in cryogenic machining of titanium alloy Ti-6Al-4V, International Journal of Machine Tools and Manufacture, 41 (2001) 2245-2260.

[44] A.K. Nandy, M.C. Gowrishankar, S. Paul, Some studies on high-pressure cooling in turning of Ti–6Al–4V, International Journal of Machine Tools and Manufacture, 49 (2009) 182-198.

[45] F. Klocke, L. Settineri, D. Lung, P. Claudio Priarone, M. Arft, High performance cutting of gamma titanium aluminides: Influence of lubricoolant strategy on tool wear and surface integrity, Wear, 302 (2013) 1136-1144.

[46] F. Klocke, A. Krämer, H. Sangermann, D. Lung, Thermo-Mechanical Tool Load during High Performance Cutting of Hard-to-Cut Materials, Procedia CIRP, 1 (2012) 295-300.

[47] M.J. Bermingham, S. Palanisamy, D. Kent, M.S. Dargusch, A comparison of cryogenic and high pressure emulsion cooling technologies on tool life and chip morphology in Ti–6Al–4V cutting, Journal of Materials Processing Technology, 212 (2012) 752-765.

[48] G.S. Goindi, P. Sarkar, Dry machining: A step towards sustainable machining – Challenges and future directions, Journal of Cleaner Production, 165 (2017) 1557-1571.

[49] K. Weinert, I. Inasaki, J.W. Sutherland, T. Wakabayashi, Dry Machining and Minimum Quantity Lubrication, CIRP Annals, 53 (2004) 511-537.

[50] C.H. Xu, Y.M. Feng, R.B. Zhang, S.K. Zhao, X. Xiao, G.T. Yu, Wear behavior of Al2O3/Ti(C,N)/SiC new ceramic tool material when machining tool steel and cast iron, Journal of Materials Processing Technology, 209 (2009) 4633-4637.

[51] F. Klocke, S. Gierlings, M. Brockmann, D. Veselovac, Influence of Temperature on Surface Integrity for Typical Machining Processes in Aero Engine Manufacture, Procedia Engineering, 19 (2011) 203-208.

[52] V.P. Astakhov, Effects of the cutting feed, depth of cut, and workpiece (bore) diameter on the tool wear rate, The International Journal of Advanced Manufacturing Technology, 34 (2007) 631-640.

[53] C.H.R.V. Kumar, B. Ramamoorthy, Performance of coated tools during hard turning under minimum fluid application, Journal of Materials Processing Technology, 185 (2007) 210-216.

[54] A. Inspektor, P.A. Salvador, Architecture of PVD coatings for metalcutting applications: A review, Surface and Coatings Technology, 257 (2014) 138-153.

[55] K. Bobzin, High-performance coatings for cutting tools, CIRP Journal of Manufacturing Science and Technology, 18 (2017) 1-9.

[56] G.J. Wolfe, C.J. Petrosky, D.T. Quinto, The role of hard coatings in carbide milling tools, Journal of Vacuum Science & Technology A: Vacuum, Surfaces, and Films, 4 (1986) 2747-2754.

[57] P. Ettmayer, H. Kolaska, H.M. Ortner, 1.01 - History of Hardmetals, in: V.K. Sarin (Ed.) Comprehensive Hard Materials, Elsevier, Oxford, 2014, pp. 3-27.

[58] B. Breidenstein, B. Denkena, Significance of residual stress in PVD-coated carbide cutting tools, CIRP Annals, 62 (2013) 67-70.

[59] T. Leyendecker, O. Lemmer, S. Esser, J. Ebberink, The development of the PVD coating TiAlN as a commercial coating for cutting tools, Surface and Coatings Technology, 48 (1991) 175-178.

[60] A. Kimura, H. Hasegawa, K. Yamada, T. Suzuki, Effects of Al content on hardness, lattice parameter and microstructure of Ti1−xAlxN films, Surface and Coatings Technology, 120-121 (1999) 438-441.

[61] M. Zhou, Y. Makino, M. Nose, K. Nogi, Phase transition and properties of Ti–Al–N thin films prepared by r.f.-plasma assisted magnetron sputtering, Thin Solid Films, 339 (1999) 203-208.

[62] I. Tsutomu, S. Hiroshi, Phase formation and characterization of hard coatings in the Ti·Al·N system prepared by the cathodic arc ion plating method, Thin Solid Films, 195 (1991) 99-110.

[63] P.H. Mayrhofer, A. Hörling, L. Karlsson, J. Sjölén, T. Larsson, C. Mitterer, L. Hultman, Self-organized nanostructures in the Ti–Al–N system, Applied Physics Letters, 83 (2003) 2049-2051.

[64] T.I. El-Wardany, E. Mohammed, M.A. Elbestawi, Cutting temperature of ceramic tools in high speed machining of difficult-to-cut materials, International Journal of Machine Tools and Manufacture, 36 (1996) 611-634.

[65] M. Arndt, T. Kacsich, Performance of new AlTiN coatings in dry and high speed cutting, Surface and Coatings Technology, 163-164 (2003) 674-680.

[66] C.M. A. Inspektor, M. Rowe, M. Beblo, N. Waggle, Engineered Coatings for Machining Stainless Steel and High Temperature Alloys, in: 41st International Conference on Metallurgic Coatings and Thin Films, San Diego, USA, 2014.

[67] E. Le Bourhis, P. Goudeau, M.H. Staia, E. Carrasquero, E.S. Puchi-Cabrera, Mechanical properties of hard AlCrN-based coated substrates, Surface and Coatings Technology, 203 (2009) 2961-2968.

[68] H. Lind, R. Forsén, B. Alling, N. Ghafoor, F. Tasnádi, M.P. Johansson, I.A. Abrikosov, M. Odén, Improving thermal stability of hard coating films via a concept of multicomponent alloying, Applied Physics Letters, 99 (2011) 091903.

[69] H. Willmann, P.H. Mayrhofer, L. Hultman, C. Mitterer, Hardness evolution of Al–Cr–N coatings under thermal load, Journal of Materials Research, 23 (2011) 2880-2885.

[70] K. Yamamoto, S. Kujime, G. Fox-Rabinovich, Effect of alloying element (Si,Y) on properties of AIP deposited (Ti,Cr,Al)N coating, Surface and Coatings Technology, 203 (2008) 579-583.

[71] J.L. Endrino, V. Derflinger, The influence of alloying elements on the phase stability and mechanical properties of AlCrN coatings, Surface and Coatings Technology, 200 (2005) 988-992.

[72] T. Sato, T. Yamamoto, H. Hasegawa, T. Suzuki, Effects of boron contents on microstructures and microhardness in CrxAlyN films synthesized by cathodic arc method, Surface and Coatings Technology, 201 (2006) 1348-1351.

[73] R. Franz, J. Neidhardt, B. Sartory, R. Kaindl, R. Tessadri, P. Polcik, V.H. Derflinger, C. Mitterer, High-temperature low-friction properties of vanadium-alloyed AlCrN coatings, Tribology Letters, 23 (2006) 101-107.

[74] G. Gassner, P.H. Mayrhofer, K. Kutschej, C. Mitterer, M. Kathrein, A New Low Friction Concept for High Temperatures: Lubricious Oxide Formation on Sputtered VN Coatings, Tribology Letters, 17 (2004) 751-756.

[75] K.D. Bouzakis, E. Bouzakis, S. Kombogiannis, R. Paraskevopoulou, G. Skordaris, S. Makrimallakis, G. Katirtzoglou, M. Pappa, S. Gerardis, R. M'Saoubi, J.M. Andersson, Effect of silicon content on PVD film mechanical properties and cutting performance of coated cemented carbide inserts, Surface and Coatings Technology, 237 (2013) 379-389.

[76] W. Tillmann, S. Momeni, F. Hoffmann, A study of mechanical and tribological properties of self-lubricating TiAlVN coatings at elevated temperatures, Tribology International, 66 (2013) 324-329.

[77] M. Pfeiler, K. Kutschej, M. Penoy, C. Michotte, C. Mitterer, M. Kathrein, The effect of increasing V content on structure, mechanical and tribological properties of arc evaporated Ti–Al–V–N coatings, International Journal of Refractory Metals and Hard Materials, 27 (2009) 502-506.

[78] L.A. Donohue, I.J. Smith, W.D. Münz, I. Petrov, J.E. Greene, Microstructure and oxidation-resistance of Ti1 − x − y −zAlxCryYzN layers grown by combined steered-arc/unbalanced-magnetron-sputter deposition, Surface and Coatings Technology, 94-95 (1997) 226-231.

[79] P.B. Mirkarimi, K.F. McCarty, D.L. Medlin, Review of advances in cubic boron nitride film synthesis, Materials Science and Engineering: R: Reports, 21 (1997) 47-100.

[80] A. Tyagi, R.S. Walia, Q. Murtaza, S.M. Pandey, P.K. Tyagi, B. Bajaj, A critical review of diamond like carbon coating for wear resistance applications, International Journal of Refractory Metals and Hard Materials, 78 (2019) 107-122.

[81] K. Bewilogua, D. Hofmann, History of diamond-like carbon films — From first experiments to worldwide applications, Surface and Coatings Technology, 242 (2014) 214-225.

[82] A.A. Minevich, Wear of cemented carbide cutting inserts with multilayer Ti-based PVD coatings, Surface and Coatings Technology, 53 (1992) 161-170.

[83] H. Holleck, M. Lahres, P. Woll, Multilayer coatings—influence of fabrication parameters on constitution and properties, Surface and Coatings Technology, 41 (1990) 179-190.

[84] H. Holleck, H. Schulz, Preparation and behaviour of wear-resistant TiC/TiB2, TiN/TiB2 and TiC/TiN coatings with high amounts of phase boundaries, Surface and Coatings Technology, 36 (1988) 707-714.

[85] C. Ducros, F. Sanchette, Multilayered and nanolayered hard nitride thin films deposited by cathodic arc evaporation. Part 2: Mechanical properties and cutting performances, Surface and Coatings Technology, 201 (2006) 1045-1052.

[86] J.S. Koehler, Attempt to Design a Strong Solid, Physical Review B, 2 (1970) 547-551.

[87] M. Irie, H. Ohara, A. Nakayama, N. Kitagawa, T. Nomura, Deposition of Ni·TiN nano-composite films by cathodic arc ion-plating, Nuclear Instruments and Methods in Physics Research Section B: Beam Interactions with Materials and Atoms, 121 (1997) 133-136.

[88] J. Musil, P. Zeman, H. Hrubý, P.H. Mayrhofer, ZrN/Cu nanocomposite film—a novel superhard material, Surface and Coatings Technology, 120-121 (1999) 179-183.

[89] S.H. Yao, Y.L. Su, W.H. Kao, K.W. Cheng, C.T. Su, Performance of nanolayer CrN/Ag coated cutting tools, Surface Engineering, 27 (2011) 180-188.

[90] S. Veprek, P. Karvankova, M.G.J. Veprek-Heijman, Possible role of oxygen impurities in degradation of nc-TiN/a-Si3N4 nanocomposites, Journal of Vacuum Science & Technology B: Microelectronics and Nanometer Structures Processing, Measurement, and Phenomena, 23 (2005) L17-L21.

[91] T. Cselle, in: Werkzeug Technik, March 2003.

[92] M.M. T. Cselle, O. Coddet, in: Schweizer Präzisions-Fertigungstechnik, Carl Hanser Verlag, Munich, August 2005.

[93] EU Project MACHERENA, in, 6th Framework Programme, under contract no. AST 3-CT- 2003-502741.

[94] S. Vepřek, S. Reiprich, A concept for the design of novel superhard coatings, Thin Solid Films, 268 (1995) 64-71.

[95] S. Vepřek, New development in superhard coatings: the superhard nanocrystalline-amorphous composites, Thin Solid Films, 317 (1998) 449-454.

[96] O.C. T. Cselle, C. Galamand, P. Holubar, M. Jilek, J. Jilek, A. Luemkemann, M. Morstein, TripleCoatings–New Generation of PVD-Coatings for Cutting Tools, Journal of Machine Manufacturing, 49 (2009) 19-25.

[97] M. Jilek, T. Cselle, P. Holubar, M. Morstein, M.G.J. Veprek-Heijman, S. Veprek, Development of novel coating technology by vacuum arc with rotating cathodes for industrial production of nc-(Al1− x Ti x)N/a-Si3N4 superhard nanocomposite coatings for dry, hard machining, Plasma Chemistry and Plasma Processing, 24 (2004) 493-510.

[98] S. Anwar, A. Islam, S. Anwar, Mechanical studies of thermally annealed nc-W2N embedded a-Si3N4 nanocomposite films, Thin Solid Films, 636 (2017) 93-98.

[99] S. Anwar, A. Islam, S. Bajpai, S. Anwar, Structural and mechanical studies of W2N embedded Si3N4 nanocomposite hard coating prepared by reactive magnetron sputtering, Surface and Coatings Technology, 311 (2017) 268-273.

[100] P.E. Hovsepian, A.P. Ehiasarian, I. Petrov, TiAlCN/VCN nanolayer coatings suitable for machining of Al and Ti alloys deposited by combined high power impulse magnetron sputtering/unbalanced magnetron sputtering, Surface Engineering, 26 (2010) 610-614.

[101] P.E. Hovsepian, A.P. Ehiasarian, I. Petrov, Structure evolution and properties of TiAlCN/VCN coatings deposited by reactive HIPIMS, Surface and Coatings Technology, 257 (2014) 38-47.

[102] W. Tillmann, M. Dildrop, Influence of Si content on mechanical and tribological properties of TiAlSiN PVD coatings at elevated temperatures, Surface and Coatings Technology, 321 (2017) 448-454.

[103] S.K. Mishra, S. Ghosh, S. Aravindan, Characterization and machining performance of laser-textured chevron shaped tools coated with AlTiN and AlCrN coatings, Surface and Coatings Technology, 334 (2018) 344-356.

[104] S. Shoujin, B. Milan, P.T.M. John, Evolution of tool wear and its effect on cutting forces during dry machining of Ti-6Al-4V alloy, Proceedings of the Institution of Mechanical Engineers, Part B: Journal of Engineering Manufacture, 228 (2013) 191-202.

[105] Chetan, B.C. Behera, S. Ghosh, P.V. Rao, Wear behavior of PVD TiN coated carbide inserts during machining of Nimonic 90 and Ti6Al4V superalloys under dry and MQL conditions, Ceramics International, 42 (2016) 14873-14885.

[106] J.L. Cantero, M.M. Tardío, J.A. Canteli, M. Marcos, M.H. Miguélez, Dry drilling of alloy Ti–6Al–4V, International Journal of Machine Tools and Manufacture, 45 (2005) 1246-1255.

[107] G.S. Fox-Rabinovich, A.I. Kovalev, M.H. Aguirre, B.D. Beake, K. Yamamoto, S.C. Veldhuis, J.L. Endrino, D.L. Wainstein, A.Y. Rashkovskiy, Design and performance of AlTiN and TiAlCrN PVD coatings for machining of hard to cut materials, Surface and Coatings Technology, 204 (2009) 489-496.

[108] A. Biksa, K. Yamamoto, G. Dosbaeva, S.C. Veldhuis, G.S. Fox-Rabinovich, A. Elfizy, T. Wagg, L.S. Shuster, Wear behavior of adaptive nano-multilayered AlTiN/MexN PVD coatings during machining of aerospace alloys, Tribology International, 43 (2010) 1491-1499.

[109] M.S.I. Chowdhury, S. Chowdhury, K. Yamamoto, B.D. Beake, B. Bose, A. Elfizy, D. Cavelli, G. Dosbaeva, M. Aramesh, G.S. Fox-Rabinovich, S.C. Veldhuis, Wear behaviour of coated carbide tools during machining of Ti6Al4V aerospace alloy associated with strong built up edge formation, Surface and Coatings Technology, 313 (2017) 319-327.

[110] S. Sharif, E.A. Rahim, Performance of coated- and uncoated-carbide tools when drilling titanium alloy—Ti–6Al4V, Journal of Materials Processing Technology, 185 (2007) 72-76.

[111] A. Ugarte, R. M'Saoubi, A. Garay, P.J. Arrazola, Machining Behaviour of Ti-6Al-4V and Ti-5553 All0oys in Interrupted Cutting with PVD Coated Cemented carbide, Procedia CIRP, 1 (2012) 202-207.

[112] Z. Hongxia, Z. Jun, W. Fuzeng, Z. Jiabang, L. Anhai, Cutting forces and tool failure in high-speed milling of titanium alloy TC21 with coated carbide tools, Proceedings of the Institution of Mechanical Engineers, Part B: Journal of Engineering Manufacture, 229 (2014) 20-27.

[113] J. A. Ghani, C.H. Che Haron, S.H. Hamdan, A.Y. Md Said, S.H. Tomadi, Failure mode analysis of carbide cutting tools used for machining titanium alloy, Ceramics International, 39 (2013) 4449-4456.

[114] F. Nabhani, Wear mechanisms of ultra-hard cutting tools materials, Journal of Materials Processing Technology, 115 (2001) 402-412.

[115] Z. Liu, Q. An, J. Xu, M. Chen, S. Han, Wear performance of (nc-AlTiN)/(a-Si3N4) coating and (nc-AlCrN)/(a-Si3N4) coating in high-speed machining of titanium alloys under dry and minimum quantity lubrication (MQL) conditions, Wear, 305 (2013) 249-259.

[116] J. Musil, Hard and superhard nanocomposite coatings, Surface and Coatings Technology, 125 (2000) 322-330.

[117] S. Veprek, A.S. Argon, Towards the understanding of mechanical properties of super- and ultrahard nanocomposites, Journal of Vacuum Science & Technology B: Microelectronics and Nanometer Structures Processing, Measurement, and Phenomena, 20 (2002) 650-664.

[118] A.A. Voevodin, C. Muratore, S.M. Aouadi, Hard coatings with high temperature adaptive lubrication and contact thermal management: review, Surface and Coatings Technology, 257 (2014) 247-265.

[119] A. Erdemir, A crystal-chemical approach to lubrication by solid oxides, Tribology Letters, 8 (2000) 97.

[120] K. Kutschej, P.H. Mayrhofer, M. Kathrein, P. Polcik, C. Mitterer, A new low-friction concept for Ti1−xAlxN based coatings in high-temperature applications, Surface and Coatings Technology, 188-189 (2004) 358-363.

[121] R. Franz, C. Mitterer, Vanadium containing self-adaptive low-friction hard coatings for high-temperature applications: A review, Surface and Coatings Technology, 228 (2013) 1-13.

[122] A. Erdemir, Solid lubricants and self-lubricating films, in: B. Bhushan (Ed.) Modern Tribology Handbook, CRC Press, 2001, pp. 787-825.

[123] M.R. Hilton, R. Bauer, P.D. Fleischauer, Tribological performance and deformation of sputter-deposited MoS2 solid lubricant films during sliding wear and indentation contact, Thin Solid Films, 188 (1990) 219-236.

[124] Y. Liu, A. Erdemir, E.I. Meletis, An investigation of the relationship between graphitization and frictional behavior of DLC coatings, Surface and Coatings Technology, 86-87 (1996) 564-568.

[125] K.J. Wahl, D.N. Dunn, I.L. Singer, Wear behavior of Pb–Mo–S solid lubricating coatings, Wear, 230 (1999) 175-183.

[126] J.J. Hu, J.E. Bultman, C. Muratore, B.S. Phillips, J.S. Zabinski, A.A. Voevodin, Tribological properties of pulsed laser deposited Mo–S–Te composite films at moderate high temperatures, Surface and Coatings Technology, 203 (2009) 2322-2327.

[127] M.A. Hamilton, L.A. Alvarez, N.A. Mauntler, N. Argibay, R. Colbert, D.L. Burris, C. Muratore, A.A. Voevodin, S.S. Perry, W.G. Sawyer, A Possible Link Between Macroscopic Wear and Temperature Dependent Friction Behaviors of MoS2 Coatings, Tribology Letters, 32 (2008) 91-98.

[128] F. Gustavsson, S. Jacobson, A. Cavaleiro, T. Polcar, Ultra-low friction W–S–N solid lubricant coating, Surface and Coatings Technology, 232 (2013) 541-548.

[129] A.A. Voevodin, J.S. Zabinski, Load-adaptive crystalline–amorphous nanocomposites, Journal of Materials Science, 33 (1998) 319-327.

[130] A.A. Voevodin, C. Rebholz, A. Matthews, Comparative Tribology Studies of Hard Ceramic and Composite Metal-DLC Coatings in Sliding Friction Conditions, Tribology Transactions, 38 (1995) 829-836.

[131] M. Stüber, H. Leiste, S. Ulrich, H. Holleck, D. Schild, Microstructure and properties of low friction TiC·C nanocomposite coatings deposited by magnetron sputtering, Surface and Coatings Technology, 150 (2002) 218-226.

[132] G. Gassner, P.H. Mayrhofer, J. Patscheider, C. Mitterer, Thermal stability of nanocomposite CrC/a-C:H thin films, Thin Solid Films, 515 (2007) 5411-5417.

[133] H. Liu, A. Tanaka, K. Umeda, The tribological characteristics of diamond-like carbon films at elevated temperatures, Thin Solid Films, 346 (1999) 162-168.

[134] A. Erdemir, A crystal chemical approach to the formulation of self-lubricating nanocomposite coatings, Surface and Coatings Technology, 200 (2005) 1792-1796.

[135] K. Miyoshi, Solid lubricants and coatings for extreme environments: state-of-the-art survey, (2007).

[136] J.S. Zabinski, J.H. Sanders, J. Nainaparampil, S.V. Prasad, Lubrication using a microstructurally engineered oxide: performance and mechanisms, Tribology Letters, 8 (2000) 103-116.

[137] C. Muratore, A.A. Voevodin, Chameleon Coatings: Adaptive Surfaces to Reduce Friction and Wear in Extreme Environments, Annual Review of Materials Research, 39 (2009) 297-324.

[138] A.A. Voevodin, J.S. Zabinski, Supertough wear-resistant coatings with 'chameleon' surface adaptation, Thin Solid Films, 370 (2000) 223-231.

[139] S.M. Aouadi, H. Gao, A. Martini, T.W. Scharf, C. Muratore, Lubricious oxide coatings for extreme temperature applications: A review, Surface and Coatings Technology, 257 (2014) 266-277.

[140] A. Magneli, Structures of the ReO3-type with recurrent dislocations of atoms: `homologous series' of molybdenum and tungsten oxides, Acta Crystallographica, 6 (1953) 495-500.

[141] N. Fateh, G.A. Fontalvo, C. Mitterer, Tribological Properties of Reactive Magnetron Sputtered V2O5 and VN–V2O5 Coatings, Tribology Letters, 30 (2008) 21-26.

[142] J.S. Zabinski, M.S. Donley, V.J. Dyhouse, N.T. McDevitt, Chemical and tribological characterization of PbO·MoS2 films grown by pulsed laser deposition, Thin Solid Films, 214 (1992) 156-163.

[143] W. Gulbiński, T. Suszko, Thin films of Mo2N/Ag nanocomposite—the structure, mechanical and tribological properties, Surface and Coatings Technology, 201 (2006) 1469-1476.

[144] C. Muratore, A.A. Voevodin, Molybdenum disulfide as a lubricant and catalyst in adaptive nanocomposite coatings, Surface and Coatings Technology, 201 (2006) 4125-4130.

[145] F.P. Bowden, F.P. Bowden, D. Tabor, The friction and lubrication of solids, Oxford university press, 2001.

[146] H.E. Sliney, The Use of Silver in Self-Lubricating Coatings for Extreme Temperatures, A S L E Transactions, 29 (1986) 370-376.

[147] A.A. Voevodin, J.J. Hu, J.G. Jones, T.A. Fitz, J.S. Zabinski, Growth and structural characterization of yttria-stabilized zirconia–gold nanocomposite films with improved toughness, Thin Solid Films, 401 (2001) 187-195.

[148] A.A. Voevodin, J.J. Hu, T.A. Fitz, J.S. Zabinski, Tribological properties of adaptive nanocomposite coatings made of yttria stabilized zirconia and gold, Surface and Coatings Technology, 146-147 (2001) 351-356.

[149] J.J. Hu, C. Muratore, A.A. Voevodin, Silver diffusion and high-temperature lubrication mechanisms of YSZ–Ag–Mo based nanocomposite coatings, Composites Science and Technology, 67 (2007) 336-347.

[150] C. Muratore, A.A. Voevodin, J.J. Hu, J.S. Zabinski, Tribology of adaptive nanocomposite yttria-stabilized zirconia coatings containing silver and molybdenum from 25 to 700°C, Wear, 261 (2006) 797-805.

[151] S. Calderon Velasco, A. Cavaleiro, S. Carvalho, Functional properties of ceramic-Ag nanocomposite coatings produced by magnetron sputtering, Progress in Materials Science, 84 (2016) 158-191.

[152] G. Skordaris, K.D. Bouzakis, T. Kotsanis, P. Charalampous, E. Bouzakis, B. Breidenstein, B. Bergmann, B. Denkena, Effect of PVD film's residual stresses on their mechanical properties, brittleness, adhesion and cutting performance of coated tools, CIRP Journal of Manufacturing Science and Technology, 18 (2017) 145-151.

[153] V. Teixeira, Mechanical integrity in PVD coatings due to the presence of residual stresses, Thin Solid Films, 392 (2001) 276-281.

[154] G. Abadias, Stress and preferred orientation in nitride-based PVD coatings, Surface and Coatings Technology, 202 (2008) 2223-2235.

[155] F.M. D'Heurle, Aluminum films deposited by rf sputtering, Metallurgical and Materials Transactions B, 1 (1970) 725-732.

[156] P.A. Papi, C.P. Mulligan, D. Gall, CrN–Ag nanocomposite coatings: Control of lubricant transport by diffusion barriers, Thin Solid Films, 524 (2012) 211-217.

[157] C. Wang, X. Yu, M. Hua, Microstructure and mechanical properties of Ag-containing diamond-like carbon films in mid-frequency dual-magnetron sputtering, Applied Surface Science, 256 (2009) 1431-1435.

[158] Y. Wu, J. Chen, H. Li, L. Ji, Y. Ye, H. Zhou, Preparation and properties of Ag/DLC nanocomposite films fabricated by unbalanced magnetron sputtering, Applied Surface Science, 284 (2013) 165-170.

[159] P. Basnyat, B. Luster, Z. Kertzman, S. Stadler, P. Kohli, S. Aouadi, J. Xu, S.R. Mishra, O.L. Eryilmaz, A. Erdemir, Mechanical and tribological properties of CrAlN-Ag self-lubricating films, Surface and Coatings Technology, 202 (2007) 1011-1016.

[160] S.M. Aouadi, A. Bohnhoff, T. Amriou, M. Williams, J.N. Hilfiker, N. Singh, J.A. Woollam, Vacuum ultra-violet spectroscopic ellipsometry study of single- and multi-phase nitride protective films, Journal of Physics: Condensed Matter, 18 (2006) S1691-S1701.

[161] C.P. Mulligan, T.A. Blanchet, D. Gall, CrN–Ag nanocomposite coatings: Effect of growth temperature on the microstructure, Surface and Coatings Technology, 203 (2008) 584-587.

[162] C.C. Tseng, J.H. Hsieh, W. Wu, S.Y. Chang, C.L. Chang, Emergence of Ag particles and their effects on the mechanical properties of TaN–Ag nanocomposite thin films, Surface and Coatings Technology, 201 (2007) 9565-9570.

[163] H. Köstenbauer, G.A. Fontalvo, C. Mitterer, J. Keckes, Tribological Properties of TiN/Ag Nanocomposite Coatings, Tribology Letters, 30 (2008) 53-60.

[164] C.P. Mulligan, T.A. Blanchet, D. Gall, CrN–Ag nanocomposite coatings: High-temperature tribological response, Wear, 269 (2010) 125-131.

[165] S.M. Aouadi, D.P. Singh, D.S. Stone, K. Polychronopoulou, F. Nahif, C. Rebholz, C. Muratore, A.A. Voevodin, Adaptive VN/Ag nanocomposite coatings with lubricious behavior from 25 to 1000°C, Acta Materialia, 58 (2010) 5326-5331.

[166] C.P. Mulligan, D. Gall, CrN–Ag self-lubricating hard coatings, Surface and Coatings Technology, 200 (2005) 1495-1500.

[167] D.S. Stone, S. Harbin, H. Mohseni, J.E. Mogonye, T.W. Scharf, C. Muratore, A.A. Voevodin, A. Martini, S.M. Aouadi, Lubricious silver tantalate films for extreme temperature applications, Surface and Coatings Technology, 217 (2013) 140-146.

[168] C. Muratore, J.J. Hu, A.A. Voevodin, Adaptive nanocomposite coatings with a titanium nitride diffusion barrier mask for high-temperature tribological applications, Thin Solid Films, 515 (2007) 3638-3643.

[169] C. Muratore, A.A. Voevodin, J.J. Hu, J.S. Zabinski, Multilayered YSZ–Ag–Mo/TiN adaptive tribological nanocomposite coatings, Tribology Letters, 24 (2006) 201-206.

[170] S.M. Aouadi, Y. Paudel, B. Luster, S. Stadler, P. Kohli, C. Muratore, C. Hager, A.A. Voevodin, Adaptive Mo2N/MoS2/Ag Tribological Nanocomposite Coatings for Aerospace Applications, Tribology Letters, 29 (2008) 95-103.

[171] S.M. Aouadi, Y. Paudel, W.J. Simonson, Q. Ge, P. Kohli, C. Muratore, A.A. Voevodin, Tribological investigation of adaptive Mo2N/MoS2/Ag coatings with high sulfur content, Surface and Coatings Technology, 203 (2009) 1304-1309.

[172] J. Xiong, M.Z. Ghori, B. Henkel, T. Strunskus, U. Schürmann, M. Deng, L. Kienle, F. Faupel, Tuning silver ion release properties in reactively sputtered Ag/TiOx nanocomposites, Applied Physics A, 123 (2017) 470.

[173] K. Jun, Y. Shimogaki, Development of TiSiN CVD process using TiCl4/SiH4/NH3 chemistry for ULSI anti-oxidation barrier applications, Science and Technology of Advanced Materials, 5 (2004) 549-554.

[174] M. Diserens, J. Patscheider, F. Lévy, Mechanical properties and oxidation resistance of nanocomposite TiN–SiNx physical-vapor-deposited thin films, Surface and Coatings Technology, 120-121 (1999) 158-165.

[175] J.B. Choi, K. Cho, M.-H. Lee, K.H. Kim, Effects of Si content and free Si on oxidation behavior of Ti–Si–N coating layers, Thin Solid Films, 447-448 (2004) 365-370.

[176] M. Nose, Y. Deguchi, T. Mae, E. Honbo, T. Nagae, K. Nogi, Influence of sputtering conditions on the structure and properties of Ti–Si–N thin films prepared by r.f.-reactive sputtering, Surface and Coatings Technology, 174-175 (2003) 261-265.

[177] Y. Zhang, Y. Yang, Y. Zhai, P. Zhang, Effect of negative substrate bias on the microstructure and mechanical properties of Ti–Si–N films deposited by a hybrid filtered cathodic arc and ion beam sputtering technique, Applied Surface Science, 258 (2012) 6897-6901.

[178] J.C. Oliveira, F. Fernandes, F. Ferreira, A. Cavaleiro, Tailoring the nanostructure of Ti–Si–N thin films by HiPIMS in deep oscillation magnetron sputtering (DOMS) mode, Surface and Coatings Technology, 264 (2015) 140-149.

[179] V. Kouznetsov, K. Macák, J.M. Schneider, U. Helmersson, I. Petrov, A novel pulsed magnetron sputter technique utilizing very high target power densities, Surface and Coatings Technology, 122 (1999) 290-293.

[180] D. Lundin, K. Sarakinos, An introduction to thin film processing using high-power impulse magnetron sputtering, Journal of Materials Research, 27 (2012) 780-792.

[181] J.A. Hopwood, The role of ionized physical vapor deposition in integrated circuit fabrication, in: J.A. Hopwood (Ed.) Thin Films, Elsevier, 2000, pp. 1-7.

CHAPTER III – Sample deposition and characterization techniques

The importance of Ag content for optimizing the machining performance of Ti-Si-(Ag)-N coatings

3 Introduction

This chapter deals with the deposition of the Ti-Si-(Ag)-N films, the type of substrates used on the deposition for different types of characterizations and subsequent characterization techniques used to assess and analyse all the characteristics and parameters deemed relevant for this thesis. All the coatings, including the ones deposited on the cutting inserts, were done by HiPIMS working in Deep Oscillation Magnetron Sputtering (DOMS). This technique uses oscillations in the pulses to basically just reduce arcing during the depositions. The characterization techniques used range from Scanning Electron Microscopy (SEM) to Energy-dispersive spectroscopy (EDS) to X-Ray Diffraction (XRD) to Thermogravimetric Analysis (TGA) and nanonindentation for hardness measurements.

3.1 Deposition of Ti-Si-(Ag)-N coatings

TiSiN coatings alloyed with silver were deposited in a Hartec chamber in reactive mode using an high power impulse magnetron sputtering - HiPIMS power supply (HiPIMS Cyprium™ III plasma generator, Zpulser Inc.) working in deep oscillation magnetron mode - DOMS. The chamber has two cathodes forming an angle of 90° as shown in Figure III-1a. One high purity Cr target (used to produce the interlayer), was placed in cathode 2. In cathode 1, one high purity Ti target (99.9%) was allocated, containing 20 holes of 10 mm diameter evenly distributed along the preferential erosion zone and 20 holes of 2 mm diameter at similar positions but slightly deviated for the boundaries of the race track (see Figure III-1b).
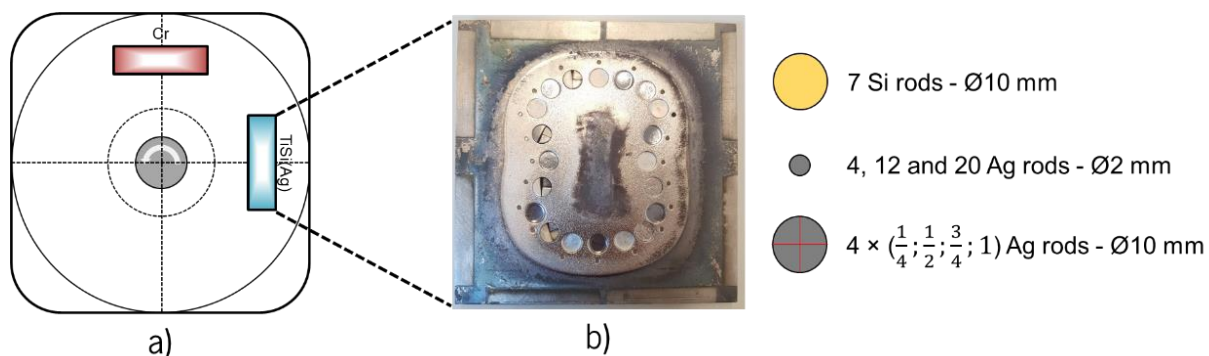
Figure III-1 Schematic configuration and representation of the a) deposition chamber and b) target and respective pellets used

This Ti target architecture allows to easily tune the chemical composition of the films by filling/changing the holes with rods of the different elements. The targets dimensions were 150×150×8 mm. Seven 10 mm holes were filled with Si (99.9%) cylindrical rods and the remaining holes with Ti (99.9%) or Ag (99.9%)

cylindrical rods. To achieve a progressive increase of Ag content on the TiSiN films, the 2 mm empty holes were progressively filled with Ag rods (4, 12 and 20) and, then, 4 of the 10 mm holes, initially containing Ti rods, were partially/totally filled with 1/4, 1/2, 3/4 and 4/4 of Ag rods (see Figure III-1b).

Different types of substrate were used depending on the type of characterization and will be detailed later. Nonetheless, independently of the type of substrate, prior to the depositions, all were ultrasonically cleaned in acetone and alcohol for 15 min each and then mounted on a rotating substrate holder that revolved at 23 rpm in relation to the centre axis of the chamber. Before the depositions, the chamber was evacuated down to a pressure of 1×10^{-4} Pa. The Ti target was then cleaned in Ar (discharge pressure - 0.3 Pa) for 10 min by applying an average peak power (P_a) of 1200 W, charging voltage (DC_{int}) of 340 V, pulse duration (D) of 1500 μs, while having the shutter in front to avoid cross contamination between the target and the substrate. Then, by moving the shutter to the front of the Cr target, the cleaning proceeded by applying 250 W at a DC power supply (Hüttinger PFG 7500 DC) at the same time that the substrates were etched with Argon ions by establishing the discharge close to the substrate holder (discharge pressure – 0.3 Pa) using roughly 490 V and 250 kHz in a DC-pulsed power supply (Pinnacle Plus, Advanced Energy), for 50 min.
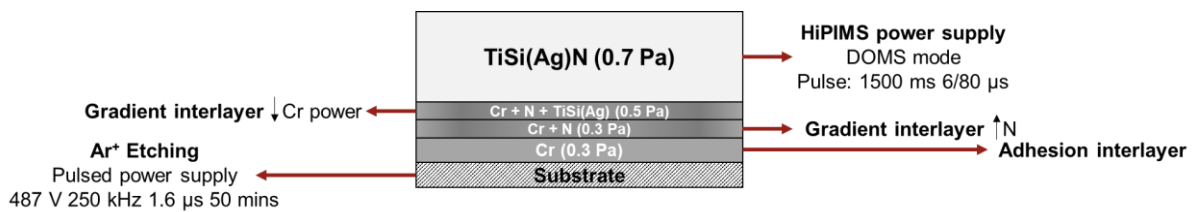
Figure III-2 Schematic representation of the different layers used for the deposition of Ti-Si-(Ag)-N coatings

As for the deposition itself, a series of interlayers with the purpose of increasing adhesion to the substrate were deposited before the final Ti-Si-(Ag)-N layer. A schematic representation of this series of layers is shown on Figure III-2. The sequence of interlayers were produced with a negative bias applied to the substrates of 60 V and follows, sequentially: i) Cr layer produced with 1200 W to the Cr target for 5 min (deposition pressure - 0.3 Pa); ii) gradient layer, keeping the same power, with increasing N content each minute until the final deposition partial pressure of 0.5 Pa, during 5 min; iii) gradient layer by turning on the HiPIMS power supply and progressively decrease the power applied to the Cr target by 200 W each min for 5 min, until switching off. The total thickness of the interlayer was close to 700 nm. The final TiSi(Ag)N layers were then conducted in reactive mode, using N_2/Ar partial pressure ratios of 1/4 (total pressure of 0.7 Pa). The following parameters were kept constant during the depositions: average peak power at the target of 1200 W, charging voltage of 340 V established at the capacitors, constant on time

(t_{on}) of 6 µs, an oscillation period (T) of 80 µs and a pulse duration of 1500 µs. To allow keeping these parameters constant, the pulse frequency (F) was automatically adjusted by the DOMS power supply software. The power supply operating parameters were the same used by Oliveira et al. [1] in a previous work, which allowed the production of TiSiN coatings with nanocomposite structure. In all the cases the deposition time was set for 180 min. For comparison purposes, a TiSiN film was deposited using the same deposition DOMS parameters. The denomination of the coatings was given accordingly to the at.% of silver present in the coatings as in TiSiNAgx; where x represents the Ag concentration. Table III-1 summarizes the deposition conditions used to deposit the Ti-Si-(Ag)-N coatings.

Table III-1 Main deposition parameters of the Ti-Si-(Ag)-N coatings

COATING	NO OF AG PELLETS	THICKNESS [µM] (FILM ONLY)	DEPOSITION RATE [NM/MIN]	HIPIMS PARAMETERS			
				V_P [V]	I_P [A]	P_P [KW]	F_t [HZ]
TiSiN	0	2.2	12.1	1145	44.1	50.5	252
TiSiNAg1	4 (Ø 2mm)	2.3	12.9	1153	41.3	47.6	249
TiSiNAg2	12 (Ø 2mm)	2.4	13.1	1153	38.5	44.4	250
TiSiNAg3	20 (Ø 2mm)	2.8	15.3	1153	41.3	47.6	251
TiSiNAg6	4 × ¼ (Ø 10mm)	2.3	12.8	1130	51.6	58.3	259
TiSiNAg10	4 × ½ (Ø 10mm)	2.3	12.9	1132	51.4	58.2	258
TiSiNAg17	4 × ¾ (Ø 10mm)	2.8	15.6	1148	47.8	54.9	253
TiSiNAg29	4	4.6	25.7	1145	46.5	53.3	251

The substrates used for the deposition can be summarized as function of final characterization:

- **(111) silicon wafers** for chemical, cross-section and surface morphology analysis;
- **FeCrAlY alloy** (20×20×1 mm; 72,8% Fe, 22% Cr, 5% Al, 0,1% Y, 0,1% Zr, in wt. %) for structural analysis and used for the thermal annealing treatments (both protective and oxidized atmospheres) and for mechanical properties (mainly hardness and Young's modulus measurements);
- **Polished AISI 316** (⌀ 25×0.5 mm) for residual stresses calculations and evaluation;
- **Alumina - Al₂O₃** (20×20×1 mm) for thermal annealing tests and characterization;

- **Tungsten carbide discs - WC - 6% Co** (20 mm diameter), used for the tribological tests at room and high temperatures;
- **Tungsten carbide inserts** (further details in section 3.5) used for the turning tests of TiAl6V4 alloy in dry condition.

3.2 Sample characterization techniques

Multiple techniques were used for different characterizations of the coatings during this work, with some of the techniques being of recurrent use in practically every different area of characterization due to their flexibility, such as the scanning electron microscopy. The following sub-sections will detail the equipment's used, focusing mainly on the experimental procedure and relevant parameters used for the characterization.

3.2.1 Scanning electron microscopy and Energy-dispersive spectroscopy (SEM-EDS)

A high resolution FEG - Zeiss Merlin Gemini 2 scanning electron microscope, equipped with secondary electron detector and energy dispersive x-ray spectrometer was used to analyse the surface and cross-section morphologies of the coatings. This technique was quite transversal and enable to complete information regarding several functional properties. Therefore, all the images of surfaces and cross-sections presented throughout this thesis, be it as-deposited coatings, after treatment coatings, wear tracks or cutting edges of the tungsten carbide inserts, were acquired using this equipment. The energy-dispersive spectrometer was used for all the cases with 10 kV accelerating voltage to acquire chemical composition of the coatings and all the elemental line profiles and elemental maps presented for the thermal stability and tribology tests that allowed to assess the silver whereabouts. This accelerating voltage was used to assure that the energy was high enough to excite all the energy levels needed to have representation of all the elements in study while, also ensuring that the electron beam was not picking up any signal from the substrates.

3.2.2 X-Ray diffraction

X-Ray diffraction characterization was performed in a PANalytical X'Pert PRO MPD using Cu Kα radiation (1.540598 Å, 45 kV and 40 mA) to characterize the structure of the as-deposited, annealed and oxidized coatings. The diffractograms were either acquired in conventional and/or grazing modes to study the preferential orientation and phase composition of the films and to remove the contribution of the diffraction peaks from the substrate, respectively. The XRD diffraction peaks were fitted using a pseudo-

Voigt function to calculate both the full width at half maximum (FWHM) and the peak position (2θ) and the grain size of the films was then calculated using the Scherrer's equation [2]. The lattice parameter was obtained by applying Bragg's law followed by the geometrical relationship equation of lattice parameter with interplanar distance and the Miller indices.

As for the study of the effect of temperature on the structure of the TiSiNAg6 coating in Chapter V, a Philips X'Pert MPD in-situ high-temperature X-ray diffraction (XRD) equipment was used. The test was conducted in open air in a temperature range of 700 °C to 950 °C in steps of 50°C, using Co Kα radiation (1.789010 Å). All the diffractograms were acquired with Bragg-Brentano geometry. A holding time of 5 min for thermal stabilization was given at each selected temperature step followed by an acquisition time of 45 min.

3.2.3 Nanoindentation (Hardness) and residual stresses

The hardness and Young's modulus of the coatings before and after thermal annealing in protective atmosphere were assessed by depth-sensing indentation (Micro Materials NanoTest) using a Berkovich diamond pyramid indenter with an applied load of 30 mN.

The residual stresses level was calculated by measuring the deflection of the film-substrate prior and after deposition by using the Stoney's equation [3].

3.3 Thermal annealing and Thermogravimetric Analysis (TGA) tests

The thermal annealing in protective atmosphere was conducted in an oven in hydrogenated argon (Ar - balance + H$_2$ - 5 vol%) protective atmosphere. The substrates were placed in a cylindrical glass tube which was connected to a vacuum system with a base pressure of 3×10^{-2} Pa. Hydrogenated argon was then introduced in the tube (reaching a pressure of 0.1 Pa) to perform the annealing treatments. The specimens were exposed to a constant linear temperature ramp (from room temperature (RT) up to specified isothermal temperature of 800°C at a rate of 20 °C/min), maintained at such temperature for 2 h, and then cooled down until room temperature.

The oxidation resistance of the coatings was evaluated by thermogravimetric analysis (TGA) using industrial air (99.9% purity). To determine the onset point of oxidation of the coatings, the films deposited specific substrates were heated from room temperature up to 1200°C with a constant heating rate of 20°C/min. Then, based on that, the selected specimens were submitted to isothermal annealing tests

at different selected temperatures for 2 h with a heating rate of 20°C/min. An air flux of 50 ml/min was used on the experiments. Weight gain due to oxidation was continuously recorded during the tests by using a microbalance with an accuracy of 0.01 mg at regular intervals of 2 s.

3.4 Tribological tests

The tribological behaviour of the films was evaluated on a high temperature pin-on disc tribometer compatible for tribological tests up to 1000°C from DUCOM Instruments (PoD 4.0). The temperature control is done through furnace heating and K-type thermocouple. The data acquisition and control was done using Labview based WinDucom software. Two types of counterbodies were used on the experiments: Al_2O_3 and TiAl6V4 6 mm diameter balls. The tests with each ball were carried out in two locations at different DUCOM premises, Groningen in Netherlands and India, for Al_2O_3 and TiAl6V4 balls, respectively.

The tribology tests performed against Al_2O_3 balls were carried out at room temperature (RT) and 600°C under a normal load of 5 N, a constant linear speed of 0.1 ms^{-1} (variable rotation speeds depending on the wear track radius used to keep the linear speed constant), for 2500 cycles. Note that, in some specific cases, the test conditions remained the same but a lower number of cycles (1500) was used to try to keep the wear in measurable levels. Tribology tests against TiAl6V4 balls were done under the same testing conditions as for the alumina balls but a new testing temperature of 900°C was introduced to simulate temperatures closer to those generated on the contact of the machining tools [4].

The specific wear rate of the coatings was determined through the evaluation of the cross section area of the 2D profiles obtained in 4 different zones of the wear track, using a 2D profilometer. Archard's law [5] was then applied to calculate the specific wear rate.

3.5 Machining tests (turning operation)

For the machining tests, the Ti-Si-(Ag)-N coatings were deposited in two types of inserts, both provided by Palbit S.A, for two different kind of tests: a) tungsten carbide inserts with reference "CNMG 120408-SF" used for "laboratorial" tests in a conventional lathe and b) tungsten carbide inserts with reference "CCGT 09T304-LN" tested in a CNC machine from Palbit S.A., emulating a modern industrial environment. The shape/dimensions of the inserts as well as the chip breaker for both the inserts are shown in Figure III-3.
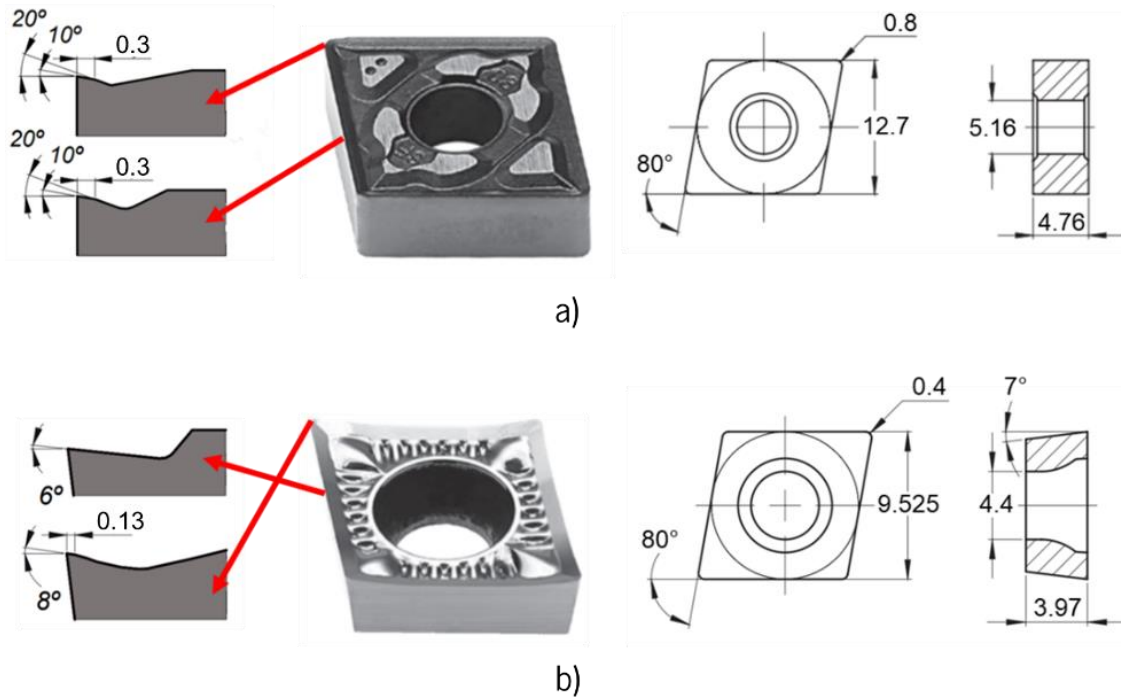
Figure III-3 Shape and dimensions of the inserts used for the machining tests: a) CNMG 120408-SF and b) CCGT 09T304 (all the dimensions in mm)

Table III-2 Chemical composition of the TiAl6V4 alloy

WT.%						
Al	**V**	**Fe**	**C**	**N**	**O**	**Ti**
6.24	3.98	0.17	0.023	0.003	0.181	Balance

As for the tests themselves, the machining operation selected was conventional orthogonal turning. A TiAl6V4 titanium alloy bar (Ø 85 x 540 mm) was used as workpiece for the tests. The chemical composition of the alloy is given in Table III-2. All the turning tests were conducted without any lubricant, i.e. in dry conditions. The laboratorial tests were conducted with the inserts with reference "CNMG 120408-SF" in a conventional mechanical lathe with a constant feed rate of 0.3 mm/rev and penetration depth of 0.2 mm using three different cutting speeds (70, 80 and 100 m/min). The flank wear on the inserts was mapped after, roughly, every 2 min of cutting. The tool life was estimated through the wear on the flank edge, according to the standard ISO 3685-1993 [6] for orthogonal turning tests, which considers a maximum flank wear of 0.3 mm as failure criterion. An example of how this flank wear is measured is shown on Figure III-4. As for the industrial tests, the cutting inserts with reference "CCGT 09T304-LN" were used and tested in a CNC machine at a higher cutting speed of 120 m/min, using a

feed rate of 0.15 mm/rev and a penetration depth of 0.2 mm. Similarly, the tool life was estimated considering a failure criterion of a maximum of 0.3 mm for the flank wear. For these tests and for benchmarking purposes, commercial AlTiN coated inserts, provided by Palbit S.A., were also tested. Table III-3 summarizes the cutting conditions used for the testing of both the types of inserts.

$V_{bmáx} = 0.3$ mm

500 µm
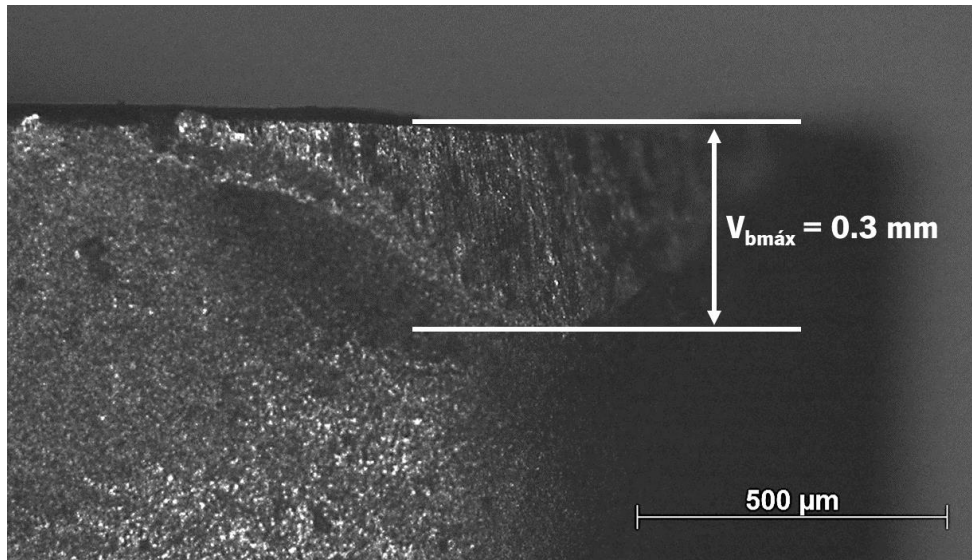
Figure III-4 Schematic representation of the flank wear measurement in the cutting inserts

Table III-3 Cutting conditions for the different types of inserts

INSERTS REFERENCE	CONDITION	CUTTING SPEED [M/MIN]	FEED RATE [MM/REV]	PENETRATION DEPTH [MM]
CNMG 120408-SF PH7910 (LABORATORIAL TESTS)	Dry	70 80 100	0.3	0.2
CCGT 09T304-LN PH0910 (INDUSTRIAL TESTS)	Dry	120	0.15	0.2

3.6 References

[1] J.C. Oliveira, F. Fernandes, F. Ferreira, A. Cavaleiro, Tailoring the nanostructure of Ti–Si–N thin films by HiPIMS in deep oscillation magnetron sputtering (DOMS) mode, Surface and Coatings Technology, 264 (2015) 140-149.

[2] P. Scherrer, Bestimmung der inneren Struktur und der Größe von Kolloidteilchen mittels Röntgenstrahlen, in: R. Zsigmondy (Ed.) Kolloidchemie Ein Lehrbuch, Springer Berlin Heidelberg, Berlin, Heidelberg, 1912, pp. 387-409.

[3] G.G. Stoney, The tension of metallic films deposited by electrolysis, Proc. R. Soc. Lond. A, 82 (1909) 172-175.

[4] T.I. El-Wardany, E. Mohammed, M.A. Elbestawi, Cutting temperature of ceramic tools in high speed machining of difficult-to-cut materials, International Journal of Machine Tools and Manufacture, 36 (1996) 611-634.

[5] J.F. Archard, Contact and Rubbing of Flat Surfaces, Journal of Applied Physics, 24 (1953) 981-988.

[6] I.O.f. Standardization, ISO 3685: Tool-life Testing with Single-point Turning Tools, ISO, 1993.

CHAPTER IV – Chemical and Structural Characterization of Ti-Si-(Ag)-N Coatings

The importance of Ag content for optimizing the machining performance of Ti-Si-(Ag)-N coatings

4 Introduction

Chapter II showed how the addition of silver to a ceramic matrix can open a multitude of new functional properties, since silver promote changes on the coating structure and phase composition. All, the possible changes on the chemical compositions, surface and cross-section morphologies and the structure of the coatings are key factors in understanding the functional characteristics of the films that will be target of discussion throughout the following chapters of this thesis.

This chapter in particular, deals with the chemical, morphological and structural characterization of the coatings deposited by HiPIMS with different silver contents and the influence of the deposition parameters on those characteristics. The coatings were initially analysed by its chemical composition by energy-dispersive spectroscopy (EDS) with further analysis conducted by scanning electron microscopy (SEM) and x-ray diffraction (XRD). As this was the first set of characterizations, all of the coatings deposited were analysed and discussed. In the future chapters, only specific coatings will be characterized as a selection of coatings is done throughout the work developed, based on the results found for the specific type of characterization in study, until only the most promising ones for the machining tests are left.

Just as shown on chapter III in section 3.1, the designation of the coatings given throughout this whole thesis, to facilitate sample identification, is done by associating the elements present on the coating system followed by the correspondent atomic percentage of silver present. For example, the TiSiNAg6 coating, means that this coating is the film possessing an amount of silver corresponding to 6 at.%. Consequently, this denomination will be used at all times to specify and identify the coating being referred to.

4.1 Results and discussion

4.1.1 Chemical and morphological analysis

The chemical composition and the Ti/Si ratio are shown in Table IV-1. Accurate composition of the nitrogen content in EDS analysis is not reliable due to the overlapping between the Ti Ll and N Kα X-ray lines, but it is possible for the titanium, silicon and silver since the main X-ray lines for these elements present no overlaps. The non-normalized accurate composition in wt.% for the Ti, Si and Ag were obtained through comparison of peaks with that of the standards (similar to the wavelength dispersive spectroscopy procedure). By normalizing these elements to atomic percentages and by assuming that, to keep the

stoichiometry ($TiN + Si_3N_4$), the $(Ti+Si)/N$ ratio should be slightly inferior to 1, it is possible to estimate the nitrogen content on the films.

Table IV-1 Elemental chemical composition of the coatings and ratio between the titanium and silicon

COATING	NUMBER OF AG PELLETS	AG (AT.%)	TI (AT.%)	SI (AT.%)	N (AT.%)	TI/SI
TiSiN	0	0.0	40.3	8.3	51.4	4.8
TiSiNAg1	4 (Ø 2mm)	0.7	39.7	8.5	51.1	4.7
TiSiNAg2	12 (Ø 2mm)	1.9	38.7	8.9	50.5	4.4
TiSiNAg3	20 (Ø 2mm)	3.2	36.1	10.6	50.2	3.4
TiSiNAg6	4 × ¼ (Ø 10mm)	6.1	36.7	8.8	48.4	4.2
TiSiNAg10	4 × ½ (Ø 10mm)	9.5	35.0	8.8	46.7	4.0
TiSiNAg17	4 × ¾ (Ø 10mm)	16.9	32.0	8.2	42.9	3.9
TiSiNAg29	4	29.2	26.6	7.5	36.7	3.5

As expected, increasing the number of Ag rods at the Ti target gives rise to coatings with progressively increasing Ag content. Although all films were produced using the same DOMS parameters, the Ti/Si ratio gradually decreases with the size and/or position of Ag rods incorporated in the target except for the TiSiNAg3 film that shows a slight increase in the Si content. This gradual decrease is easily explained by a combination of the increasingly smaller area of Ti on the target, due to the introduction of the silver pellets, with the consequent increasingly higher contents of silver being deposited. The replacement of Ti pellets by Ag pellets at the centre of the race track is accompanied by an increase of the peak power (P_P in Table III-1 of chapter III) which, as it will be shown later, directly influence the deposition rate, the structure and the morphology of the films. This increase of P_P is resulting mainly from an increase of the peak discharge current (I_P in Table III-1 of chapter III), which can be explained by the probable change on the electric properties of the target induced by this replacement of pellets.
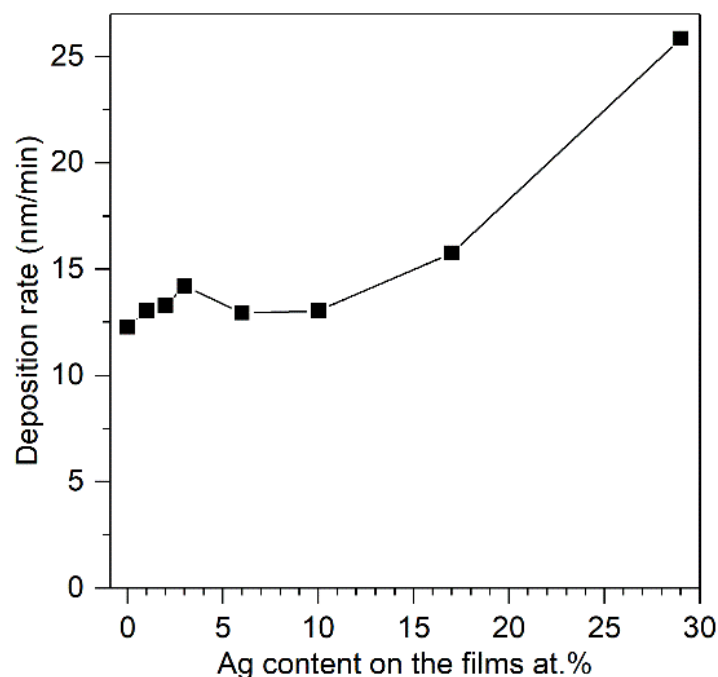
Figure IV-1 Deposition rate of the coatings as a function of Ag content

The deposition rate of the different coatings is shown in Figure IV-1. Reference TiSiN film displays the lowest deposition rate among all the films. Increasing the Ag content up to 3 at.% progressively increases the deposition rate of the films. Since the deposition pressure and the electric properties of the Ti target did not significantly change with the increasing of 2 mm Ag rods incorporated in the Ti target (see P_P values in Table III-1 of chapter III), this is an expected result since: i) additional material is being sputtered with the incorporation of the Ag rods and ii) deposition rate of Ag is several times higher than any element, or compounds with it formed (working in reactive compound mode has taken place), being sputtered. However, there is a sudden decrease of the deposition rate for the film with an Ag content of 6 at.%. It is well known that the deposition rate of films produced by HiPIMS depends, beyond the usual deposition parameters (discharge pressure, substrate bias and power applied to the target), mainly on the ionized fraction of the sputtered material [1]. The increase of this fraction, as observed by the increase of the peak current (I_P on Table III-1 of chapter III), led to the decrease of the deposition rate due to the increase of the metallic ion back-attraction to the target. Further increments on the area of Ag pellets in the target give rise to higher deposition rates reaching a maximum value of 26 nm/min for the coating with the highest Ag content, in good agreement with the higher sputtering yield of Ag. Moreover, for the two coatings with the highest Ag content a decrease of P_P was found which also can give a small contribution to the increase of the deposition rate.
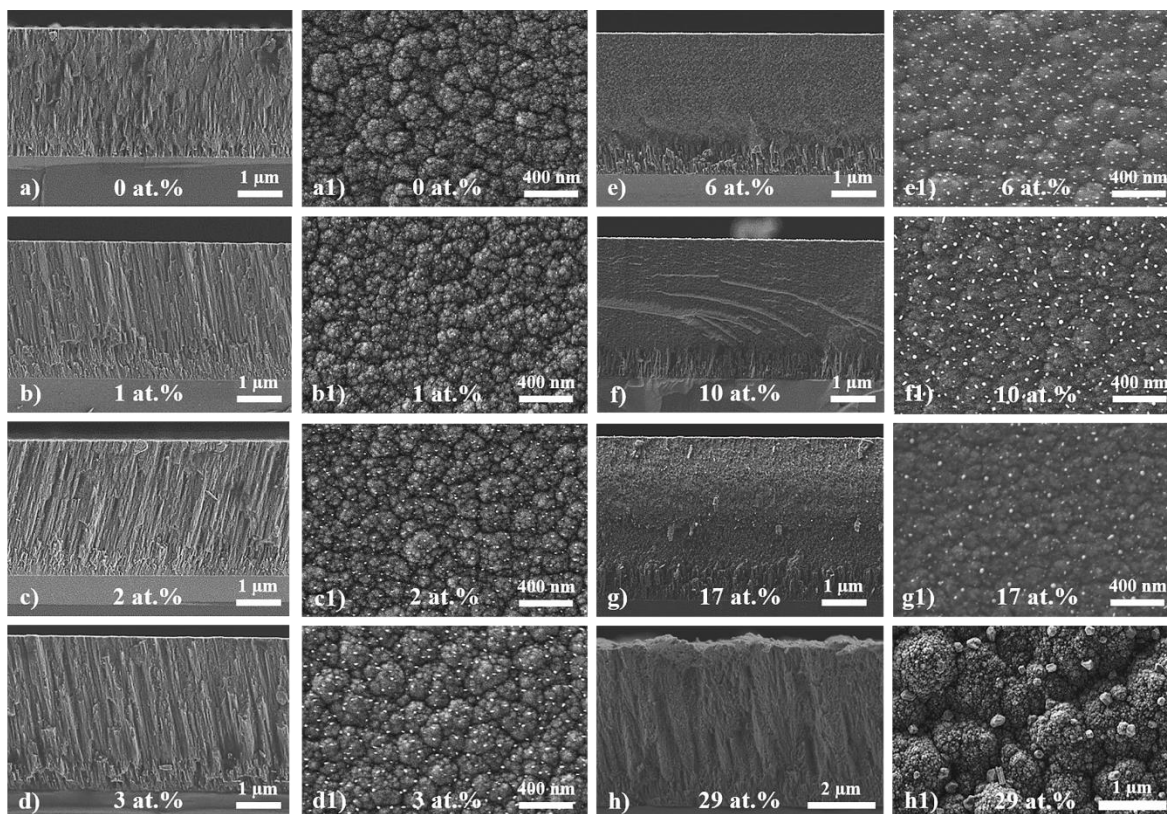
Figure IV-2 Cross-section and surface morphology micrographs of the TiSi(Ag)N coatings with: a) and a1) 0% at.% Ag; b) and b1) 1 at.% Ag; c) and c1) 2 at.% Ag; d) and d1) 3 at.% Ag; e) and e1) 6 at.% Ag; f) and f1) 10 at.% Ag; g) and g1) 17 at.% Ag; h) and h1) 29 at.% Ag

The cross section and surface morphology of the coatings are shown in Figure IV-2. Reference TiSiN coating displays a columnar although rather dense morphology (Figure IV-2a), with columns spanning from the substrate up to the top of the film. Surface morphology of this coating (Figure IV-2a1) display a cauliflower type aspect, where small grains combine to form larger structures of the size of the columns observed in cross section. No significant changes on both cross section and surface morphology occurred with low silver additions to the reference film (up to 3 at.% Ag), in good agreement with the electric properties of the target. Transition from columnar to a very compact morphology was observed when 6 at.% of Ag (Figure IV-2e) was added to the reference coating. This abrupt change might be explained by the increase of P_P which, primarily due to the increase of I_P (see I_P on Table III-1 of chapter III), boosts the fraction of ionized species reaching the growing film, promoting the surface mobility of the adatoms and fighting the shadowing effect due to the higher number of ions arriving perpendicularly to the growing film surface, consequently, raising a spontaneous compact morphology [2]. Additionally, the higher adatom mobility will induce an easier Ag nanoparticle formation enhancing the competitive growth between Ag and TiSiN (nc-TiN + a-SiN$_x$) phases, which may also contribute to this densification effect. Increasing the silver content on the films up to 17 at.% still promotes the formation of a compact morphology without

changing the surface morphology. However, for the coating with 29 at.% of silver (Figure IV-2h) a very columnar and porous morphology is established. This inversion on the morphology can be understood based on the combined effect of: i) slight decrease of P_P and ii) high concentration of Ag on the films giving rise to a much higher number of nucleation sites where the silver, due to its very high mobility, can segregate and coalesce into larger particles which, owing to their poor affinity with the other compounds, grows a porous spontaneous morphology. No significant changes on the surface morphologies of the films were observed, excepting for the coating with higher Ag content which displays a rough morphology, in good agreement with its cross section morphology. Small white clusters can be observed on the surface of Ag rich coatings. The size of these particles increase with the Ag concentration, corroborating the rise of Ag content on the films. Finally, in all the coatings an intermediate columnar layer, in-between the substrate and functional top coating, can be identified as the interlayer deposited to improve the adhesion of the coatings.

4.1.2 Structure analysis

The XRD diffraction patterns of the as-deposited coatings acquired in grazing mode and the conventional diffraction patterns of the TiSiN and TiSiNAg6 coatings are shown in Figure IV-3, respectively. Reference TiSiN coating displays well defined crystalline diffraction peaks assigned to a f.c.c NaCl type TiN phase (ICDD card n.º 01-087-0633). No peaks associated with crystalline Si-N phase are detected revealing its amorphous character. These results corroborate the findings of Oliveira et al. [2] and Fernandes et al. [3], where for such deposition parameters a nanocomposite film structure (nc-TiN surrounded by an amorphous SiN_x matrix) was formed, although small amounts of Si were still present in solid solution on the TiN lattice. All the TiN diffraction peaks are shifted toward lower angles from the reference card confirming the high level of compressive residual stresses (~4 GPa) measured on the film (see Figure IV-4). Diffraction peak located at ~43.4°, positioned in-between the Cr_2N and CrN phases suggests the formation of a middle compound between these phases. This signal is tentatively explained by the gradient Cr-N interlayer used to make the transition between the Cr interlayer and the final TiSiN film. In fact, XRD diffraction pattern acquired in grazing incident mode does not present such peak, supporting this statement. Peak positioned at ~44.4° corresponds to superimposing signal coming from the CrN_x interlayer and the FeCrAlY substrate. Again, XRD diffraction pattern obtained in grazing incidence mode supports this affirmation, although a very small peak is still observed. As it will be discussed later this peaks also overlap the (200) reflection of the Ag.
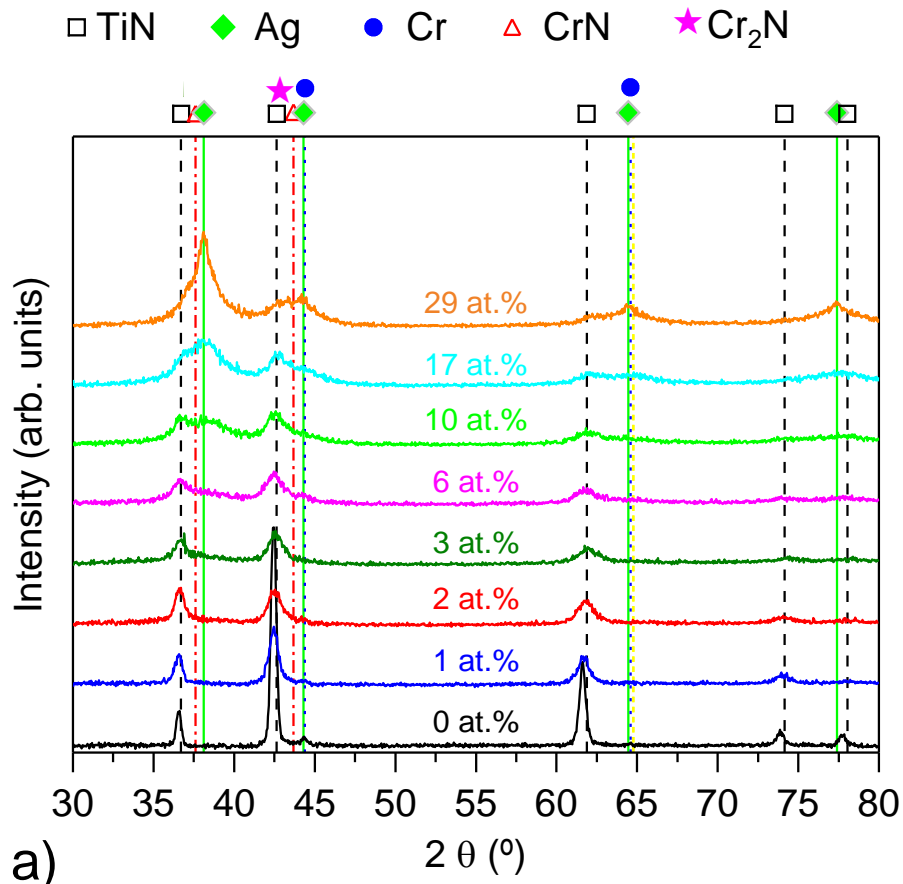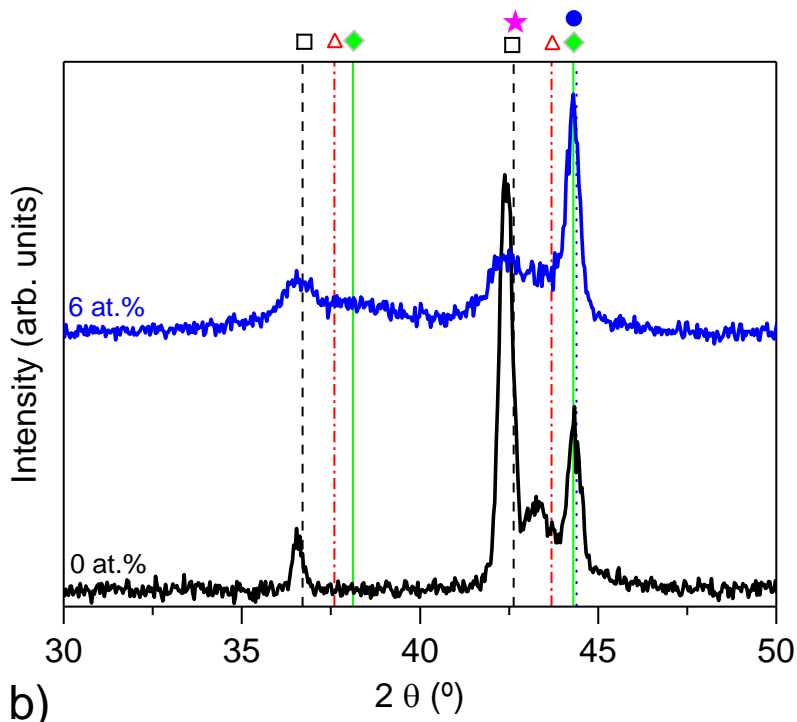
Figure IV-3 XRD diffraction patterns of the as-deposited films acquired in a) grazing mode and b) conventional XRD for reference TiSiN and TiSiNAg6 coatings

Using Scherrer's equation [4], the grain size of the reference film can be estimated to ~24 nm (see Figure IV-5b). The relative intensities of the TiN diffraction peaks show that the film has a (200) preferential orientation, as the intensity of the (111) peak from the ICDD card, is only 72.9% of the intensity of the (200), which represents 100%. Ehiasarian et al. [5] showed that the structure of TiN films deposited by HiPIMS is developed gradually by competitive growth of the grains which highly depends on the molecular-to-atomic nitrogen ratio in the discharge gas, the amount of ionized metal species and the ion-to-neutral flux ratio. The (200) preferential orientation of the films is typical of high energy bombarding conditions, high metal ion-to-metal neutral ratio and/or high N_2 dissociation rate [6].
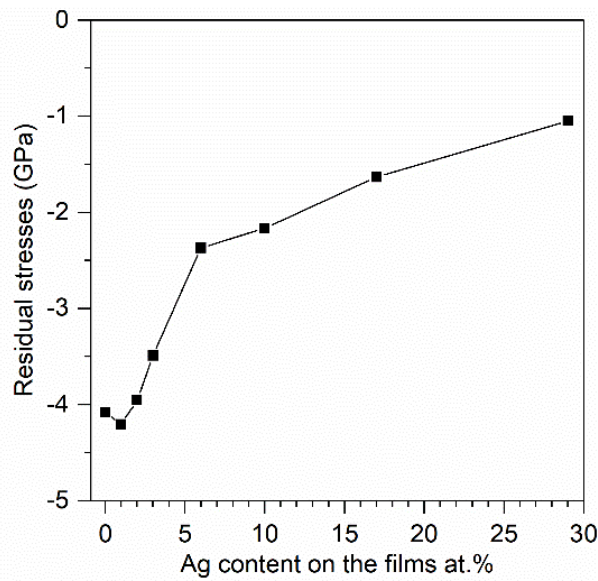
Figure IV-4 Residual stresses measured on the TiSiN(Ag) coatings as a function of the Ag concentration
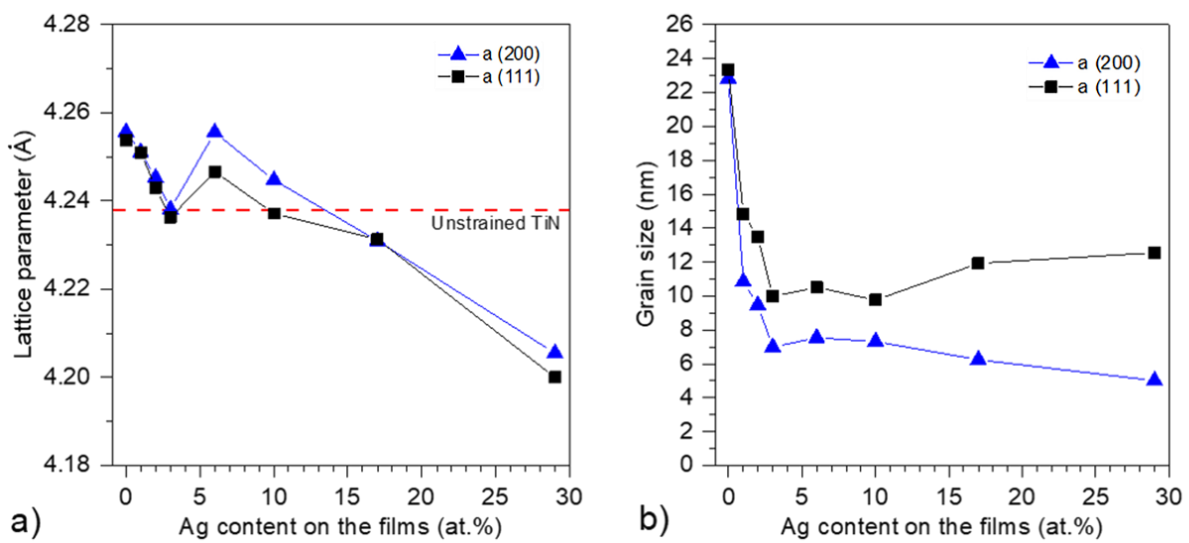
Figure IV-5 a) Lattice parameter and b) grain size of the as-deposited TiSiNAg films

The incorporation of Ag induces changes on the structure of TiSiN reference film, as it follows: i) it changes the preferential orientation (PO) of the films from (200) to (111), ii) it significantly broadens the TiN diffraction peaks, suggesting a lower degree of structural order and the formation of a nanocrystalline structure, iii) for low Ag content it abruptly decreases the grain size of TiN crystallites from 24 nm to 11-7 nm (depending on the crystal orientation) followed, for higher Ag contents, by small variations which suggests that the grain size is independent of the Ag content on the films (see Figure IV-5b) and, iv) it leads to the appearance of a broad diffraction peak (38°) assigned to Ag, which progressively increases of intensity with Ag addition in good agreement with the films chemical composition. The broadening of the TiN diffraction peaks, i.e. the decrease of grain size, with silver incorporation can be explained based on the competitive growth between Ag, TiN grains and the Si-N segregation. In fact, the addition of Ag increases the number of nucleation sites, inhibiting the TiN crystallites growth and thus producing a nanocomposite microstructure composed by these crystallites, a Si-N phase and Ag nanoparticles. This behaviour agrees well with the work of Dang et al. [7] which, although did not calculate and discuss the grain size evolution with increasing Ag additions to TiSiN films deposited by multi-arc ion plating, seems from their XRD diffraction patterns, to show a similar behaviour. It should be noted that Ag has no affinity to ceramic matrixes which, together with its very high mobility, will make it tendentiously grow as nanoparticles. This corroborates the presence of the white spots seen in on the top surface morphology of the films containing Ag (see Figure IV-2b$_1$ to h$_1$). In addition, the presence of Ag nanoclusters corroborates well with the work of several authors who evaluated the influence of Ag alloying on other coating systems [8-10].

The lattice parameter of films calculated from the TiN (111) and (200) diffraction peaks is shown in Figure IV-5a) as function of the Ag concentration. For comparison purposes, the lattice parameter of the unstrained TiN (ICDD card 01-087-0633) is also shown. TiSiN film displays a higher lattice parameter than that of unstrained TiN in good agreement with its high level of compressive residual stresses shown before (see Figure IV-4). Alloying with Ag contents up to 3 at.% progressively decreases the lattice parameter to similar values than that of the unstrained card, however, a sudden increase of this parameter is reached for 6 at.% of Ag. Further increase of the Ag decreases the lattice parameter of the films. These variations on the lattice parameter can be interpreted based on the level of residual stress on the films and on the variation of the deposition conditions. For low Ag concentration coatings (≤3 at.%), which were deposited under similar conditions, the decrease of the lattice parameter is a consequence of the decrease of the level of residual stresses on the films (Figure IV-4). However, interestingly enough, the film with 3 at.% Ag, still presents a considerable high level of compressive residual stresses which

should translate in a higher value of lattice parameter than that of the unstrained TiN. This suggests that an additional event is counteracting the effect of these compressive stresses. This event might be associated with the presence of Si in solid solution on the TiN lattice [11]. Indeed, Si has a lower atomic radius than that of Ti and therefore, if incorporated on the TiN lattice, will result in a decrease of the lattice parameter, effectively "negating" the residual stresses effect. Despite the continuous decrease of the level of residual stresses, the coating with 6 at.% Ag, shows a steep increase in the lattice parameter which can be tentatively explained by the increase in the peak power observed for this coating. Under such deposition conditions, the energy of the adatoms is increased which facilitates the Si segregation out from the TiN lattice, cancelling out the lattice deformation imposed by the solid substitution effect. Further Ag additions progressively decrease the lattice parameter as a consequence of the combined effect of the decrease of residual stresses and of the peak power. Considering the level of residual stresses and the lower value of the lattice parameter in relation to that of the unstrained TiN for these coatings (> 6 at.% Ag), suggests that the presence of Si in solid solution is still occurring.

4.2 Conclusions

This chapter reported the influence of Ag additions on the chemical composition, the morphological microstructure and the structure evolution of TiSiN(Ag) coatings deposited by HiPIMS working in DOMS mode. Comparison of the results with those achieved for a reference TiSiN film was also presented. According to XRD analysis, all coatings showed an fcc NaCl-type structure assigned to crystalline TiN. Ag additions to the TiSiN reference film, significantly broadens the TiN diffraction peaks and leads to the appearance of a broad diffraction peak assigned to Ag. A decrease of TiN grain size is observed when the first Ag content is added to the reference film due to the competitive growth between Ag, TiN grains and the SiN phases. However, further increase of Ag content does not seem to alter significantly the TiN grain size which suggests the grain size is independent of the silver content. Transition from columnar to very compact morphology, decrease of the deposition rate and increase of the lattice parameter was observed when 6 at.% of Ag was added to the reference coating due to the increase of peak power promoted by the introduction of bigger Ag pellets at the center of the race track of the target. Reverse to a columnar morphology was observed for the coating with highest Ag concentration due to both the slight decrease of peak power and the high concentration of Ag on the film which due to its very high mobility grows a porous spontaneous morphology. The increase of the lattice parameter, although contradicting the decrease of the level of compressive residual stresses, is explained by the increase of the peak power

which increases the mobility of the adatoms and consequently allows the diffusion of the Si remaining in solid solution in the TiN lattice.

After this analysis, the next chapter will deal with the thermal stability of these coatings while also making an analysis of the hardness of these coatings before and after annealing. Hardness analysis was not shown on this chapter for that same reason, since this way it is possible to make the analysis as a comparison with the as-deposited and the after-annealing coatings.

4.3 References

[1] A. Anders, Deposition rates of high power impulse magnetron sputtering: Physics and economics, Journal of Vacuum Science & Technology A, 28 (2010) 783-790.

[2] J.C. Oliveira, F. Fernandes, F. Ferreira, A. Cavaleiro, Tailoring the nanostructure of Ti–Si–N thin films by HiPIMS in deep oscillation magnetron sputtering (DOMS) mode, Surface and Coatings Technology, 264 (2015) 140-149.

[3] F. Fernandes, J.C. Oliveira, A. Cavaleiro, Self-lubricating TiSi(V)N thin films deposited by deep oscillation magnetron sputtering (DOMS), Surface and Coatings Technology, 308 (2016) 256-263.

[4] P. Scherrer, Bestimmung der inneren Struktur und der Größe von Kolloidteilchen mittels Röntgenstrahlen, in: R. Zsigmondy (Ed.) Kolloidchemie Ein Lehrbuch, Springer Berlin Heidelberg, Berlin, Heidelberg, 1912, pp. 387-409.

[5] A.P. Ehiasarian, A. Vetushka, Y.A. Gonzalvo, G. Sáfrán, L. Székely, P.B. Barna, Influence of high power impulse magnetron sputtering plasma ionization on the microstructure of TiN thin films, Journal of Applied Physics, 109 (2011) 104314.

[6] J.E. Greene, J.E. Sundgren, L. Hultman, I. Petrov, D.B. Bergstrom, Development of preferred orientation in polycrystalline TiN layers grown by ultrahigh vacuum reactive magnetron sputtering, Applied Physics Letters, 67 (1995) 2928-2930.

[7] C. Dang, J. Li, Y. Wang, Y. Yang, Y. Wang, J. Chen, Influence of Ag contents on structure and tribological properties of TiSiN-Ag nanocomposite coatings on Ti–6Al–4V, Applied Surface Science, 394 (2017) 613-624.

[8] F. Fernandes, T.B. Yaqub, A. Cavaleiro, Influence of Ag additions on the structure, mechanical properties and oxidation behaviour of Cr-O coatings deposited by HiPIMS, Surface and Coatings Technology, 339 (2018) 167-180.

[9] N.K. Manninen, R.E. Galindo, S. Carvalho, A. Cavaleiro, Silver surface segregation in Ag-DLC nanocomposite coatings, Surface and Coatings Technology, 267 (2015) 90-97.

[10] P. Basnyat, B. Luster, Z. Kertzman, S. Stadler, P. Kohli, S. Aouadi, J. Xu, S.R. Mishra, O.L. Eryilmaz, A. Erdemir, Mechanical and tribological properties of CrAlN-Ag self-lubricating films, Surface and Coatings Technology, 202 (2007) 1011-1016.

[11] R.F. Zhang, S. Veprek, Crystalline-to-amorphous transition in $Ti_{1-x}Si_x N$ solid solution and the stability of fcc SiN studied by combined ab initio density functional theory and thermodynamic calculations, Physical Review B, 76 (2007) 174105.

CHAPTER V – Thermal characterization of Ti-Si-(Ag)-N Coatings

The importance of Ag content for optimizing the machining

performance of Ti-Si-(Ag)-N coatings

5 Introduction

After dealing with the fundamental characterization of the TiSiNAg coatings in the as-deposited state in previous chapter, it is now of utmost importance to study and assess the behaviour of these coatings at higher temperatures since it is this environment expected when dealing with the machining of titanium alloys. Therefore, this chapter refers to the thermal characterization of the TiSiNAg coatings in protective atmosphere as well as in oxidizing atmosphere. The tests performed at protective atmosphere will give information related with structural changes as function of the temperature. Besides these structural changes, another issue is focused on the silver diffusion on the coatings, in order understand the role of the Si-N amorphous matrix as a diffusion barrier. To assess phase transformations, oxidation resistance, while evaluating oxide growth effect on the silver diffusion, thermal treatments at oxidizing atmosphere tests were also performed.

First, the coatings were evaluated in relation to thermal stability by exposing them at increasing temperatures in a protective atmosphere followed by hardness measurement and structural analysis, evaluated by nanoindentation and XRD, respectively. After that, the phase evolution with increasing temperature was evaluated. Then the onset point of oxidation of the films was evaluated by thermogravimetric analysis (TGA). The films were exposed at a constant linear-temperature ramp and the oxidation weight gain continuously measured. Then, the coatings were exposed to isothermal oxidation tests and the oxidation weight gain of the different films was compared. SEM in conjunction with EDS were then used to characterize the distribution of the main elements in the cross section of the films, the oxide scale growth and therefore the chemical composition of different oxides and the distribution of silver on the coating.

Although for the protective atmosphere environment all of the coatings were evaluated, the results shown in section 5.1.1 pertain only some of them, as the behaviour observed was found to be representative for the rest of the coatings. However, for the oxidizing atmosphere environment, some of the coatings were not tested at all. Actually, the selection was made based on significant differences on the silver content. The tests were performed for low (TiSiNAg2), medium (TiSiNAg6) and high (TiSiNAg10 and TiSiNAg17) silver additions. Obviously, it would seem that the TiSiNAg29 could be consider as the "high" silver content but it was also the first coating to be discarded since it was the only one showing an extremely poor adhesion, very low hardness and a very porous morphology anticipating its bad behaviour in real applications. Also of note, is that for the in-situ high temperature X-ray diffraction, only the TiSiNAg6 coating was tested since it was the most promising sample.

5.1 Results

5.1.1 Annealing of the Ti-Si-(Ag)-N coatings in protective atmosphere

All coatings were annealed at 800°C in a protective atmosphere for 2h to assess the effect of temperature on the structural and mechanical properties and to characterize the distribution of the silver in the coatings. In order to understand the possible changes on the mechanical properties during machining tests, the Hardness (H) and Young's modulus (E) of both the as-deposited coatings and the ones after being submitted to annealing at 800°C are shown on Figure V-1.
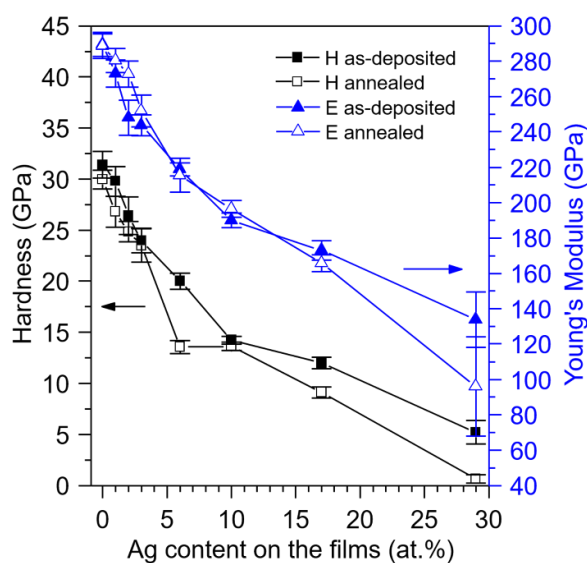
Figure V-1 Hardness (H) and Young's modulus (E) of the as-deposited and annealed coatings

Reference TiSiN coating has a hardness of ~32 GPa and a Young's modulus of ~290 GPa which agrees well with the values referred in the literature for nanocomposite structured TiSiN coatings within this range of Si contents [1]. As expected, the introduction of increasing contents of silver in the coatings leads to a steady decrease of the mechanical properties as the amount of the soft phase is increasing facilitating grain boundary sliding. Moreover, the decrease in the compressive residual stresses, shown before (see Figure IV-4 in Chapter IV), may also contribute to the observed decline of hardness. Submitting the films to the annealing treatment did not promote significant changes in the mechanical properties of the coatings in good agreement with the XRD results that will follow the discussion in more detail (see Figure V-2). Albeit, a steeper decrease is observed for the coating with the highest silver content (29 at.%) in good agreement with the presence of the soft and continuous Ag layer that remained "engraved" on the surface, despite the cleaning procedure. The hardness obtained approaches thus that of the bulk silver (~0.25 GPa).
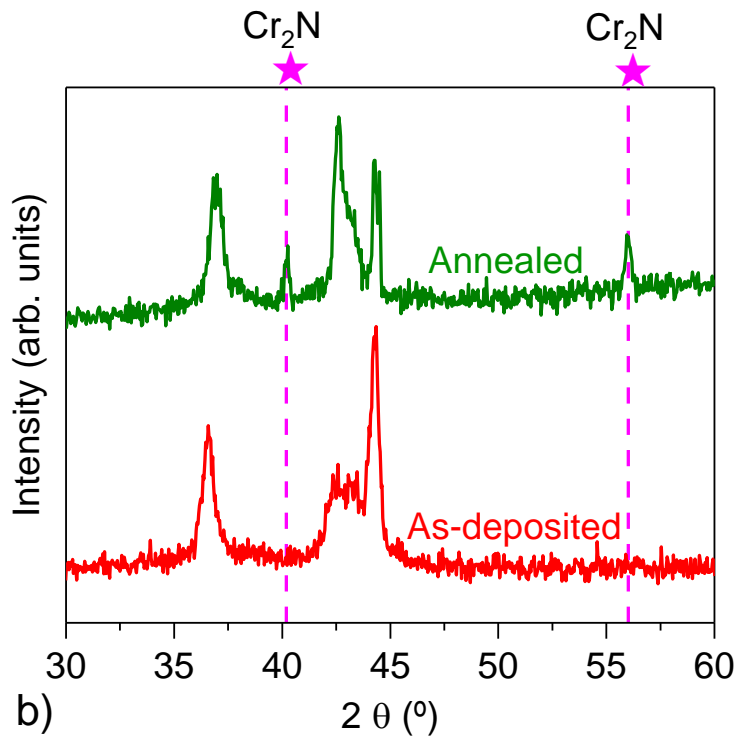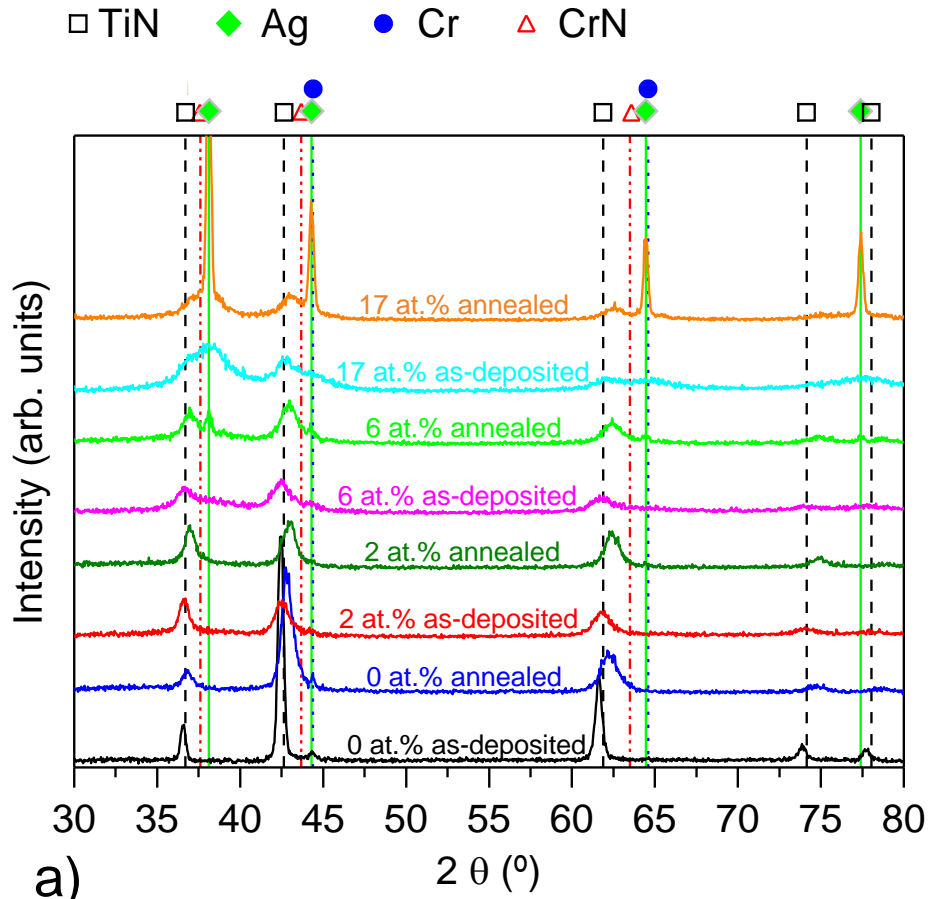
Figure V-2 a) XRD diffraction patterns of the TiSiN, TiSiNAg2, TiSiNAg6 and TiSiNAg17 as-deposited and annealed films, obtained in grazing incident mode and b) As deposited and annealed XRD diffraction patterns of TiSiNAg2 coating acquired in conventional mode

Following this mechanical property, the structural characterization is now assessed with the XRD diffraction patterns, in grazing mode, of the selected coatings as-deposited and after annealing being shown on Figure V-2a. No major changes on the structure/phase composition were observed for all the coatings in good agreement with the results obtained by Xu et al [2] in the TiSiN system deposited by cathodic arc evaporation, who reports that changes in the structure and mechanical properties only started occurring after submitting the coatings to temperatures higher than 1000°C.
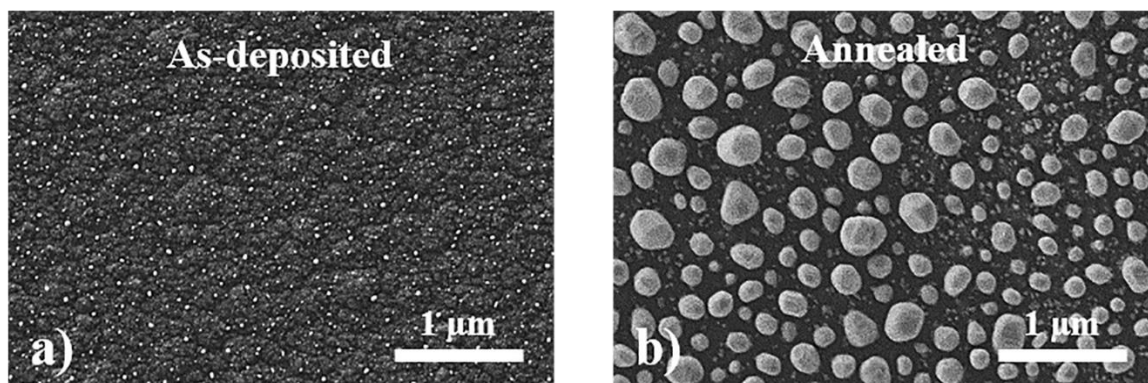
Figure V-3 Surface morphology of the TiSiNAg17 coating: a) as-deposited and b) after annealing

Nevertheless, an increase in the intensity of the silver peaks was observed, especially for the coatings with medium (6 at.%) and high (17 at.%) silver contents. This increase can be explained if we take into account the silver diffusion that occurred to the surface denoted by the increase in size of the particles on the surface as shown on Figure V-3, representative for all the coatings. Also of note is that, all the peaks associated with the TiN phase are now shifted towards higher angles than those of the correspondent reference ICDD card. Although not calculated, changes in the residual stresses induced by the annealing treatment and the subsequent cooling might explain this shift. Segregation of the silver to either the grain boundaries or the surface promotes the release of stresses with the consequent shift of the XRD peaks to higher angles [3]. This process is obviously enhanced by the high temperature used in the annealing process which facilitates the Ag diffusion. During the cooling process the disparity in the thermal expansion coefficients between the film and the substrate may induce tensile stresses also shifting the peaks towards higher angles. Finally, in the conventional mode XRD diffractogram (see XRD pattern of TiSiNAg2 film shown in Figure V-2b, representative for all the coatings), two new reflections appear in the annealed coatings at ~40° and at ~56° which were found to be associated with the Cr_2N phase inherent to the gradient layer. This can be tentatively explained by the nitriding of this phase occurring during the annealing process. Nitriding of the remaining metallic Cr parts via a solid state reaction was reported to occur for temperatures as low as 700°C [4].
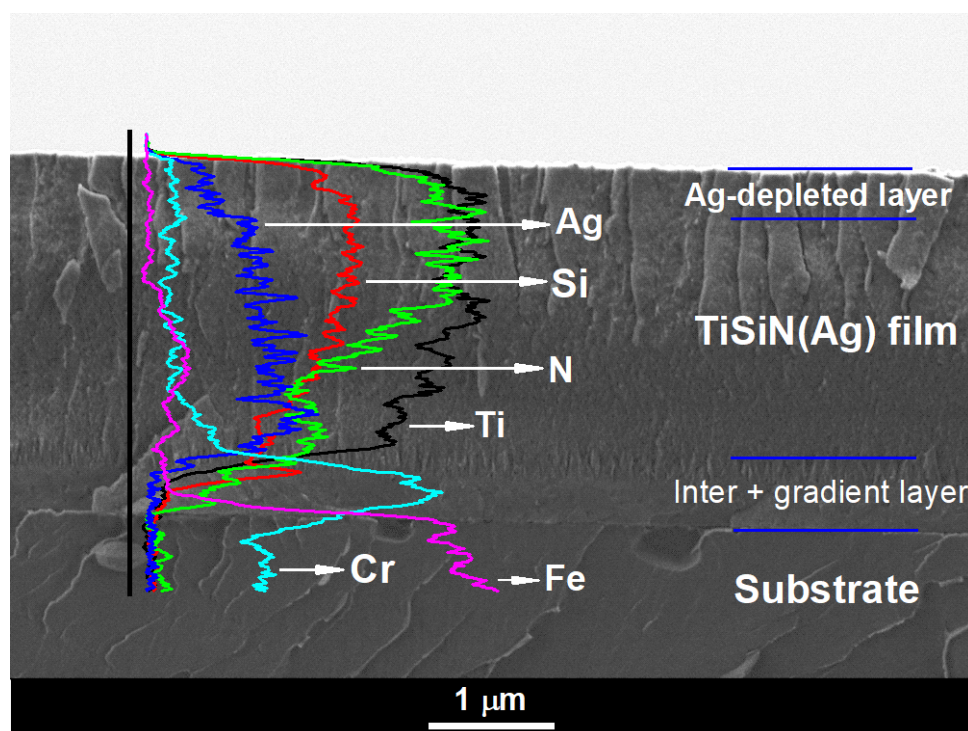
Figure V-4 Fracture cross section morphology and EDs line scan of the annealed TiSiNAg6 coating

After XRD analysis and prior to the silver distribution assessment and hardness measurements, all the coatings were submitted to a surface cleaning procedure with alcohol, which removed the superficial Ag particles shown on Figure V-3b. The cross section observation of the TiSiNAg6 coating (Figure V-4), showed, no significant changes in the morphology of the films representative for all the coatings tested, corroborating the XRD results shown before. However, a small dual layer was formed close to the surface of the films. Elemental chemical composition lines revealed the presence of an Ag-deficient TiSiN with the previous Ag rich layer on top formed due to the diffusion of silver from this sub-layer below (before sample cleaning). Elemental line profiles also revealed an accumulation of Ag and Si near the interface of the film/interlayer. Similar results were observed by Fernandes et. al [5] for the CrO(Ag) system. Independently of the previous observations and based on the observable homogeneous distribution of the silver on the rest of the coating, it could be considered that the TiSiN system offers a somewhat effective barrier to the Ag diffusion.

5.1.2 Annealing of the Ti-Si-(Ag)-N coatings in oxidizing atmosphere

Following the tests in protective atmosphere, the oxidation resistance of the TiSiNAg coatings was now evaluated. To start, the phase evolution of the TiSiNAg6 coating (representative of the silver content between the "low" and "high") at increasing higher temperatures was studied through in-situ X-ray

diffraction. After that, the thermogravimetric analysis of the coatings in dynamic mode was done followed by the observation of the isothermal curves.
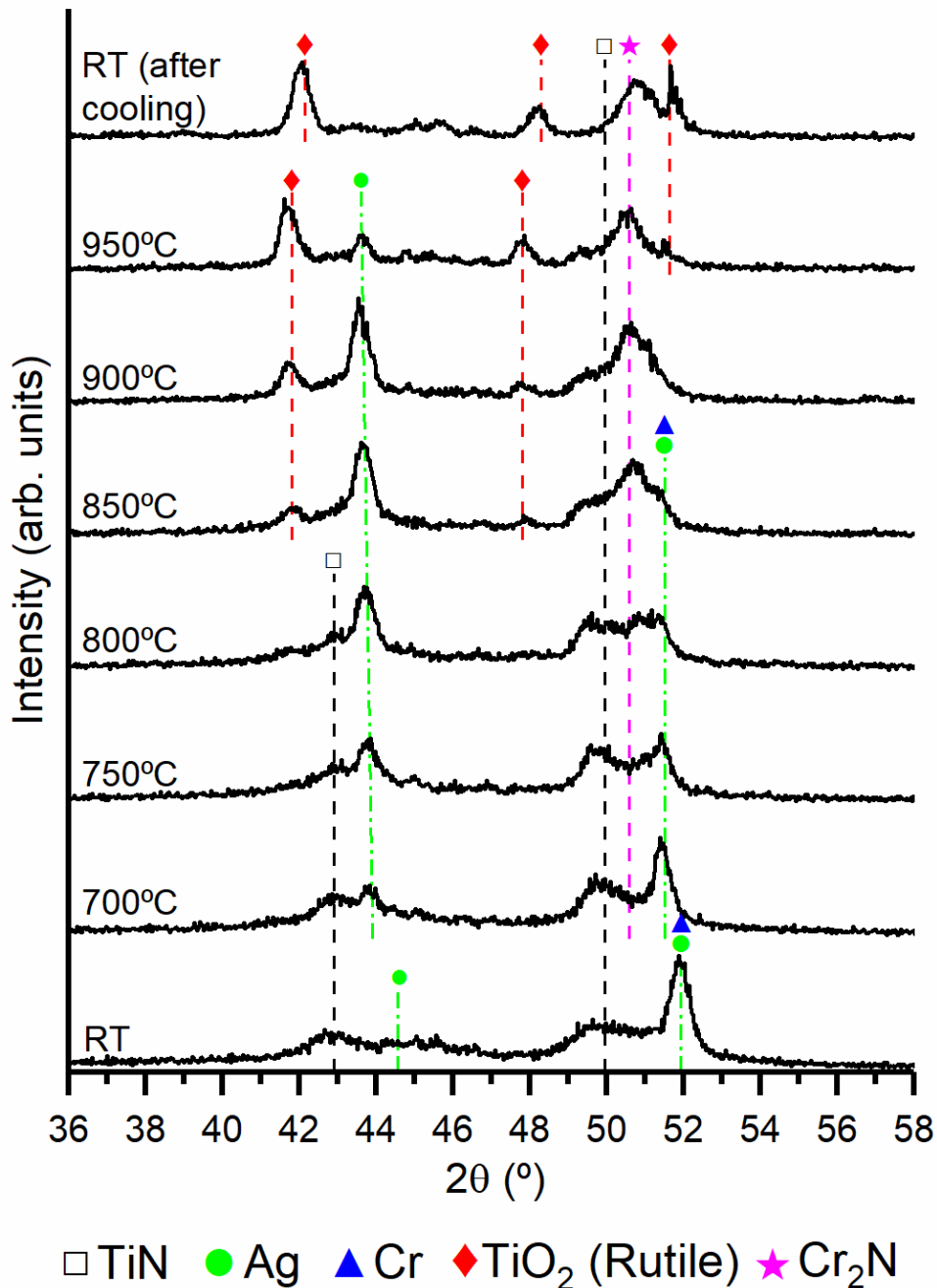
Figure V-5 XRD spectra of the TiSiNAg6 film at different temperatures. Spectra were obtained in conventional mode using a Co Kα radiation (λ = 1.789010 Å)

The in-situ high temperature XRD diffractograms evolution of TiSiNAg6 coating, representative for all the Ag rich coatings, is shown on Figure V-5. It should be noted, for XRD comparison purposes, that these diffractograms were obtained in conventional mode and with Co Kα radiation, instead of Cu Kα, which

explains why similar peaks are now positioned at higher angles than those showed previously in Chapter IV. The film before annealing displayed broad diffraction peaks positioned at ~43° and ~50°, both assigned to TiN (ICDD card no 87-633) and at ~44.5°, assigned to Ag (111) (ICDD card no 87-597). Furthermore, a crystalline peak centred close to ~52° correlates to Cr from the interlayer, which is overlapped to the (200) peak of Ag. By increasing the temperature to 700°C, the Ag (111) diffraction peak, located at around ~44°, shows higher intensity whereas the decrease of the intensity of the Ag (200) peak suggests a change in the preferential orientation of the silver. This agrees well with the preferential orientation expected from the ICDD card. All XRD diffraction peaks are shifted to lower angles (more noticeable for Ag ones), explained by a combination of the thermal expansion of the lattice and the build-up of stresses resulting from the growing of the oxide scales. Corroborating this is the return of the peaks to their "normal" positions after cooling down. At 750°C and 800°C, a very small diffraction peak can be detected as a shoulder in the left of the overlapped Ag and CrN peaks, which can be correlated to the Cr$_2$N phase resulting from the recrystallization of the CrN gradient layer. Also observable, is the reinforcement of the changes in the Ag (111) and (200) plans, further highlighting the change in the preferential orientation of the silver. When the temperature reaches 850°C, the first signs of oxidation start to be detected with the appearance of two small peaks at around ~42° and ~48°, assigned to the tetragonal TiO$_2$ rutile phase (ICDD card no 76-0649) peaks that become more and more intense with increasing temperature, suggesting an increase in the thickness of the oxide scale. This corroborates the progressive suppression of the TiN diffraction peaks intensity. At 950°C, the trend in the intensity of Ag diffraction peaks is inverted, showing lower values. Taking into account, the melting point of the silver (960°C) and the size of the Ag nanoparticles, this decrease in the intensity should be attributed to the melting of the Ag nanoparticles and/or the consequent loss of silver by evaporation [6, 7]. Thermogravimetric results of the films (shown in the following TGA study) confirm this trend as a more detailed explanation will also follow later. In addition to the appearance of a new peak at ~51.5°, related to rutile, the signal of TiN crystallites is still detected, confirming that film is not totally oxidized at this temperature. After cooling down, the same phases as identified at 950 °C were indexed, with exception of the Ag signal. Only vestiges of TiN and Ag peaks are detected after cooling down. This agrees well with the elemental map distribution of the cross section of the film, shown in Figure V-6, where only weak signals of Ag, Ti and N are visible.
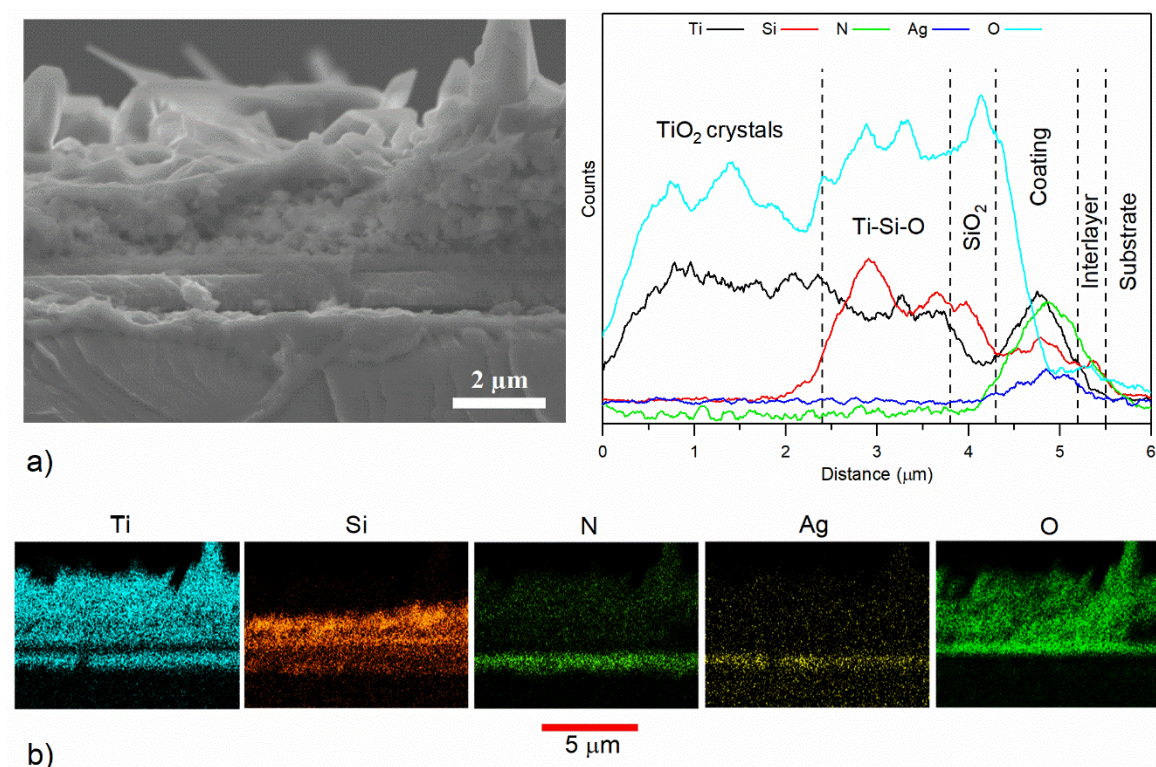
Figure V-6 Cross section morphology and corresponding elemental line profiles (a) and elemental maps (b) of the TiSiNAg6 film after in-situ high temperature oxidation

The SEM cross section micrograph and corresponding elemental maps and elemental lines distribution of TiSiNAg6 after in-situ high temperature XRD evolution are shown in Figure V-6. Four different layers can be distinguished on the cross section of the annealed film: i) a top layer formed by crystals, majorly composed of Ti-O, corroborating the rutile signal detect by XRD, ii) below a porous layer composed of a mix of Ti and Si oxides, iii) further below, a glass like compact layer of SiO_2 and iv) the remaining un-oxidized film. Dissociation of the nitrogen, inward diffusion of the oxygen and the outward diffusion of the titanium coupled with the higher affinity of oxygen to titanium explain the formation of the permeable rutile TiO_2 crystals on the top of the film [8]. On the contrary, SiO_2 is reported to be an efficient barrier to the oxygen diffusion [9], however, in this case, a porous structure is firstly observed, over the protective SiO_2 layer. In some cases, the fast outward diffusion of the titanium can lead to porosity and disrupt the formation of an adequate SiO_2 oxidation barrier [8]. Signal of silver on the oxide scale was very weak, corroborating the low signal in the XRD analysis (see Figure V-5) after cooling down. However, on the non-oxidized part of the film it is still possible to observe a clear and evenly dispersed silver signal, suggesting that Ag is not diffusing but is, instead, being "consumed", vanishing from the oxide scale when temperatures are high enough to promote its evaporation. As the oxidation process is evolving and progressing from the surface down to the interface, silver is kept inside the original film. However, as the

coating is being oxidized and the porous TiO_2 starts to be formed, silver has the conditions (the pores) to agglomerate and, eventually, to diffuse outwards to the oxide scale surface. Therefore, even in oxidizing atmosphere conditions, the nanocomposite TiSiN film offers an efficient barrier to Ag diffusion.
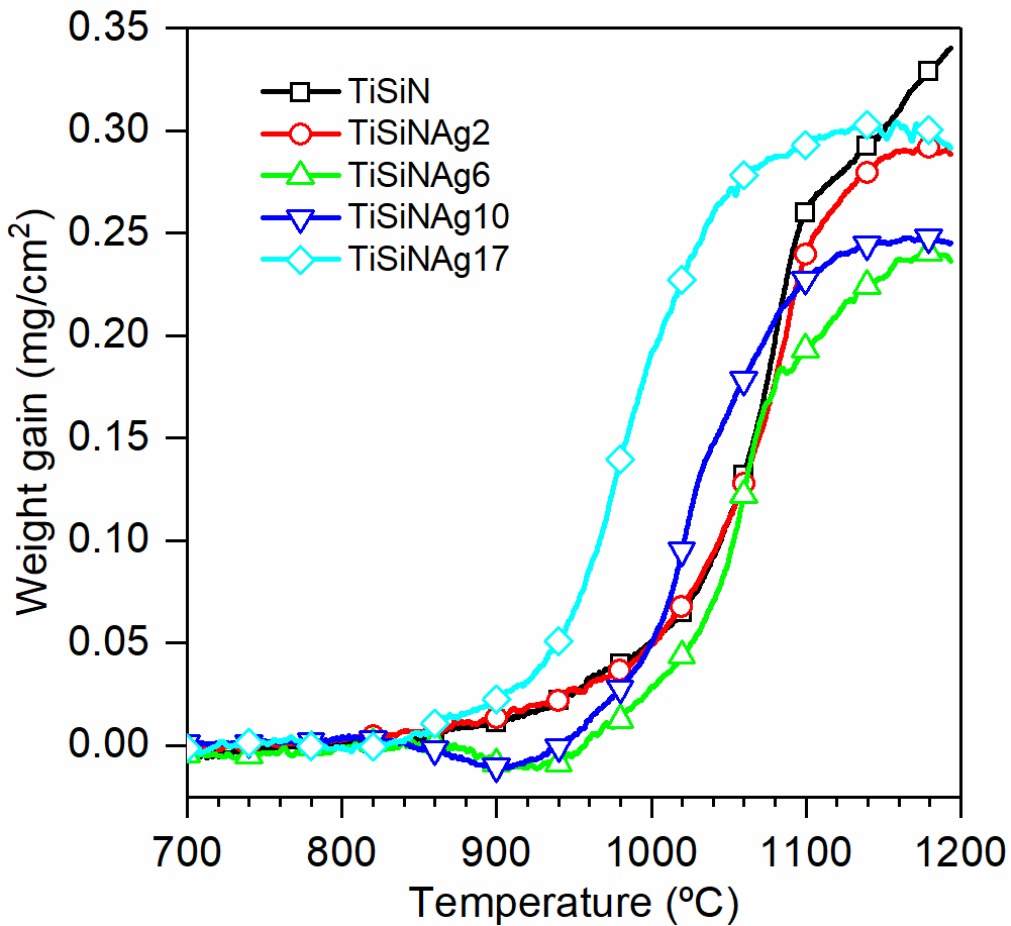
Figure V-7 Thermogravimetric oxidation rate of selected coatings performed at a constant linear temperature ramp (from RT to 1200ºC at a rate of 20ºC/min)

In order to better understand the oxidation behaviour of the TiSiNAg coatings, thermogravimetric analysis in dynamic mode with a continuous increase of the temperature from RT up to 1200 °C (see Figure V-7) was conducted. As shown in Figure V-7, the onset oxidation temperature of the reference TiSiN film is ~850 °C. Silver additions to TiSiN film does not change the onset point of oxidation. This temperature agrees well with the first oxide products detected previously in the in-situ high temperature XRD study, shown in Figure V-5. Contrarily to the observations of Fernandes et al. [10], who studied the effect of vanadium additions on the oxidation behaviour of a TiSiN film with similar Si content, vanadium induced a decrease on the onset point of oxidation of the coatings. However, in that work, TiSiN was deposited as a solid solution, i.e. with the Si replacing the Ti positions on the TiN lattice. No nanocomposite structure

was deposited. Therefore, the absence of the Si-N phase did not allow the controlled release of the lubricious phase, which in its outwards trajectory disrupted the formation of the protective Si-O layer.

After the onset oxidation temperature is reached, the oxidation process progresses, initially with a slow increase in the mass gain and, then, close to 1000°C accelerates showing very high oxidation rates. The development of the oxide scale, including a Si-O layer explains initially, the low rates and later, the high rates, when it becomes less protective. Coatings with increasing Ag contents display a similar mass gain evolution. However, the one with the highest Ag content accelerates the oxidation at a lower temperature. At about 1100°C, an inflection in the curve is then perceived which seems to indicate that the film is completely oxidized. It has been already reported that the high oxidation resistance of the TiSiN system is related with the presence of a protective silicon oxide layer that hinders the oxygen and metal ions diffusion, shielding the coating from further oxidation [11-13].

An unusual feature in the oxidation curves for the coatings with medium silver contents (6% and 10 at.%) is seen: the curves exhibit a mass loss right after the onset point of oxidation which, then, continues its "normal" evolution after the temperature reaches ~930°C. This mass loss is due to a competitive process occurring between silver aggregation and silver evaporation/sublimation. In fact, the size of the particles plays an important role in the decrease of the melting and evaporation temperature of metals i.e. the lower the size of the clusters the lower the melting and evaporation temperature points are [6, 7]. Due to the small size of Ag nanoparticles existing in the as-deposited films, when the temperature reaches the oxidation start point, the evaporation or sublimation of silver starts to occur even if the melting temperature of Ag is reached. This phenomenon proceeds as the temperature increases, up to the moment that: i) the small nanoparticles on the surface are all evaporated and/or ii) the diffusion of silver is strong enough so that agglomeration into larger clusters happens, avoiding their sublimation. For very high silver contents, Ag agglomeration is easier, giving rise to higher nanoparticles size hindering the sublimation process for temperatures lower than the melting temperature of Ag. Therefore, in the oxidation weight gain curve of the TiSiNAg17 coating, the step mass loss is absent.
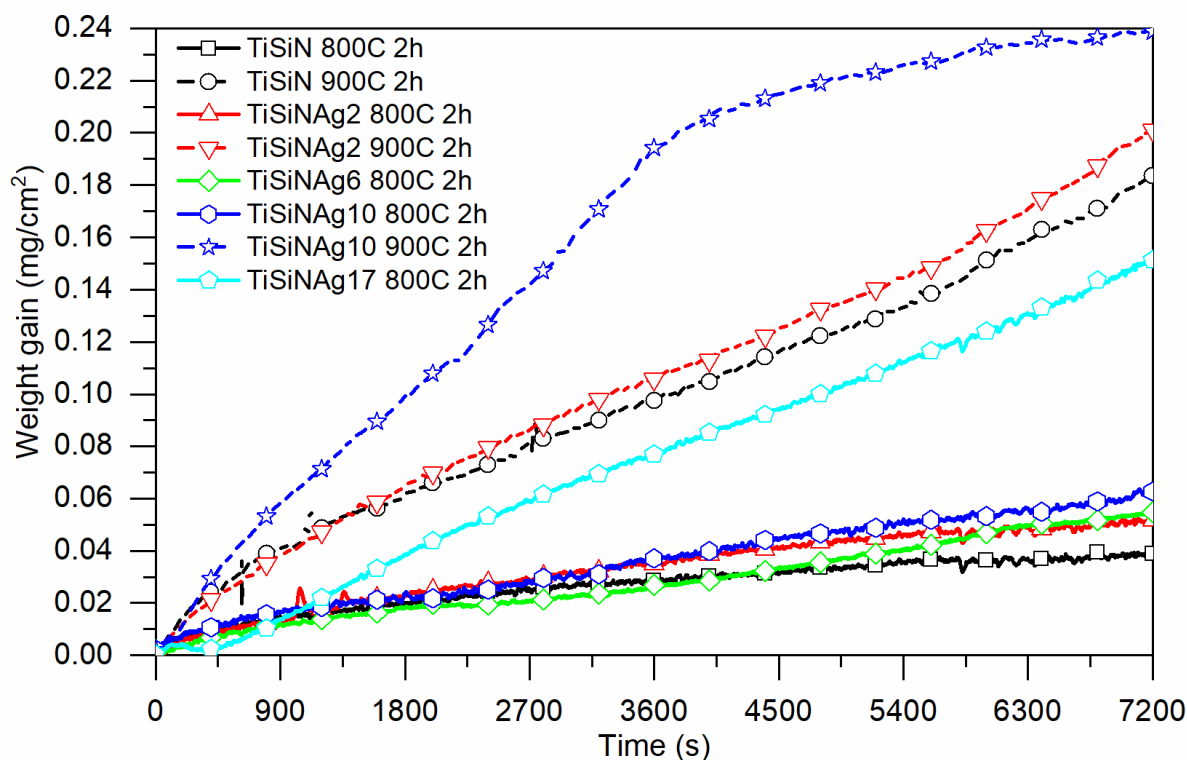
Figure V-8 Isothermal TG curves of coatings exposed at 800ºC and 900ºC for 2h

In order to better characterize the oxidation behaviour of films, isothermal analysis at 800°C and 900 °C, for 2 h, were carried out, as seen in Figure V-8. Reference TiSiN film tested at 800 °C follows a parabolic law, suggesting the formation of a protective oxide layer. Cross section morphology of the film revealed the formation of a dual oxide scale, i.e. small crystals were observed on top of the film which EDS analysis revealed to be composed of Ti and O. Below this layer, a compact layer rich in Si and O, suggesting the formation of a protective SiO_2 layer. XRD diffraction patterns confirmed the presence of the Ti-O phases (see the small rutile peaks in Figure V-9i a2), however Si-O could not be detected, suggesting its amorphous character. The parabolic behaviour of the coating can be thus explained by the formation of the protective Si-O layer, corroborating the literature results [11, 12, 14].
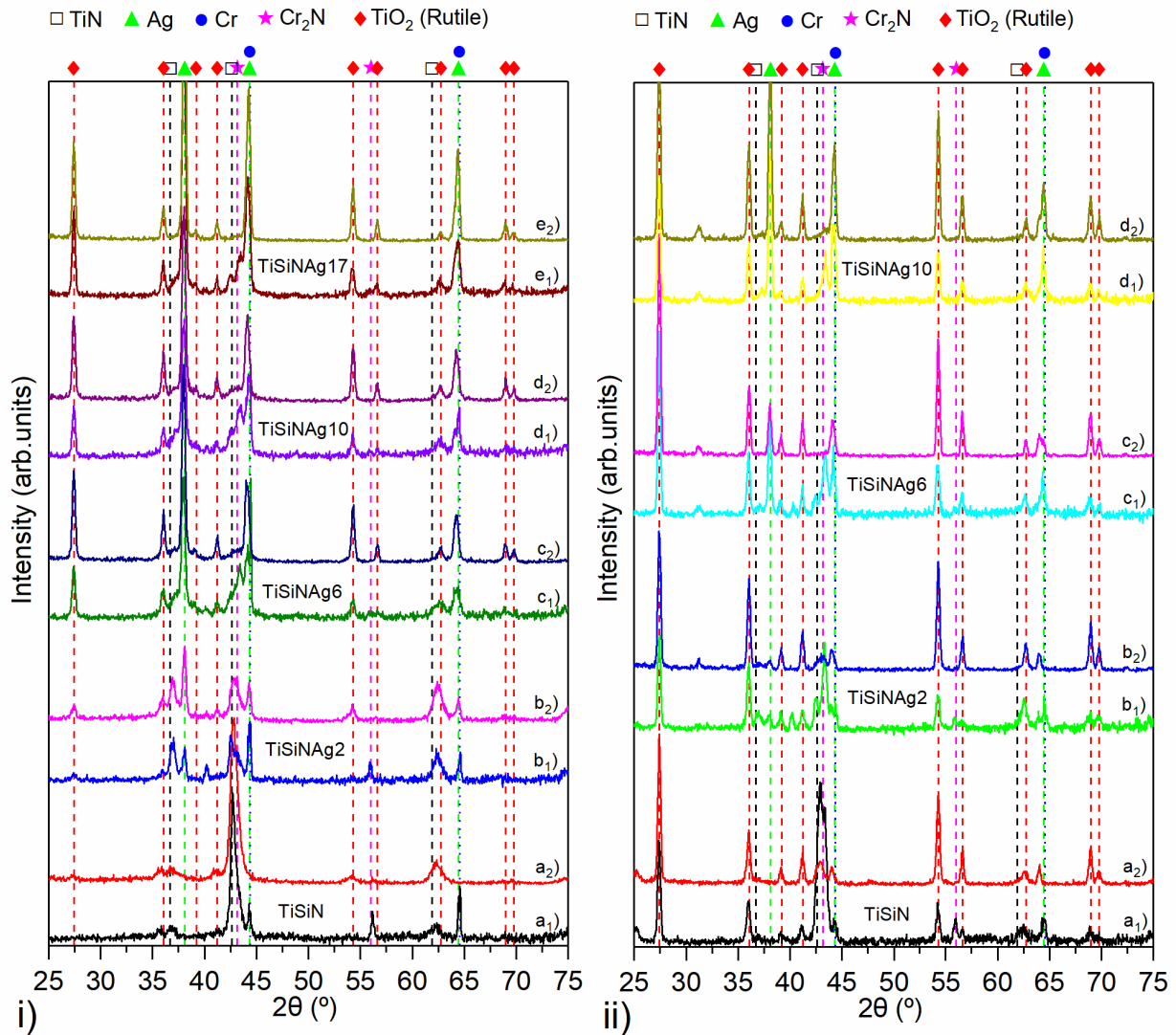
Figure V-9 XRD spectra of the coatings after isothermal tests at i) 800ºC and ii) 900ºC for 2 hours. Indexes 1 for conventional mode and indexes 2 for grazing mode.

At 900°C, the coating also shows a normal parabolic evolution but only at the very beginning (up to 900 s), then a linear law defines the oxidation rate. The linear evolution should be related to a porous Ti-Si-O layer growth below the top Ti-O layer (see Figure V-10). At the very beginning of the oxidation process, due to either the high Ti content or the higher affinity of Ti to O than Si [15], a TiO_2 layer starts growing. The depletion of Ti in that zone leads to a Si-rich layer, which in the presence of oxygen forms Si-O. In this stage, the oxidation process is governed by the inwards diffusion of O_2- through the TiO_2 layer and the outwards diffusion of Ti ions through the Si-O layer [10]. The oxidation rate, i.e. the mass gain ratio, is determined by the Ti ions able to out diffuse in the Si-O layer, since it is well known that TiO_2 oxide is not protective at these high temperatures. Therefore, oxygen will always be available for combination with Ti/Si in the interface between the TiO_2 crystals and Si-O layer. In the first moments of oxidation, Si-O is thickening which justifies the parabolic behaviour. However, after some time, the out diffusing of Ti will

leave a porous structure behind which, in addition to the higher affinity of oxygen for Ti than Si, will lead to a progressive replacement of Si on the Si-O layer forming the observed porous Ti-Si-O layer. During a period of time, Si-O layer is formed and transformed in the Ti-Si-O, keeping its thickness approximately constant and defining the linear rate registered after the parabolic behaviour (Ti diffusion through a layer with constant thickness). From the moment that the whole Si-O layer is transformed in the porous Ti-Si-O (after ~5200 s), the easy diffusion of the reactive species through this layer, increases the oxidation rate, explaining the second linear trend in the oxidation curve, now with a much higher slope.
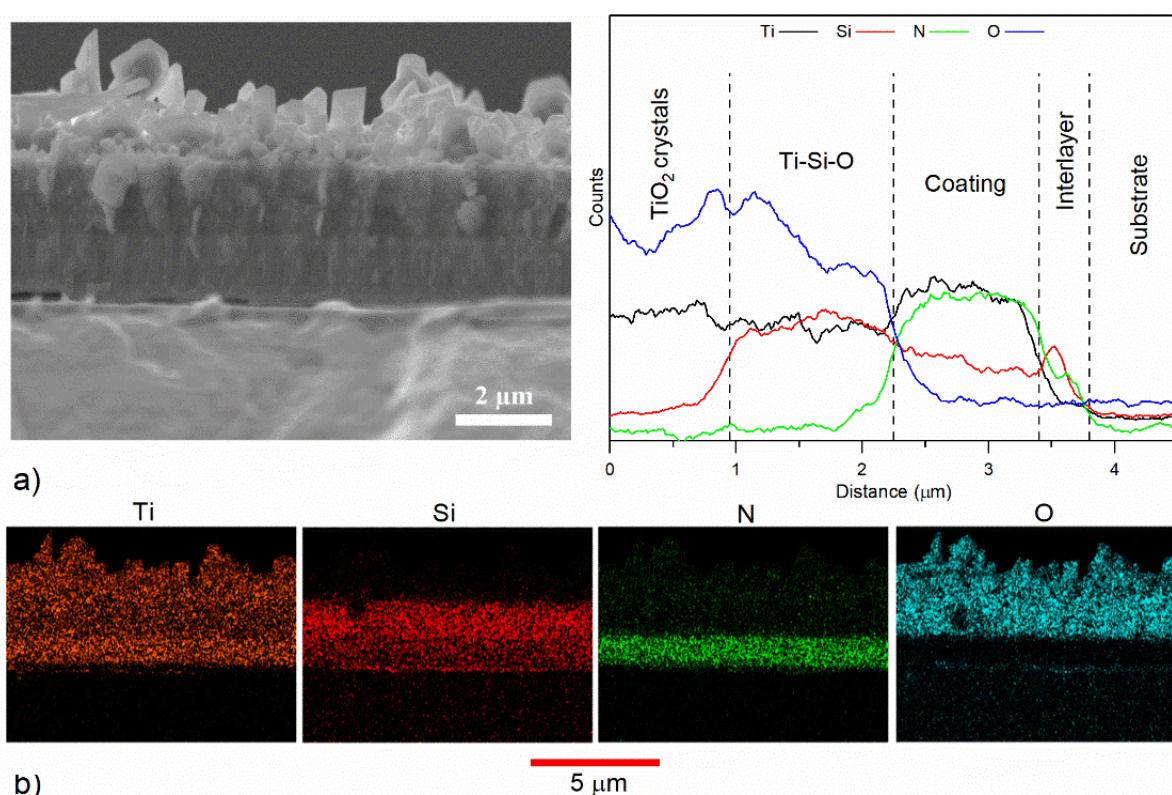
Figure V-10 Cross section and correspondent elemental line profiles (a) and elemental map profiles (b) of the TiSiN coating after annealing at 900ºC for 2 hours

TiSiNAg2, TiSiNAg6 and TiSiNAg10 coatings oxidized at 800 °C display oxidation weight gain slightly higher than TiSiN, particularly in the last part of the oxidation test, for which a transition to a linear trend is observed. In the first part of the weight gain curves, the oxidation seems to be independent of the silver content. The cross section of the oxidized films confirmed that the coatings with silver show higher thickness of the oxide scale (see Figure V-11, for TiSiNAg6 and TiSiNAg10 coatings). The coating with the highest silver content (TiSiNAg17) displayed much higher mass weight gain clearly evidencing the nefarious influence on the oxidation performance of coatings. Similarly, to the TiSiN reference film, the oxidized scale of Ag-containing films displayed two distinct oxide layers: a top layer comprised by big rutile

crystals and, below, a porous layer rich in Ag, Si and O. In addition to the phases expected at room temperature, XRD diffraction patterns detected also the presence of TiO_2 and Ag phases, corroborating the oxide scale composition. As expected, no signals of Si-O could be detected due to its amorphous character.
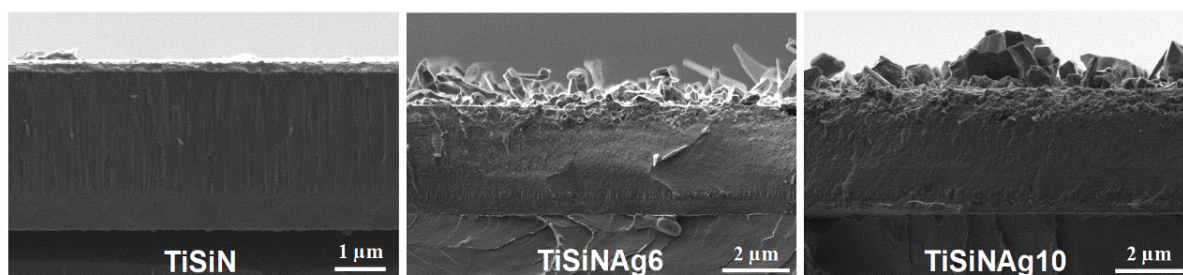
Figure V-11 Cross section morphologies of the TiSiN, TiSiNAg6 and TiSiNAg10 coatings after annealing at 800ºC for 2 hours

Elemental maps distribution shown in Figure V-12, for the TiSiNAg6 coating annealed at 800°C, showed the presence of vestiges of Ag on the outer layer, accumulation of Ag in the internal layer and a small zone depleted in Ag visible in between the film and the internal oxide layer. This suggests that: i) oxidation of Ag-containing coatings proceeds in a similar way as for reference TiSiN film, with additional diffusion of Ag, ii) Ag helps to disrupt the protective Si-O layer, favouring its transformation in the porous Ti-Si-O layer, promoting the premature change in the oxidation law from parabolic to linear and increasing oxidation; this behaviour is amplified with the increase in the Ag content, iii) Ag which diffused together with Ti to form top layer evaporates masking the real weight gain in the oxidation curves and iv) diffusion of Ag from the film to the oxide scale occurs in a limited region of the top of the un-oxidized film (i.e. down to some nanometres), as suggested by the Ag and O depleted region, but rich in Ti, Si and N, located immediately below the porous inner oxide layer shown in Figure V-12. It should be remarked that in the un-oxidised coating there is a strong and constant signal of Ag. This limited out-diffusion of Ag is well in agreement with the annealing results found in the previous sub-section during annealing with protective atmosphere, where the top Ag rich layer was formed due to the diffusion of silver from a very thin zone from the TiSiN coating below (see Figure V-4). As expected, the Ag agglomeration/concentration on the bottom of the oxide scale is as high as the original Ag content in the film.
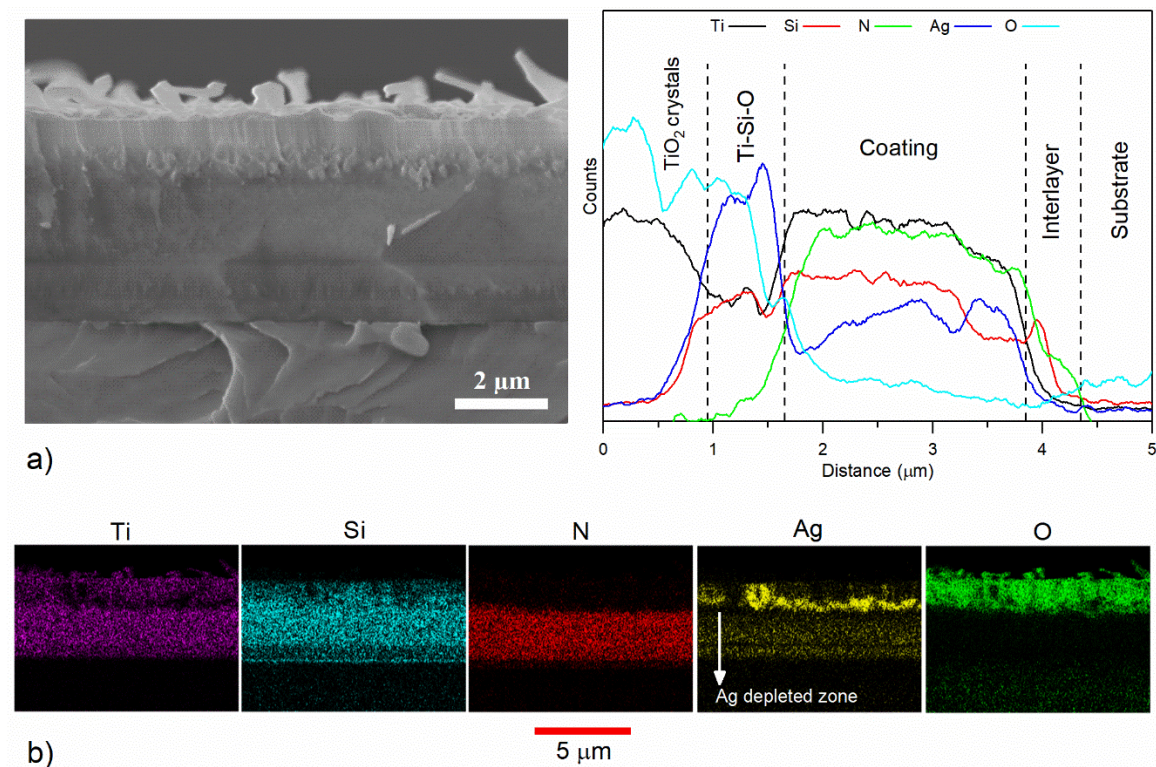
Figure V-12 Elemental map distribution of the TiSiNAg6 coating after annealing at 800ºC for 2 hours

At 900°C, higher oxidation rates are expected since all diffusion phenomena ruling the oxidation process are enhanced. TiSiNAg2 film displayed similar weight gain evolution than reference TiSiN film, as shown in Figure V-8. However, for higher Ag contents, the difference in the oxidation performance are much higher, as shown in Figure V-8 for TiSiNAg10 coating. The transformation to the second linear step, i.e. where the oxidation is ruled by the reactive species diffusion in the porous Ti-Si-O layer, occurs at approximately the same weight gain (0.14 mg/cm^2) but at a much earlier time (2300 s against 5200 s). The fully oxidation of the coating occurs before the end of the test. This result corroborates the XRD results plotted in Figure V-9 where the absence of diffraction peaks assigned to TiN could be noticed. This was not the case for the TiSiAgN6 coating for which un-oxidised film was still possible to be observed after the 2 hour test, as shown in Figure V-13. The elemental maps show that there is still a part of the original film to be oxidised. Moreover, the type and distribution of the oxide phases in the oxidised scale are very close to the ones described for the oxidation at 800 °C. Finally, and more importantly, in the un-oxidised film there is still a content of Ag homogeneously distributed, showing that even for this high temperature its outwards diffusion can be avoided, showing the beneficial contribution of the nanocomposite arrangement with the Si-N layer working as an anti-diffusion barrier to Ag.
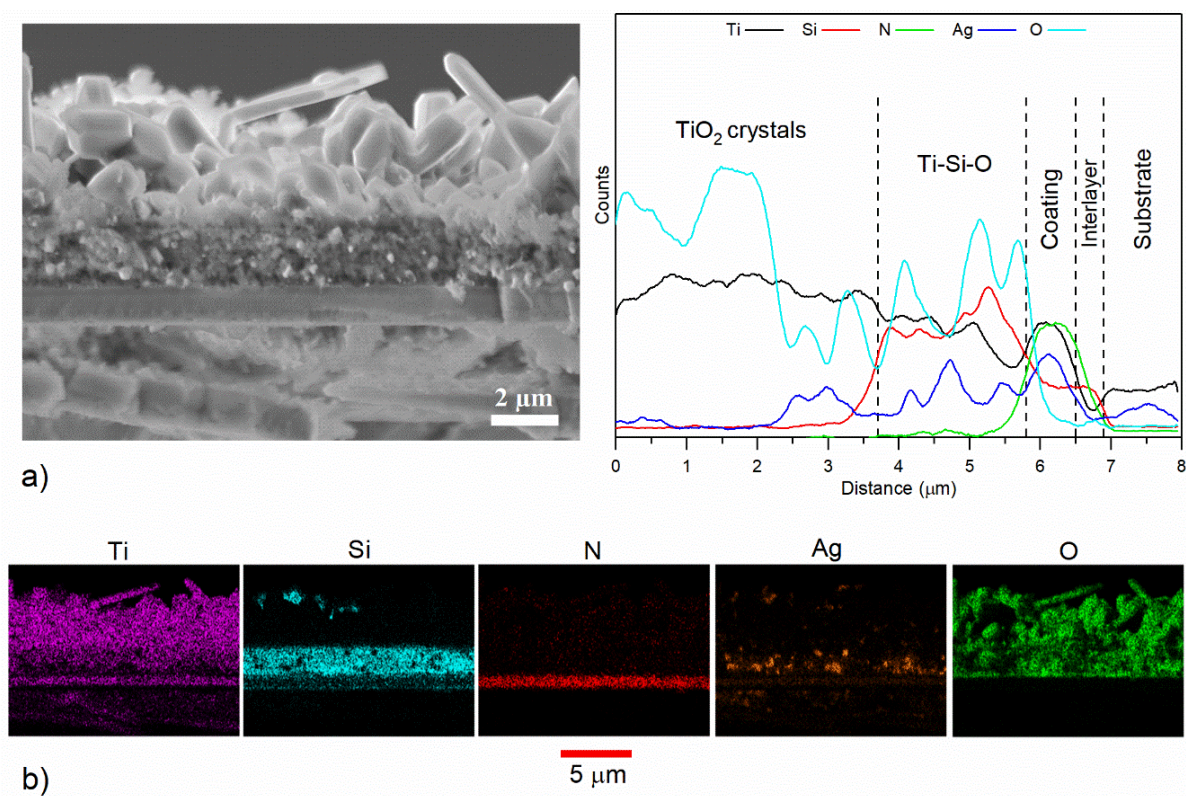
Figure V-13 Elemental map distribution of the TiSiNAg6 coating after annealing at 900ºC for 2 hours

5.2 Conclusions

In this chapter the Ag influence on the thermal stability, with and without protective atmospheres, of TiSiN(Ag) films deposited by HiPIMS working in DOMS mode was assessed. From a general perspective, annealing treatment, in protective atmosphere, did not significantly change the structure, morphology or mechanical properties of films, neither it allowed a strong diffusion of Ag to the surface, working as an effective barrier to these ions. X-ray diffraction and hardness measurements before and after annealing showed basically the same structure and hardness, with the only differences being a shift of the peaks to higher angles, due to the release of the residual stresses and the increase in the intensity of the Ag peaks due to some amounts of silver that diffused from the topmost part of the film. This was perceived by analysis of the elemental maps and profiles that allowed to see the formation of a very thin dual layer where a top Ag rich layer is formed due to the diffusion of silver from the Ag deficient TiSiN layer below. Independently of these small differences, it can be concluded that the TiSiN system can be considered as an efficient barrier to stop the diffusion of silver as the annealing treatment didn't promote any change in the homogenous distribution of the Ag in the film.

As for the coatings submitted to annealing treatment in oxidizing atmosphere, the phase evolution during in-situ high temperature XRD displayed a change in the preferential orientation of the silver from (111) to

(200). The first signs of oxidation started to appear at 850°C, with the appearance of the TiO_2 rutile peaks. The increase in the intensity of these peaks suggest the increase in the thickness of the oxide scale. At 950°C, a suppression of the Ag peaks starts to be visible which was explained by the evaporation/sublimation of the Ag nanoparticles. TGA analysis in dynamic mode allowed to confirm that silver has no influence on the onset point of oxidation of the films (850°C). However, increasing the silver content leads to an acceleration of the oxidation process, deteriorating the rate at which oxidation occurs. For the coatings with medium silver contents (TiSiNAg6 and TiSiNAg10), a mass loss in the weight gain curves is perceived. This mass loss was attributed to a competitive process occurring between silver aggregation and silver evaporation/sublimation.

Isothermal TGA tests performed at 800°C in the reference TiSiN film follow a parabolic law which can be explained by the formation of a protective Si-O layer. When the isothermal temperature was increased to 900°C, the curves follow two distinct laws. At the very beginning, a normal parabolic law, then, a linear law defines the oxidation process. The oxidation rate is governed by the Ti ions able to disrupt the protective Si-O layer and, thus, creating a porous Ti-Si-O layer instead. Coatings with low and medium silver contents (TiSiNAg2, TiSiNAg6 and TiSiNAg10) oxidized at 800°C show an oxidation weight gain slightly higher than that of the reference TiSiN. In the initial part of the process, the oxidation seems independent of the silver content in the films. However, for the coating with the highest silver content, the mass gain is much higher evidencing the deteriorating effect of the silver on the oxidation resistance. Despite these observations, yet again it was possible to realize that in the un-oxidized part of the film, the silver continued to be homogeneously distributed confirming that the TiSiN system can act as an effective barrier to the diffusion of silver.

Now that the oxidation behaviour of these coatings was conducted, the following chapter will take the characterization one step further by approximating the testing conditions to that of the in-service machining. Thus, Chapter VI will assess the friction and wear during the tribological tests conducted at increasingly higher temperatures and with a counterbody composed of the same material as the alloy of interest (TiAl6V4).

5.3 References

[1] S. Veprek, M.G.J. Veprek-Heijman, P. Karvankova, J. Prochazka, Different approaches to superhard coatings and nanocomposites, Thin Solid Films, 476 (2005) 1-29.

[2] Y.X. Xu, L. Chen, Z.Q. Liu, F. Pei, Y. Du, Improving thermal stability of TiSiN nanocomposite coatings by multilayered epitaxial growth, Surface and Coatings Technology, 321 (2017) 180-185.

[3] C.P. Mulligan, T.A. Blanchet, D. Gall, CrN–Ag nanocomposite coatings: Effect of growth temperature on the microstructure, Surface and Coatings Technology, 203 (2008) 584-587.

[4] W. Ernst, J. Neidhardt, H. Willmann, B. Sartory, P.H. Mayrhofer, C. Mitterer, Thermal decomposition routes of CrN hard coatings synthesized by reactive arc evaporation and magnetron sputtering, Thin Solid Films, 517 (2008) 568-574.

[5] F. Fernandes, T.B. Yaqub, A. Cavaleiro, Influence of Ag additions on the structure, mechanical properties and oxidation behaviour of Cr-O coatings deposited by HiPIMS, Surface and Coatings Technology, 339 (2018) 167-180.

[6] A.G. Bembel, On the Size Dependences of the Metallic Nanoparticle Evaporation and Sublimation Heats: Thermodynamics and Atomistic Modeling, Russian Physics Journal, 59 (2017) 1567-1574.

[7] V.M. Samsonov, S.A. Vasilyev, A.G. Bembel, Size dependence of the melting temperature of metallic nanoclusters from the viewpoint of the thermodynamic theory of similarity, The Physics of Metals and Metallography, 117 (2016) 749-755.

[8] F. Deschaux-Beaume, T. Cutard, N. Fréty, C. Levaillant, Oxidation of a Silicon Nitride-Titanium Nitride Composite: Microstructural Investigations and Phenomenological Modeling, Journal of the American Ceramic Society, 85 (2002) 1860-1866.

[9] J.B. Choi, K. Cho, M.-H. Lee, K.H. Kim, Effects of Si content and free Si on oxidation behavior of Ti–Si–N coating layers, Thin Solid Films, 447-448 (2004) 365-370.

[10] F. Fernandes, J. Morgiel, T. Polcar, A. Cavaleiro, Oxidation and diffusion processes during annealing of TiSi(V)N films, Surface and Coatings Technology, 275 (2015) 120-126.

[11] M. Diserens, J. Patscheider, F. Lévy, Mechanical properties and oxidation resistance of nanocomposite TiN–SiNx physical-vapor-deposited thin films, Surface and Coatings Technology, 120-121 (1999) 158-165.

[12] F. Vaz, L. Rebouta, M. Andritschky, M.F. da Silva, J.C. Soares, The effect of the addition of Al and Si on the physical and mechanical properties of titanium nitride, Journal of Materials Processing Technology, 92-93 (1999) 169-176.

[13] F. Vaz, L. Rebouta, P. Goudeau, J. Pacaud, H. Garem, J.P. Rivière, A. Cavaleiro, E. Alves, Characterisation of Ti1−xSixNy nanocomposite films, Surface and Coatings Technology, 133-134 (2000) 307-313.

[14] J. Patscheider, T. Zehnder, M. Diserens, Structure–performance relations in nanocomposite coatings, Surface and Coatings Technology, 146-147 (2001) 201-208.

[15] H.J.T. Ellingham, Reducibility of oxides and sulphides in metallurgical processes, Journal of the Society of Chemical Industry, 63 (1944) 125-133.

CHAPTER VI - High Temperature Tribological Behaviour of Ti-Si-(Ag)-N Coatings

The importance of Ag content for optimizing the machining performance of Ti-Si-(Ag)-N coatings

6 Introduction

As Chapter V dealt with the thermal characterization of the TiSiNAg coatings and having the basic characterization done in Chapter IV, the following step is now coming closer to the in-service machining performance of the coatings by first analysing their behaviour in terms of friction and wear performance. Thus, this chapter will allow to assess and determine the expected friction and wear behaviour of the TiSiNAg coatings while also using test conditions that try to mimic and approximate the environment to that generated during the machining of titanium alloys.

The coatings tribological performance were evaluated at room and at high temperatures using a high temperature pin-on-disc tribometer while sliding against two different types of counterbodies. First, an analysis pertaining the tests conducted against alumina counterbodies is done, to accelerate the wear and estimate the specific wear rate of the coatings, followed by tests against the TiAl6V4 counterbodies, to try to mimic real test machining conditions. After the tests, characterization of wear tracks was conducted by using 2D profilometry to attain the wear track depth and wear track profile to calculate the volume loss and by SEM-EDS to characterize the wear mechanisms taking place on the wear track and wear debris.

Based on the observations found on the previous chapter and taking into account that the tribology tests were conducted at different premises (Netherlands and India), the TiSiNAg2 coating was removed from the testing since it presented a similar behaviour to that of the TiSiN coating. Moreover, by eliminating the TiSiNAg2 coating, the number of different tests conducted at the premises were able to be increased, keeping a proper range of different silver contents (0, 6, 10 and 17 at.%).

As a side note, it should also be highlighted here that since the tests with alumina and TiAl6V4 were conducted at different premises and in order to compare the friction performance of the coatings against each ball, the friction curves showed in this chapter are plotted normalized to the TiSiN coating with an assumed COF value in the steady state of 1.

6.1 Results

6.1.1 Alumina counterbody (Al_2O_3)

The normalized friction curves of the coatings tested against alumina balls at room temperature and 600°C are shown in Figure VI-1. At room temperature, the friction curves exhibit two different regimes: a

running-in period followed by a steady state regime. During the running-in period, the contact stresses and the initial contact interaction of "irregular" asperities from both the film and the counterpart can lead to the observed increase in the COF values; then, the contact starts to "adapt" establishing a stable wear mechanism and consequently a stable COF. The COF curves at the steady state stage are relatively smooth and constant. Addition of silver shows no influence on the coefficient of friction with the TiSiNAg6 coating exhibiting a similar value to that of the reference. Similar behaviour was observed by Köstenbauer et al. [1] for TiN(Ag) nanocomposite coatings tested at RT against alumina balls, where, for silver contents up to 22 at.%, the COF values remained similar to that of the reference TiN. Note that further increasing the silver content shows a slight decrease in the coefficient of friction; however, as it will be explained later during the wear mechanisms analysis, the sliding was occurring against the adhesion interlayer, which masks the real COF value. As referred to before in Chapter III in section 4.3, the number of cycles for these two films was lowered to 1500 cycles. Despite this, the wear was still high enough to quickly expose the inter/gradient layer.

At 600°C, normalized COF values for the TiSiN and TiSiNAg6 films are higher than those tested at RT. As it will be explained later this can be attributed to the type of wear debris formed on the wear track of the films. Also, a progressive decrease in the COF of the films is now observed with increasing silver contents up to 10 at.%. Further Ag additions do not seem to influence the COF. Similar tendency was observed for TiN/Ag [1] and CrN/Ag [2] coating systems when sliding against alumina balls at 500°C and 600°C testing temperatures, respectively.

a)   b)
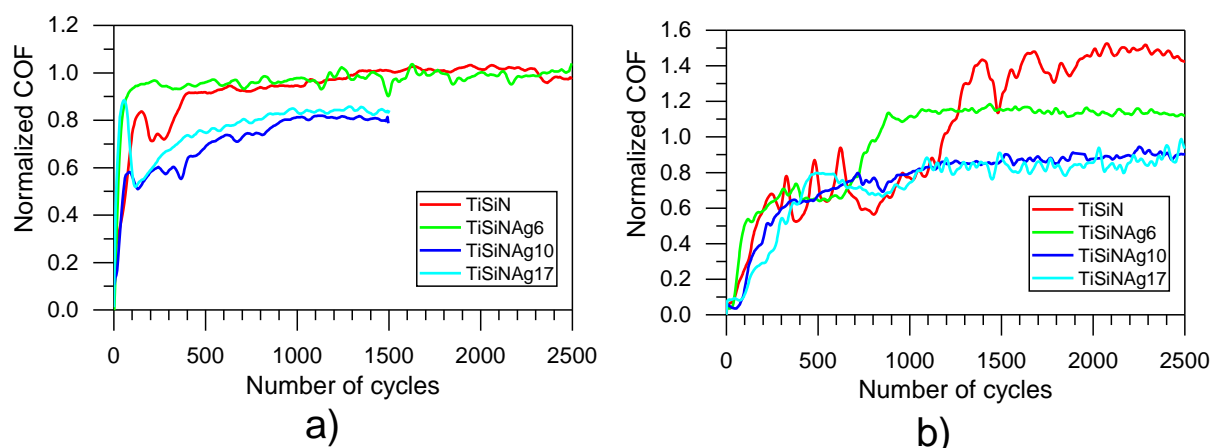
Figure VI-1 Normalized friction coefficient values as function of the number of cycles of the TiSiNAg coatings tested against alumina balls for: a) RT and b) 600ºC

The specific wear rate of the coatings tested at both room temperature and 600°C is shown in Figure VI-2. At room temperature, reference TiSiN coating shows the lowest wear rate of all the coatings. Specific

wear rate of reference film is in the range of those found in the literature [3-5]. With increasing amount of Ag content in the films, a deterioration on the wear rate is clearly observed, well correlated with the trend observed with the hardness. In fact, the wear rate for the two coatings with the highest silver content (TiSiNAg10 and TiSiNAg17) was not possible to be conveniently measured since, due to the fast wear-out of the coatings, most of the contact occurs as a counterbody/gradient interlayer interface. Even with a much lower number of cycles, it was still not possible to keep wear depths in acceptable values, corroborating that increasing silver content does deteriorate the wear resistance of the coatings at room temperature. These results are in accordance to the hardness of the coatings since, at low temperatures, the hardness is one of the most important parameters ruling the contact, helping to prevent both micro and macro scale ploughing and abrasion [6, 7], effectively reducing the wear. A similar tendency was observed by Dang et al. [8] with TiSiN(Ag) coatings which, although sliding against WC-6%Co balls, initially, displayed a decrease in the specific wear rate for Ag contents up to 8 at.% followed by a degradation of the tribological behaviour for higher silver contents due to the decrease in the mechanical properties.
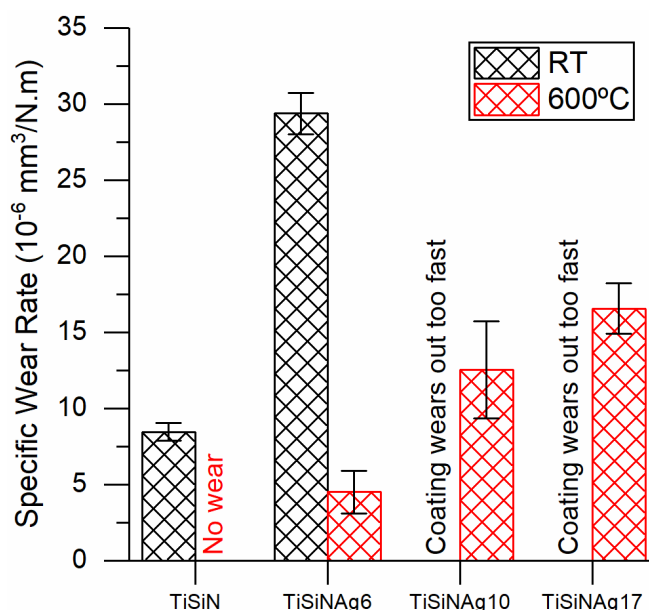
Figure VI-2 Specific wear rate of the TiSiNAg coatings tested at RT and 600ºC sliding against alumina balls

Nevertheless, these coatings are not to work at room temperature and, in this sense, when the temperature increases to 600°C, it is possible to observe a general decrease in the specific wear rates for all the coatings when compared to the tests at room temperature which suggests that silver, besides hardness, is now having a significant role in the wear of the coatings. Reference TiSiN exhibits no observable wear although the wear track, when observed by SEM-EDS, shows a tribofilm of alumina formed over the coating which explains the low wear rate achieved for this coating as it will be shown

later and explained in more detail when the wear mechanisms analysis is conducted. In spite of the better behaviour in relation to RT tests, increasing the Ag content in the films still shows a deterioration in the wear resistance. This behaviour shows the first signs of the potential lubrication effect of Ag. Although the temperature is not high enough to allow the full effect of Ag as a lubricant agent for high temperatures, it starts to show its influence, in relation to the reference TiSiN coating, in providing an anti-adherent ability, as it will be seen more prominently in the tests conducted against the TiAl6V4 balls in section 6.1.2. However, the lubrication effect is not efficient enough to sufficiently decrease the COF and protect the surface against the wear. Then, the resistance to abrasion provided by the mechanical strength is more effective in the coatings with lower Ag contents due to their higher hardness. To help to interpret the changes on the friction and specific wear rate described above and to confirm our preliminary explanation to the effect of Ag at 600 °C tests, a detailed analysis of the worn surfaces of the sliding contact was performed to better understand the wear mechanisms.

The wear track micrographs of the tested coatings at room temperature and at 600°C are shown on Figure VI-3. Reference TiSiN film displays a smooth wear track (Figure VI-3a$_1$). When silver content is increased to 6 at. % (Figure VI-3b$_1$), wear debris are formed due to the plastic deformation/failure of the film. EDS analysis conducted at the fish-like type wear debris (Figure VI-4i) revealed that they consist of oxidized material from the film mixed with some debris detached from the ball, hence the aluminium signal. Similarly, Fernandes et al. [4] observed this kind of wear debris on the worn surface when TiSiN coatings alloyed with vanadium were submitted to pin-on-disc tests at room temperature against Al$_2$O$_3$ counterparts. Due to the movement of the ball, asperities will brake producing free wear particles from either the film or the counterpart. The continuous sliding movement of the ball will drag the wear debris against the film surface promoting their oxidation and contributing to the continuous removal of the coating. The wear in the reference TiSiN film is governed by plastic deformation and micro scale abrasion. The very high hardness and higher resistance to plastic deformation, in relation to Ag-containing coatings, justifies the much better wear resistance of the TiSiN film. When 6 at.% of Ag is added to the film, the hardness and resistance to plastic deformation decreases and, consequently, a higher rate of material removal from the film occurs, with the formation of bigger wear debris. The smashing of the wear debris, their oxidation and adhesion to both elements of the contact pair, make that no improvement in the frictional behaviour can be observed in relation to the reference film. The contact between ductile metals is well known to lead to high friction coefficients [9]. Further Ag content increase (TiSiNAg10 and TiSiNAg17) led to a more severe wear mechanism promoted by the adhesion of higher amounts of wear debris to the sliding surfaces (Figure VI-3c$_1$ and VI-3d$_1$), their oxidation and the consequent higher removal

of material. The wear rate significantly increases and the exposure of the interlayer/adhesion layer occurs (see EDS in Figure VI-4ii), showing the detrimental effect of silver on the wear resistance of the films. Although the interlayer was exposed, some zones of the wear track are still intact which allow to confirm that the wear, for these coatings, is still being governed by the decrease in the mechanical strength.
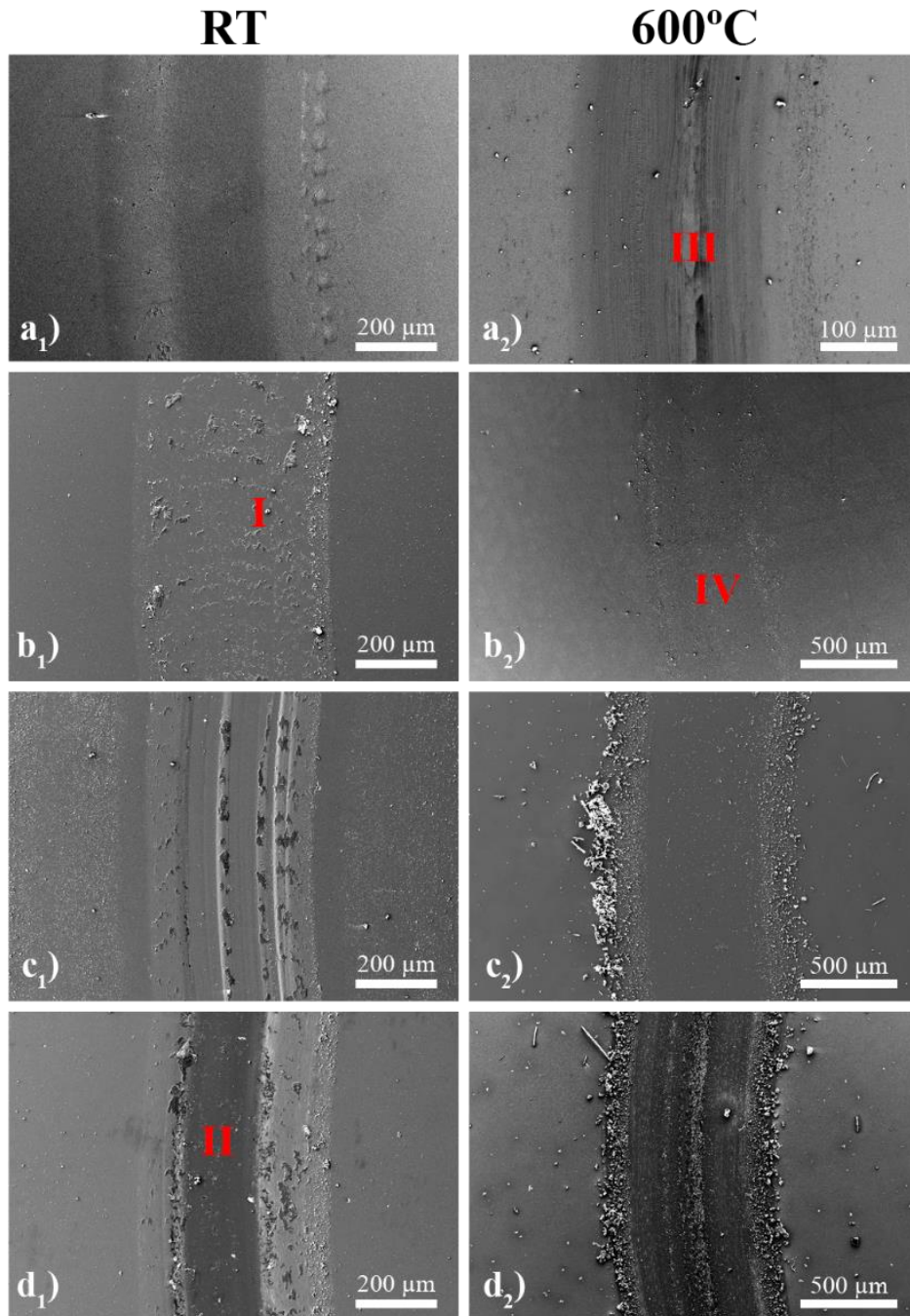
Figure VI-3 Wear track micrographs of the TiSiNAg coatings sliding against alumina balls tested at room temperature and 600ºC: a) TiSiN, b) TiSiNAg6, c) TiSiNAg10 and d) TiSiNAg17. Index 1 for RT and index 2 for 600ºC. Roman numerals correspond to EDS analysis zones

Figure VI-4 Zoomed micrographs and correspondent EDS spectras of zones I and II in Figure VI-3, of the TiSiNAg coatings tested at RT: i)TiSiNAg6 (Zone I) and ii) TiSiNAg17 (Zone II)

At 600°C, a continuous and homogenous tribolayer is observed adhered to the wear track of reference TiSiN film (Figure VI-3a$_2$), from which EDS revealed to be comprised of a mix of Ti, Si, Al and O (Figure VI-5i) suggesting that it corresponds to a mixture of Ti-O and Si-O oxides, caused by the oxidation of the film, and Al-O debris due to the wear of the ball. A continuous Ti-Si-Al-O rich tribolayer is thus established on the top of the film being the wear performance governed by the contact of the adhered tribolayer with the surface of the ball (ceramic on ceramic). This interaction may justify the higher COF of this film at 600 °C (see Figure VI-1b). Similar behaviour was observed by Ming-Chang et al. [10] when sliding ceramic-ceramic pairs in atmospheric conditions. When silver content increases, a noticeable change of the wear mechanism is observed. TiSiNAg6 and TiSiNAg10 (Figure VI-3b$_2$ and VI-3c$_2$, respectively) displayed a smooth wear track with small free wear debris evenly distributed on the wear track with no visible signs of abrasion or adhesion. SEM/EDS analysis revealed the presence of small abrasion grooves and two types of particles on the surface (Figure VI-5ii): 1) very small silver particles evenly distributed throughout the whole analysed area and 2) alumina wear debris, detached from the ball, and loosely bond to the wear track surface (EDS in Figure VI-5ii). The higher the concentration of Ag on the films, the

higher the number and size of Ag particles in the wear track. Due to temperature and movement of the ball, wear debris from the film can oxidize and, together with particles of the ball, slide against the surface of the film promoting material removal. However, the presence of the Ag clusters in the contact will: i) act as low friction agents reducing the friction, as shown in Figure VI-1b (at this temperature the mechanical behaviour of Ag is significantly reduced showing very low shear strength), and, ii) avoid the adhesion of wear debris and the formation of a continuous adhesion layer of the oxidized particles. The wear debris are impeded from adhering to the wear surface and instead, some are spread out to the border of the track (see Figure VI-3c$_2$ and VI-3d$_2$). However, those remaining in the contact will contribute to higher removal rates of the less hard films, keeping the wear rate still higher in relation to the reference TiSiN film. The progressive decrease of hardness and resistance to plastic deformation is still the main parameter ruling the wear. Nonetheless, silver has a positive effect in avoiding the adhesion of material to the wear surface which, as it will be discussed for the TiAl6V4 counterbody, is a beneficial aspect.
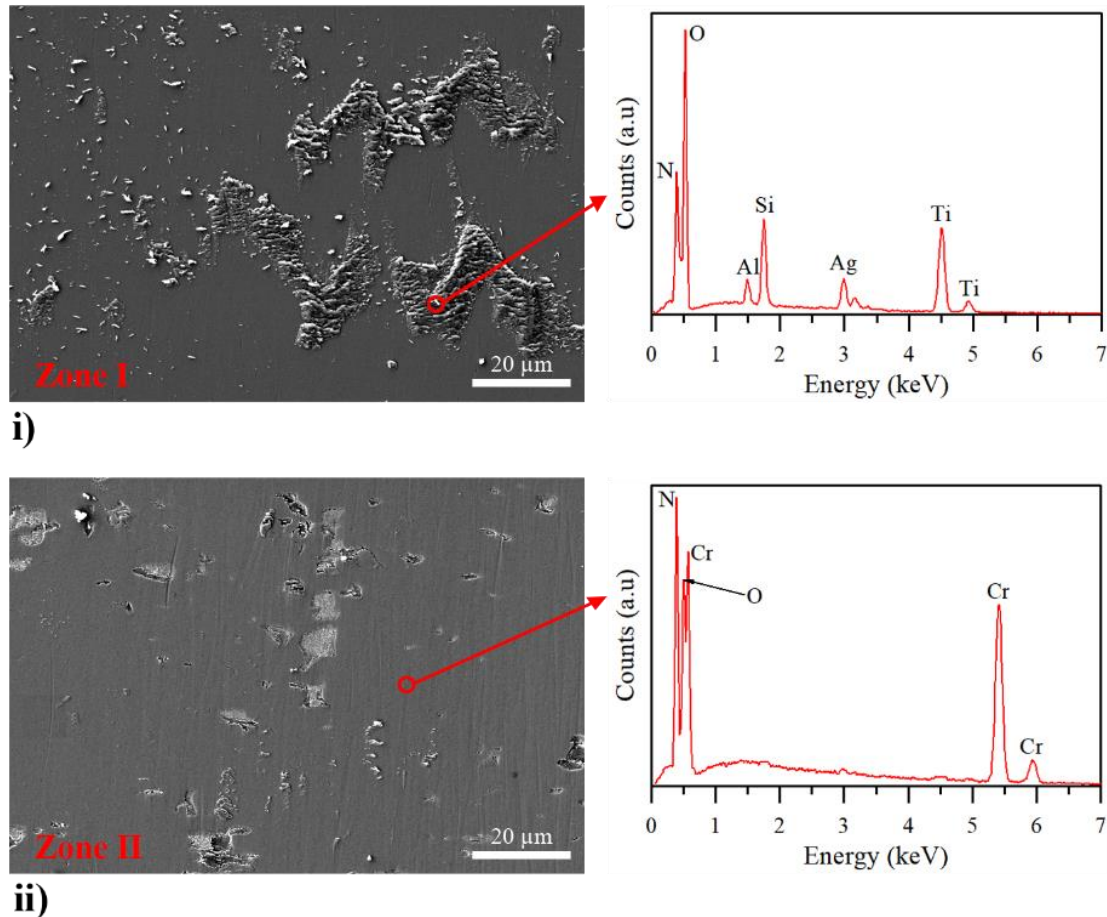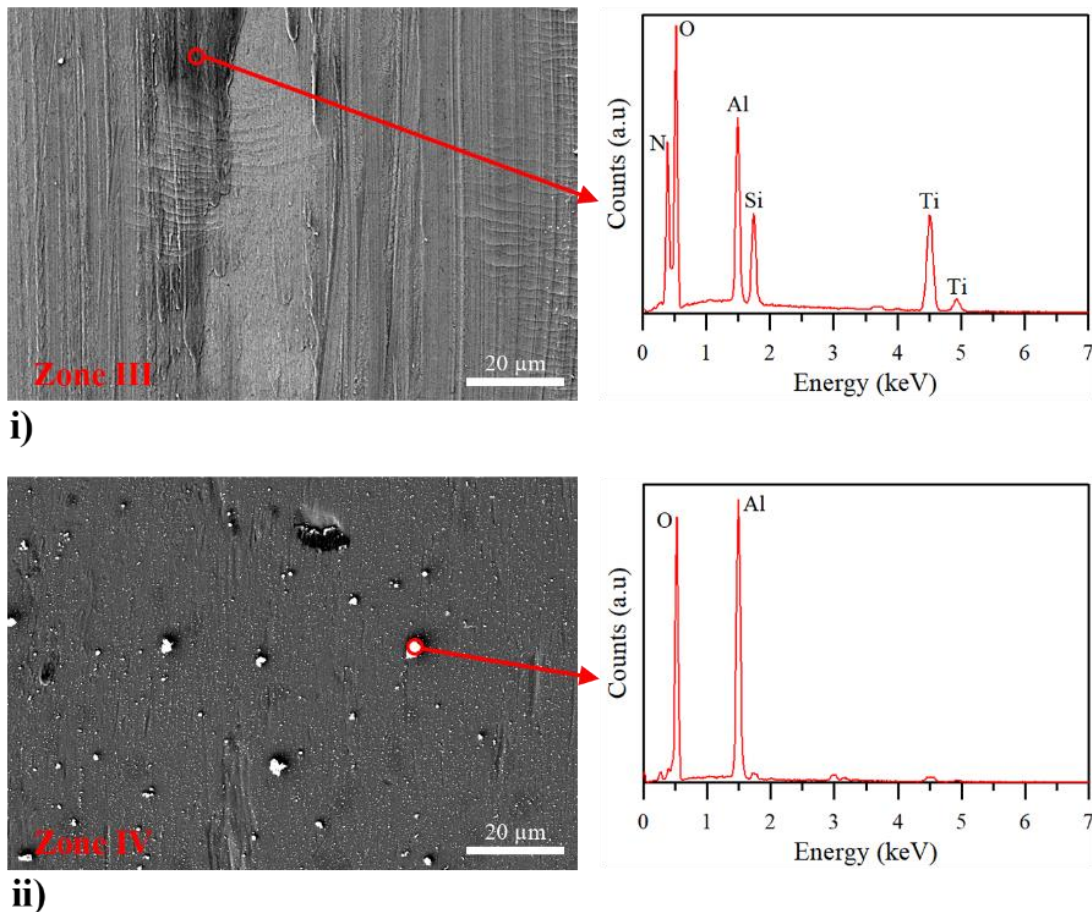

Figure VI-5 Zoomed micrographs and correspondent EDS spectras of zones III and IV in Figure VI-3, of the TiSiNAg coatings tested at 600ºC: i)TiSiN (Zone III) and ii) TiSiNAg6 (Zone IV)

6.1.2 Grade 5 titanium alloy counterbody (TiAl6V4)

Figure VI-6 shows the coefficient of friction curves for the TiSiNAg films submitted to pin-on-disc tests at different temperatures sliding against TiAl6V4 balls. Starting with room temperature, all the coatings exhibit similar curves, relatively smooth and with stable values of coefficient of friction. Opposite to what was observed with alumina balls, increasing the silver content gives rise to a noticeable decrease on the COF, with the lowest value being shown by the coating with the lowest amount of silver (TiSiNAg6). However, further increasing of the Ag content to the highest amount (TiSiNAg17) leads to an increase in the COF, which will be, later, tentatively explained by the unstable porous matrix left right below the top layer by the silver particles dragged during the sliding process. Similar evolution of COF was observed by Basnyat et al. [11] and Gulbinski et al. [12] where, for CrAlN and Mo$_2$N coatings tested at RT, small amounts of silver led to low COF values whereas, after a certain threshold of Ag content, COF increased again significantly.
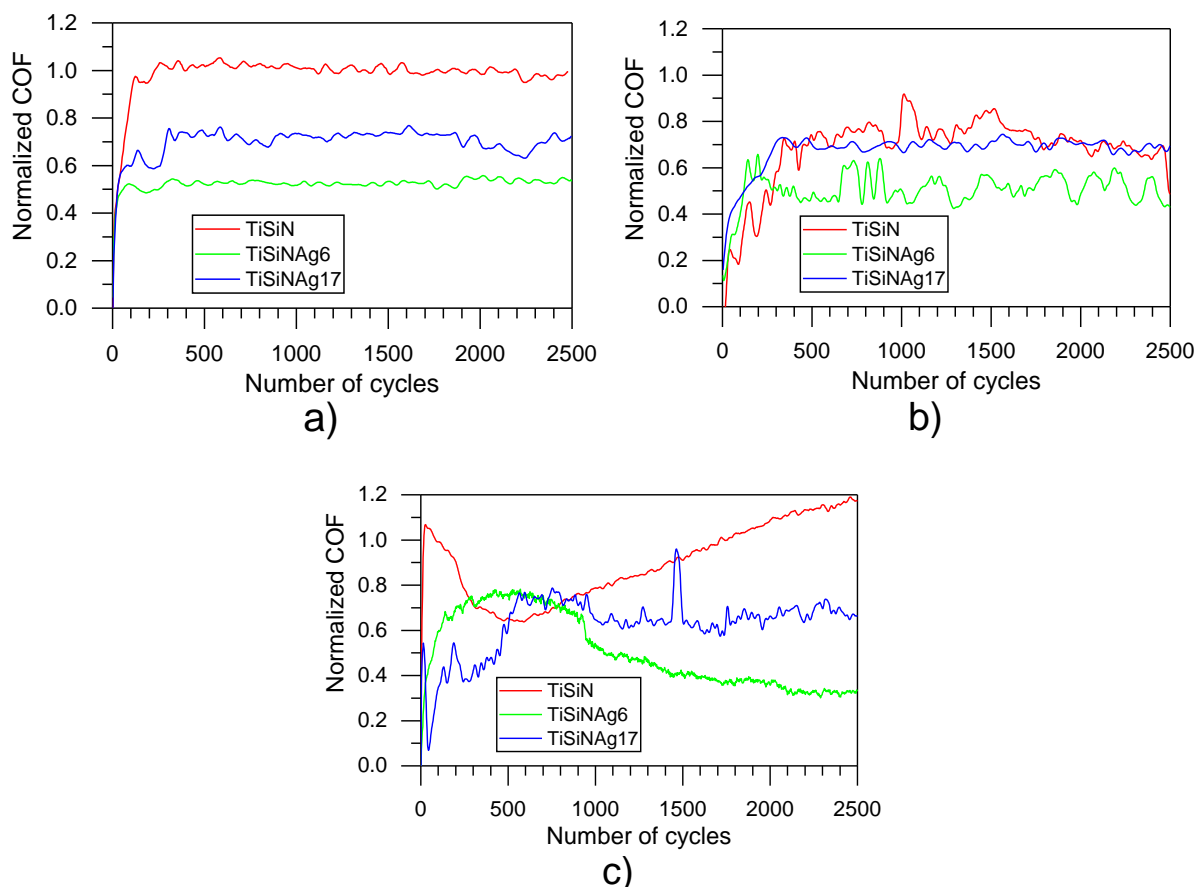
Figure VI-6 Coefficient of friction as a function of number of cycles of the TiSiNAg coatings tested against TiAl6V4 balls for: a) RT, b) 600ºC and c) 900ºC

Moving to the 600°C coefficient of friction curves, it is possible to observe a similar evolution to that of the coatings tested at room temperature. For small amounts of silver (TiSiNAg6), a decrease in the COF value is observed, followed by an increase after further incrementing the Ag content (TiSiNAg17). Although the test temperature is higher, which could suggest higher degree of silver diffusion and consequent different sliding contacts, the COF values for room temperature and 600°C seem to be roughly the same, indicating similar sliding conditions, as it will be shown later when the wear mechanisms are analysed.

When increasing the temperature to 900°C, slightly different COF curves are recorded. Reference TiSiN shows two distinct stages: a first one where the COF rapidly decreases, corresponding to the running-in period, and a second stage where the COF, after reaching a minimum value, starts slowly increasing. As it will be shown later, this last part can easily be explained by the complete wear out of the coating, leading to different types of sliding contacts (counterbody successively rubbing against film, interlayers and finally, the substrate). With the addition of Ag (TiSiNAg6), the curve shows the same two stages but inverted in relation to the reference film. Firstly, the COF increases until a maximum, corresponding to the interlocking between asperities and, then, slowly starts decreasing down to values lower than those observed for RT and 600 °C temperatures, suggesting a more prominent role of silver. For further increasing in the silver content, as for the other testing temperatures, the coefficient of friction values are also higher than for TiSiNAg6 sample. In summary and only considering COF results, the testing temperature does not significantly influence the general behaviour of the coefficient of friction. However, silver content shows a beneficial effect up until a certain threshold value.

In many of the tests performed against Ti6Al4V balls, wear was not possible to be measured, since either the formation of a tribolayer over the wear track protects the underneath materials or the coatings delaminated. At room temperature, TiSiN and TiSiNAg6 coatings showed the best results overall, showing no wear. Truly, in both of these coatings, no wear was able to be measured by profilometry. Further increasing the silver content leads to an increase in the wear rate with the TiSiNAg17 coating tested at RT being the only sample for which the wear could be measured (16×10^{-4} mm^3/N.m), confirming that, as already shown for the alumina balls, high contents of Ag deteriorate the wear resistance of the coatings, despite the reduction of COF. Similarly to what occurred with the alumina balls, these results are easily explained taking into account that hardness is the most important parameter ruling the contact at this temperature. Furthermore, the wear mechanism changes from adhesive to a harsher abrasion for the higher silver content (TiSiNAg17), contributing to the observed increase in the wear. These mechanisms will be explained in more detail during the wear mechanisms analysis, later.

Increasing the temperature to 600°C led to an improvement in the overall wear resistance of all coatings. None of the coatings, at this temperature, show any sign of measurable wear which allow to immediately realize that increasing the temperature has a beneficial effect on the wear resistance of the coatings with higher silver contents. This behaviour is similar to what was observed for the alumina balls, again, suggesting that, besides hardness, silver might now have a more important role in the contact. In fact, all the coatings have a similar adhesive mechanism ruling the wear rate despite the increase in silver, opposite to what was observed for the TiSiNAg17 coatings at room temperature. However, since no wear was able to be measured in any of the coatings, it is impossible to directly compare the effect of silver on the wear resistance between the coatings at this temperature. Notwithstanding, as it will be shown later during the wear mechanisms analysis, silver has a significant effect on the amount of adhered material from the ball to the wear surface.

Lastly, when the test temperature increases to 900°C, yet again, in none of the coatings the wear rate was able to be measured, although for different reasons than those of the 600°C tests. Reference TiSiN has no accurate measurement of wear since the film delaminated and was completely worn out. During the test, a big part of the wear took place in a brief first contact stage with the coating, then with the adhesion interlayer and, finally, with the substrate. Softening of the coating, due to the presence of either Ag or pores, and increasing amount of wear debris, that can act as three body abrasion, might explain the decrease in the wear resistance (more details following in the wear mechanisms analysis). Zhu et al. [13] and Fateh et al. [14] observed similar behaviours for TiSiN and TiN(Ag) coatings, respectively, sliding against alumina balls, where after a threshold temperature close to 500°C, the wear rapidly increases. In this case, this threshold temperature is much higher (900°C when compared to 500°C) which might be tentatively explained by the difference in the counterparts, since alumina possesses a much higher hot hardness than the TiAl6V4, effectively making alumina a much harsher test condition. Addition of Ag to the coatings clearly shows the beneficial effect of silver on their wear resistance when the temperature is increased. Similar to the situation at 600°C, wear on these coatings was not able to be measured due to the effect of silver. The much higher temperature could enhance the silver diffusion at the surface which potentially eliminates the adhesion of the material from the ball to the wear surface. Moreover, Ag can act as a lubricant, effectively reducing the friction (see Figure VI-6c) and wear, as it will be seen later. Finally, further increments of silver (TiSiNAg17) leads to the delamination of the film, due to lack of adhesion. Therefore, this film will not be subject to further studies at this temperature, since no proper tribological analysis can be conducted. All the previous statements show, that the increasing of the

temperature and of the silver content up to a threshold value has a beneficial effect on the wear resistance of the coatings against Grade 5 titanium alloy.
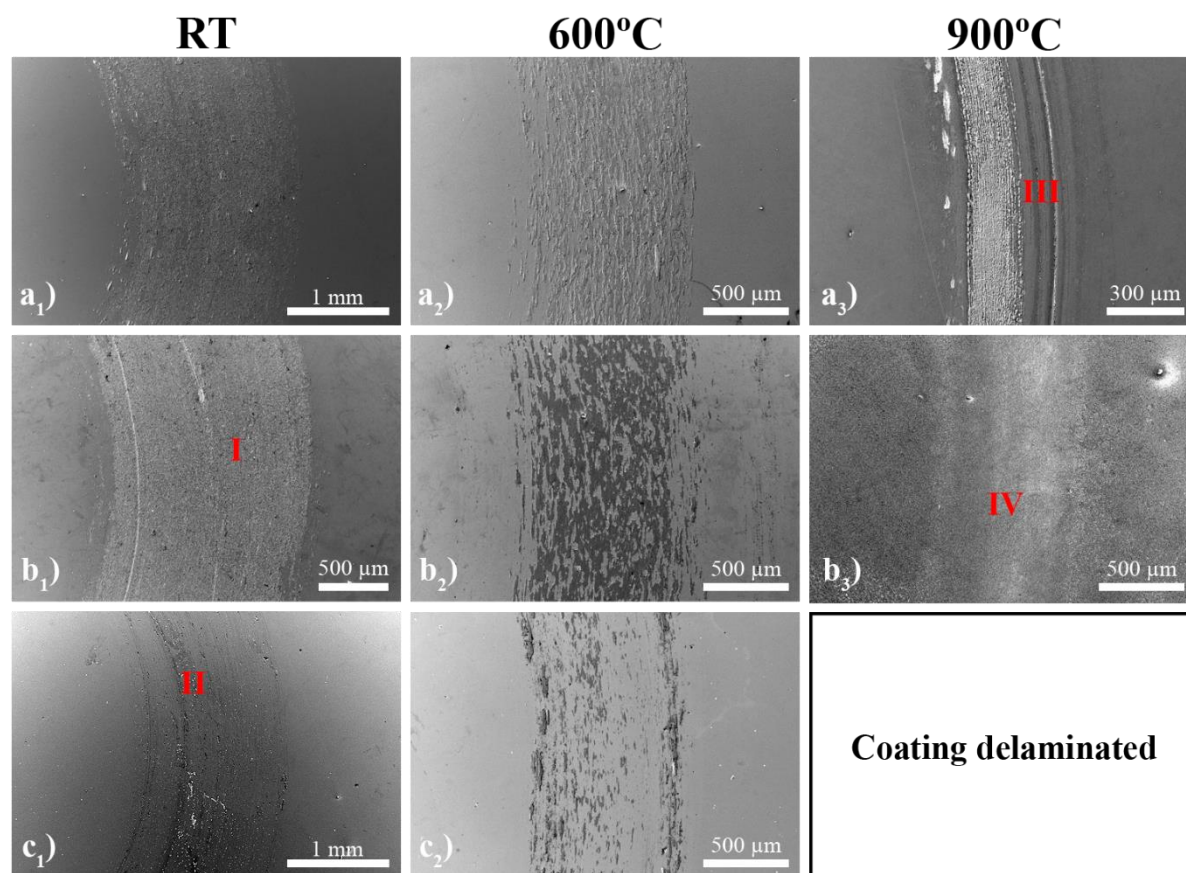
Figure VI-7 Wear track micrographs of the TiSiNAg coatings sliding against TiAl6V4 balls tested at room temperature, 600ºC and 900ºC: a) TiSiN, b) TiSiNAg6 and c) TiSiNAg17. Index 1 for RT, index 2 for 600ºC and index 3 for 900ºC. Roman numerals correspond to EDS analysis zones

The wear track micrographs of the tested coatings at room temperature, 600°C and 900°C are shown in Figure VI-7. At room temperature, the first thing to notice is that the wear tracks are different with the increasing amounts of silver. TiSiN coating (Figure VI-7a$_1$) exhibits the typical adhesive wear mechanism with a considerable amount of adhered material from the ball. However, no measurable wear was achieved, which might mean that the oxides formed from the material of the ball are actually having a protective effect. Likewise, increasing the Ag content for small amounts (TiSiNAg6) sees no change in the wear mechanism, also having high amounts of adhered material on the wear surface (Figure VI-7b$_1$). The wear on this coating was also not possible to be measured, however, the friction is lower than that of reference film (see Figure VI-6a). Both coatings having the same wear mechanism and no measurable wear can be tentatively explained by the combination of the superficial silver and the adhered material from the ball that form a protective tribofilm, reducing the COF. EDS measurements taken in the tribolayer

(Figure VI-8i) shows and a complex mixture of oxides, including Al-O which confirms that a part of the tribolayer is coming from the counterbody (TiAl6V4). Further increasing the Ag content reveals a clear change in the wear mechanism to a harsher abrasion (Figure VI-7c$_1$). On the other hand, a considerable amount of grooves are observed in the wear track that EDS analysis revealed to have material from the ball (Figure VI-8ii), i.e., for this sample, the material from the ball got ploughed inside the coating. In the surface, there are also several visible pits which, as suggested before, are created by the Ag agglomerates dragged from the sample. This effect combined with the lower hardness of the coatings, lead to either mechanical interlocking or the easy "scratching" of the sample, contributing to the observable increase in the friction (see Figure VI-6a) and wear.

Figure VI-8 Zoomed micrographs and correspondent EDS spectras of zones I and II in Figure VI-7, of the TiSiNAg coatings tested at RT: i)TiSiNAg6 (Zone I) and ii) TiSiNAg17 (Zone II)

TiSiNAg coatings at a temperature of 600°C perceive that, from a general perspective, all the coatings now exhibit the same adhesive wear mechanism with material from the ball being adhered to the wear track (Figure VI-7). No measurable wear was possible to be obtained for any of the coatings, which corroborates that increasing the temperature promotes a beneficial effect in keeping the material from

the ball adhered to the wear surface serving as a protective tribolayer, reducing the wear. Nonetheless, and perhaps one of the most interesting facts of this work, incorporating silver in the films promotes a decrease in the amount of adhered material on the wear track. It is possible to observe in the micrographs that the amount of adhered material declines with increasing silver content in the coatings. To corroborate this and to have a better visualization of this effect, the 2D profiles obtained from the wear tracks of all the coatings are shown in Figure VI-9. These profiles clearly confirm two things: i) there is no measurable wear in any of the coatings (profile goes up instead of down) and, ii) adhered material decreases with incorporation of Ag (more easily perceived for the TiSiNAg17 profile). This shows that silver, besides helping with the formation of a protective tribolayer, also stops the material from the ball to adhere to the surface which, from a machining perspective, is an interesting result since it helps prevent one of the most common failure of tools when machining titanium alloys, that is the built-up edge formation [15, 16].
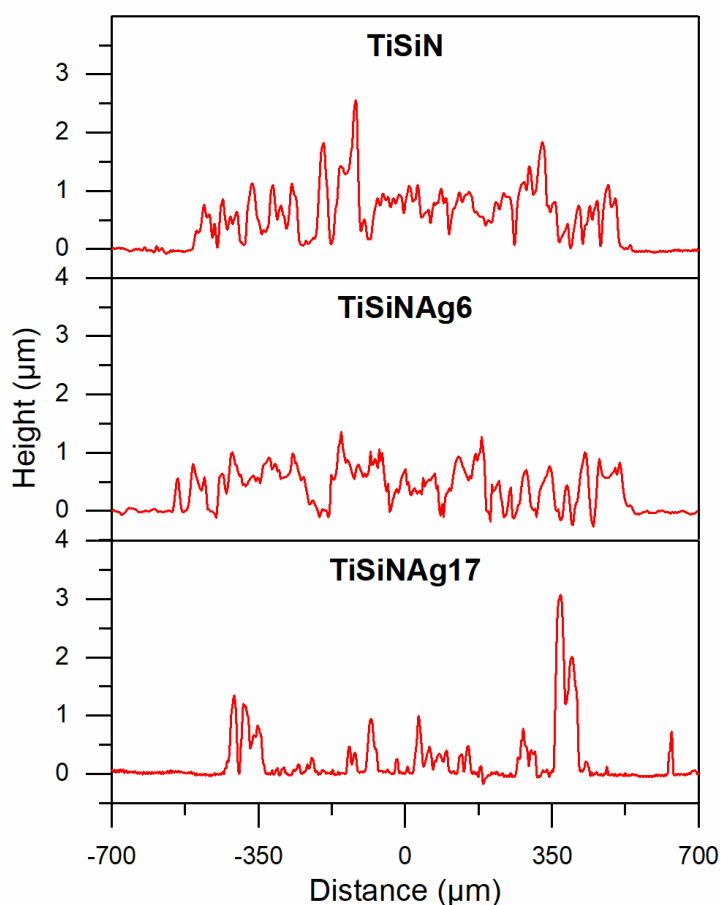
Figure VI-9 2D wear profiles of the TiSiNAg coatings sliding against TiAl6V4 balls at 600ºC

Finally, increasing the test temperature to 900°C leads to the most interesting results of all the tests. As already explained before, the TiSiNAg17 coating suffered from lack of adhesion to the substrate at this

temperature and, therefore, due to lack of proper analysis, it will not be considered in this part of the work. The reference TiSiN has a noticeable decrease in the wear resistance as denoted by the exposed substrate (Figure VI-7a$_3$). However, it seems that the wear is not homogeneous with two distinct regions observable: i) a left side whiter zone where the substrate is exposed and ii) a right side greyer area where some part of the coating still subsists. A zoomed SEM micrograph on this last zone is shown on Figure VI-10i. Looking at the image, it is possible to perceive two distinct zones: A) adhered material from the ball, that in this case, might have acted as a lubricious protective layer and B) removed material from the coating that could be associated to fatigue wear. At this temperature, oxidation of the surface can lead to a less resistant layer which, after a high number of cycles, can lead to accumulation of plastic strain and the consequent fracture, destroying the coating, as seen on zone B in Figure VI-10i. The addition of silver shows the most interesting results of all the tests. TiSiNAg6 show no measurable wear and, more interestingly, no signs of any adhered material from the ball are visible on the wear tracks (Figure VI-7b$_3$). It is also possible to observe that, at this temperature, the diffusion/agglomeration of silver occurs in the surface, as observed by the amount of white particles. A closer analysis of the wear track (Figure VI-10ii) allows to easily perceive that the only mechanism ruling the wear at this very high temperature has to be related with the silver particles. The exclusive presence of silver in the sliding contact has a tremendous beneficial effect on the wear resistance of the coatings, also acting as a lubricious layer, effectively reducing the wear and friction. To show its benefits, silver does not need to form a continuous homogenous layer but only to be present as medium sized particles. Furthermore, silver has another positive effect by completely hindering the adhesion of material from the ball to the surface, as confirmed by the lack of aluminium signal on the EDS in Figure VI-10ii. As explained before, from a machining perspective, this is a very interesting result in the way that it might effectively negate one of the most important failure modes of cutting tools when machining this type of alloys (BUE – built-up edge). Since the effect of silver is clearly more prominent as the test temperature increases, a further positive achievement is found: an increase in the cutting speeds during the machining process can be allowed (since higher cutting speeds lead to higher temperatures in the contact). To summarize, it is clear that increasing the silver content shows a beneficial effect in reducing the friction and increasing the wear resistance of the coatings. Moreover, silver also prevents the adhesion of material from the ball to the wear surface. However, temperature is an important parameter to potentiate the effect of Ag, as Ag benefits tremendously from temperature. In order for Ag to show its true potential, high temperatures have to be present.
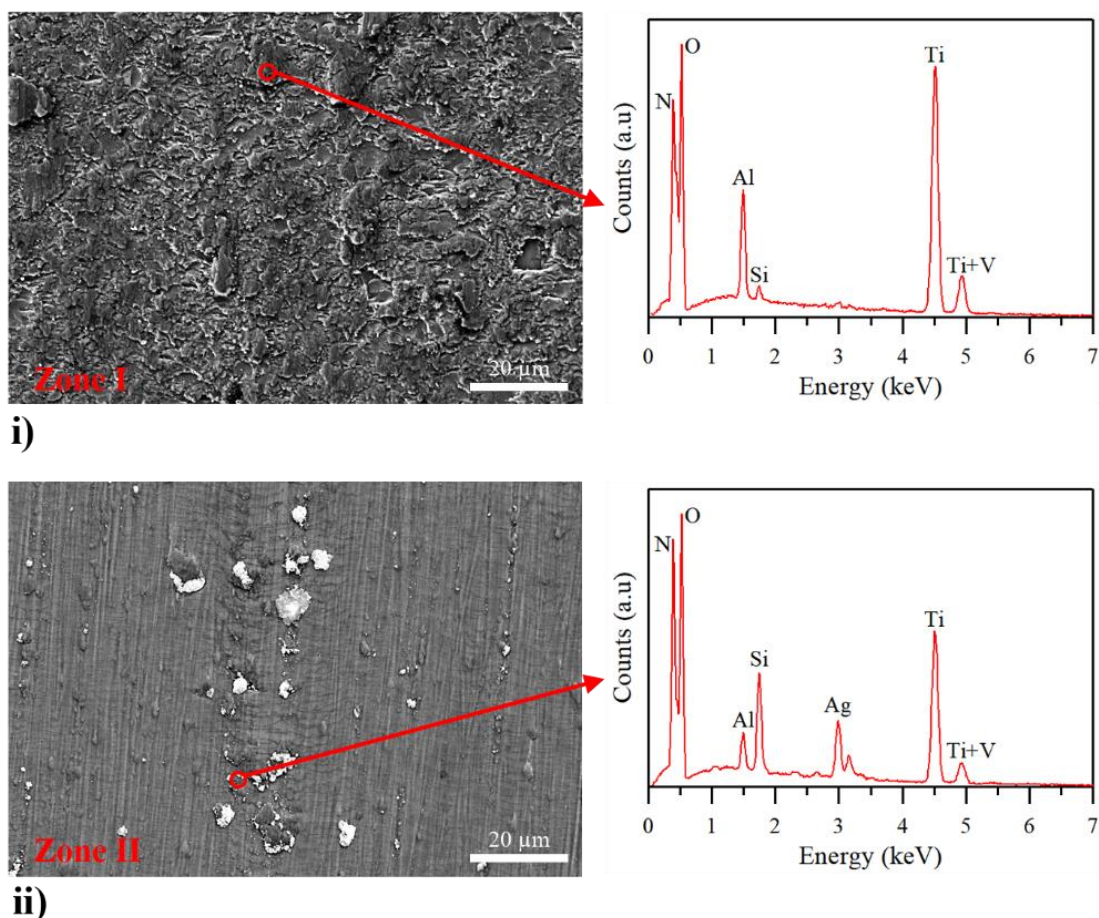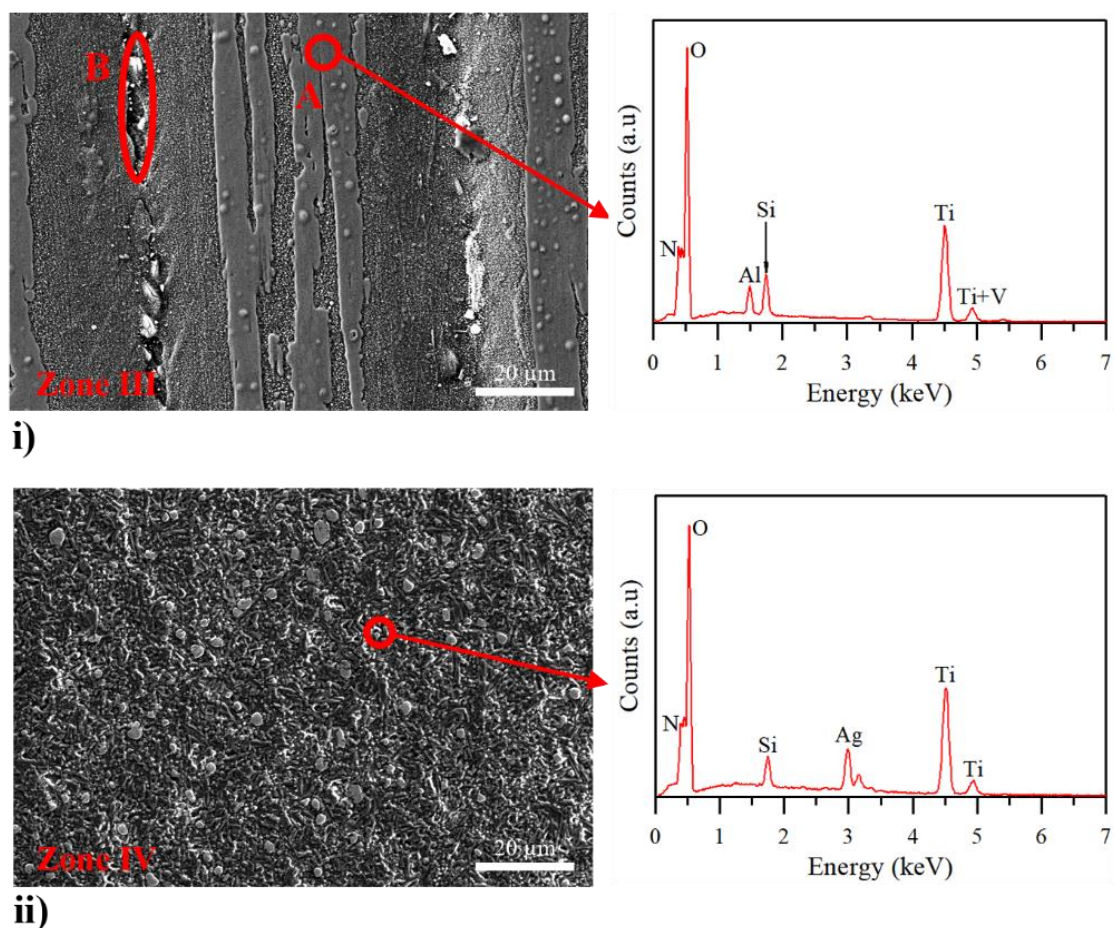
Figure VI-10 Zoomed micrographs and correspondent EDS spectras of zones III and IV in Figure VI-7, of the TiSiNAg coatings tested at 900ºC: i) TiSiN (Zone III) and ii) TiSiNAg6 (Zone IV)

6.2 Conclusions

In this chapter, the tribological behaviour of the TiSiNAg coatings at room and at high temperatures and the influence of silver in this behaviour was assessed. For room temperature tests against the alumina balls, Ag additions clearly show the detrimental effect on the specific wear resistance of the films, independently of the COF decrease for the higher Ag concentrations. This was explained based on the decrease of the hardness of the coatings with Ag increments, which is the most important parameter ruling the wear at RT. At 600°C, a general increase in the wear resistance for all the coatings is observed, however, the reference TiSiN still exhibits the best result overall with no measurable wear. Some signs of the effect of Ag start to be visible although, the main parameter ruling the wear is still the hardness. Notwithstanding, the beneficial effect of silver impending the adhesion of material to the wear surface starts to be shown.

When sliding against TiAl6V4 balls, friction was revealed to decrease with increasing Ag additions, however, no measurable wear was able to be attained for the tests, independently of the temperature. At room temperature and similarly to the sliding experiments against alumina balls, the decrease in the wear resistance for the TiSiNAg17 film can be explained by the hardness decrease. At 600°C, no measurable wear could be attained for any of the coatings. At this temperature, SEM micrographs allow to start perceiving the ability of silver to hinder the adhesion of material to the wear surface, which is much more pronounced at 900°C with low silver amounts (6 at %).

In summary and from a general perspective, tests conducted against TiAl6V4 balls, revealed that silver shows a promising effect in reducing the friction and increasing the wear resistance of the coatings while also adding the beneficial effect, from a machining perspective, of preventing the adhesion of material to the wear surface and thus the formation of undesirable building edges. As such, the following chapter will deal with the in-service machining behaviour of these coatings for increasing cutting speeds (which means increasing temperatures at the contact zone), which will allow to correlate and corroborate the results with the observations found on this chapter.

6.3 References

[1] H. Köstenbauer, G.A. Fontalvo, C. Mitterer, J. Keckes, Tribological Properties of TiN/Ag Nanocomposite Coatings, Tribology Letters, 30 (2008) 53-60.

[2] K. Kutschej, C. Mitterer, C.P. Mulligan, D. Gall, High-Temperature Tribological Behavior of CrN-Ag Self-lubricating Coatings, Advanced Engineering Materials, 8 (2006) 1125-1129.

[3] F. Fernandes, J.C. Oliveira, A. Cavaleiro, Self-lubricating TiSi(V)N thin films deposited by deep oscillation magnetron sputtering (DOMS), Surface and Coatings Technology, 308 (2016) 256-263.

[4] F. Fernandes, T. Polcar, A. Cavaleiro, Tribological properties of self-lubricating TiSiVN coatings at room temperature, Surface and Coatings Technology, 267 (2015) 8-14.

[5] D. Goldbaum, P. Manimuda, G. Kamath, S. Descartes, J.E. Klemberg-Sapieha, R.R. Chromik, Tribological behavior of TiN and Ti (Si,C)N coatings on cold sprayed Ti substrates, Surface and Coatings Technology, 291 (2016) 264-275.

[6] K. Holmberg, H. Ronkainen, A. Matthews, Wear Mechanisms of Coated Sliding Surfaces, in: D. Dowson, C.M. Taylor, T.H.C. Childs, M. Godet, G. Dalmaz (Eds.) Tribology Series, Elsevier, 1993, pp. 399-407.

[7] K. Holmberg, H. Ronkainen, A. Matthews, Tribology of thin coatings, Ceramics International, 26 (2000) 787-795.

[8] C. Dang, J. Li, Y. Wang, Y. Yang, Y. Wang, J. Chen, Influence of Ag contents on structure and tribological properties of TiSiN-Ag nanocomposite coatings on Ti–6Al–4V, Applied Surface Science, 394 (2017) 613-624.

[9] I. Hutchings, P. Shipway, 3 - Friction, in: I. Hutchings, P. Shipway (Eds.) Tribology (Second Edition), Butterworth-Heinemann, 2017, pp. 37-77.

[10] J. Ming-Chang, Y. Li-Yung, Environmental effects on wear behaviour of alumina, Wear, 161 (1993) 111-119.

[11] P. Basnyat, B. Luster, Z. Kertzman, S. Stadler, P. Kohli, S. Aouadi, J. Xu, S.R. Mishra, O.L. Eryilmaz, A. Erdemir, Mechanical and tribological properties of CrAlN-Ag self-lubricating films, Surface and Coatings Technology, 202 (2007) 1011-1016.

[12] W. Gulbiński, T. Suszko, Thin films of Mo2N/Ag nanocomposite—the structure, mechanical and tribological properties, Surface and Coatings Technology, 201 (2006) 1469-1476.

[13] Y. Zhu, M. Dong, J. Li, L. Wang, Wear failure mechanism of TiSiN coating at elevated temperatures, Applied Surface Science, 487 (2019) 349-355.

[14] N. Fateh, G.A. Fontalvo, G. Gassner, C. Mitterer, Influence of high-temperature oxide formation on the tribological behaviour of TiN and VN coatings, Wear, 262 (2007) 1152-1158.

[15] A. Inspektor, P.A. Salvador, Architecture of PVD coatings for metalcutting applications: A review, Surface and Coatings Technology, 257 (2014) 138-153.

[16] S. Pervaiz, A. Rashid, I. Deiab, M. Nicolescu, Influence of Tool Materials on Machinability of Titanium- and Nickel-Based Alloys: A Review, Materials and Manufacturing Processes, 29 (2014) 219-252.

CHAPTER VII - Ag Influence in the Ti-Si-(Ag)-N Coatings During Turning of the TiAl6V4 Aerospace Alloy

The importance of Ag content for optimizing the machining performance of Ti-Si-(Ag)-N coatings

7 Introduction

Taking into account the results encountered in the previous chapters, especially the deterrence of the silver diffusion, the low wear achieved for higher temperatures and the hindering of adhered material to wear surfaces, the next and final step is to take all together and realize if these promising results translate themselves into a proper machining performance. This is the main point of this chapter as it ties everything together to assess the main objective of this thesis that is, as the title implies, the machining performance of the Ti-Si-(Ag)-N coatings.

This chapter will then assess the machining performance for increasing cutting speeds in two distinct environments both without the application of any liquid coolant. First, an analysis of the coatings performance in a laboratorial environment is conducted using a conventional lathe using three different increasing cutting speeds (70, 80 and 100 m/min) allowing to study the effect of silver when the operating temperatures are increased (higher cutting speeds will lead to higher operating temperatures). After this analysis, another study followed by testing the same coatings in an industrial environment at an even higher cutting speed (120 m/min) and by comparing them against a commercial coating commonly used in the machining of this titanium alloys. This last test will allow to benchmark the coating solution proposed in this thesis to eventually be applied in industrial applications. In both the environments, the tool life curves were obtained followed by the study of the wear mechanisms for each of the inserts tested.

Taking into account the results encountered in the previous chapters and having in mind the delamination that occurred at the 900 °C tribology tests for the TiSiNAg17 coating, this same coating was not considered for testing in this chapter. Thus, the coatings considered for the machining tests were then, obviously, the TiSiN which is taken as our reference coating throughout this whole thesis and the "surviving" silver coatings that withstood and presented the most promising results throughout all the characterizations (TiSiNAg6 and TiSiNAg10 coatings).

7.1 Results

7.1.1 Laboratorial tests performance of Ti-Si-(Ag)-N coatings (CNMG 120408-SF inserts)

The flank wear evolution as a function of the machining distance of the uncoated and coated inserts tested at 70, 80 and 100 m/min cutting speeds are shown in Figure VII-1. For the lowest cutting speed of 70 m/min (Figure VII-1a), it is possible to observe that the uncoated tool showed the worst tool life, especially as this insert suffered from premature breakage of the tip (Figure VII-2a).
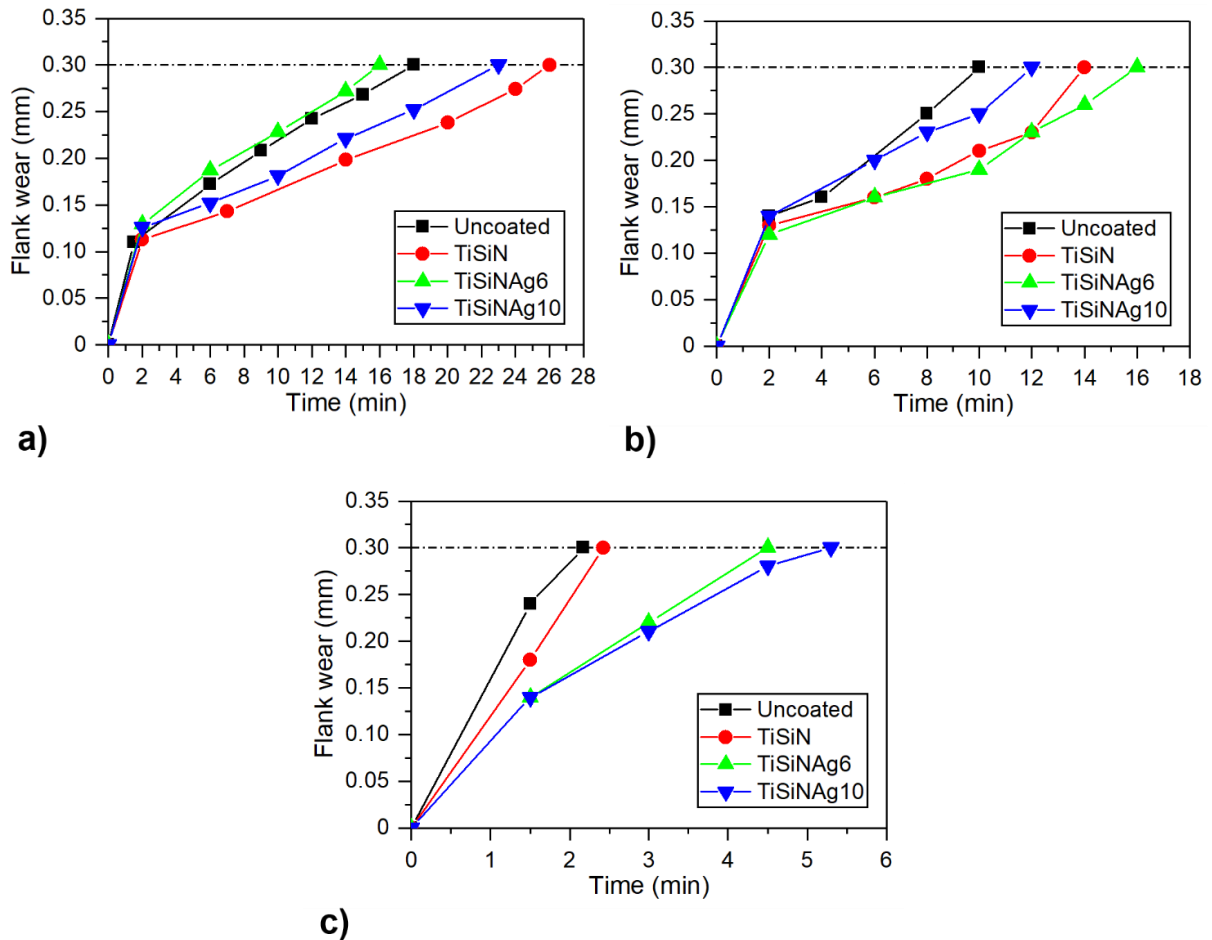
Figure VII-1 Flank wear vs machining time of the uncoated and TiSiN(Ag) coatings for the different cutting speeds: a) 70 m/min, b) 80 m/min and c) 100 m/min

This phenomenon was attributed to the combined effect of an abrasion wear mechanism and the formation of built-up edges as it will be discussed in more detail lately. Furthermore, the curves also show that the reference TiSiN showed the highest tool life (26 min). Silver addition (TiSiNAg6 and TiSiNAg10) to the coatings seems to have no benefits on the tool life, as these inserts showed a tool life only slightly superior to the uncoated one. All-in-all, generally this cutting speed does not generate high temperatures which suggests that the main parameter ruling the wear of the tools is the hardness. Indeed, the reference TiSiN, as the hardest coating of the bunch, clearly shows the best tool life and with the introduction of silver, a decrease on the hardness values occurs and, thus, a deterioration in the tool life. This suggestion, is in accordance with the high temperature tribological behaviour of these coatings reported in Chapter VI. In fact, for the lowest temperature sliding tests against TiAl6V4 balls, the coatings containing silver showed a deterioration in the wear resistance in relation to TiSiN one, due to the decrease in the hardness.

When the cutting speed is increased to 80 m/min (Figure VII-1b), a significant improvement of the machining performance of the TiSiNAg6 coating, side by side with the reference TiSiN, is observed. That

coating presented the highest tool life among all the coatings, suggesting that now, the introduction of silver in the coatings might actually show a benefit role in the tool life. With this cutting speed, the uncoated and TiSiNAg10 tools show the worse performances. Undoubtedly, increasing the silver content up to a certain threshold (6 at. %) leads to an increase in the tool life when compared to the reference TiSiN. This behaviour can be explained by the compromise between the hardness of the tools and the higher temperature reached induced by the increase in the cutting speed. On one hand, the achieved temperature can be enough to promote the lubricious effect of the silver; however, on the other hand, the hardness must still rule the wear rate, since the TiSiNAg10 coating does not show a good performance in spite of its higher amount of silver while the TiSiNAg6 coating still displays a relatively high hardness and enough Ag to get the combination of benefits that propels this coating to display the best tool life. The reference TiSiN coating, benefits from its highest hardness still presenting a high tool life. Nonetheless and despite the lower tool life of the TiSiNAg10 coating, all the coatings show promising results as the estimated tool lives are still relatively high and higher than the uncoated tools.

Finally, when the cutting speed was increased to 100 m/min, the effect of silver as solid lubricant outperforms the hardness effect on the wear. A quick look at the curves in Figure VII-1c shows that, now, the worst coating is actually the reference TiSiN only overtaking the uncoated tool. By adding silver to the coatings the tool life was considerably increased. This suggests, contrarily to what was observed for the lowest cutting speed (70 m/min), that hardness is not the determinant factor on the wear of the inserts. Indeed, the higher cutting speed might now be enough to generate the necessary heat for the silver to develop its lubricious effect, reducing the friction and wear on the tools. These achievements are completely aligned with the previous tribological results found in Chapter VI, where, for a temperature of 900°C, when sliding against TiAl6V4 balls, the addition of silver clearly increased the wear resistance of the coatings. In summary, Ag rich coated inserts show promising results for reducing the tool wear and improving the life of the tools, mainly for high cutting speeds. This performance should result in an increasing material removal rate in the machining of Ti alloys without using any liquid lubrication.
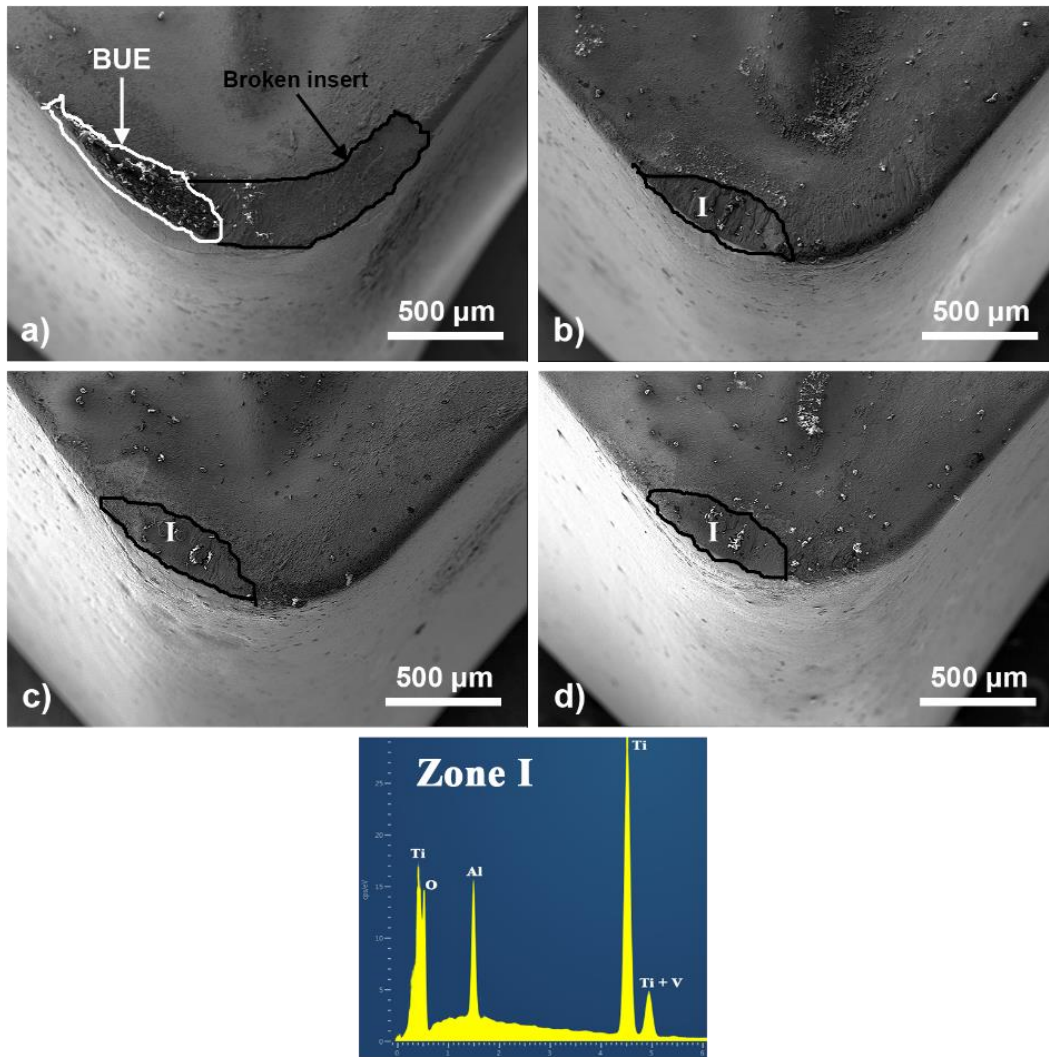
Figure VII-2 Post-mortem SEM micrographs of the tips of the inserts for the cutting speed of 70 m/min and correspondent zones EDS spectra: a) Uncoated, b) TiSiN, c) TiSiNAg6 and d) TiSiNAg10

The tip SEM micrographs of all the inserts post-mortem, for the lowest cutting speed (70 m/min), are shown in Figure VII-2. From a general perspective, it seems that the main culprit for the flank wear on the inserts is abrasion promoted by the chip sliding on the insert. In the uncoated tool, the formation of the built-up edge (BUE) in the rake face is observed (Figure VII-2a). The formation of BUEs may lead to the change of the cutting geometry leading to increased flank wear and consequent premature tool failure. Additionally, BUE breakage may lead to the edge fracture due to the welding of the chip to the tool and the weakened cutting edges as it is shown for the uncoated inserts in Figure VII-2a, where it is possible to observe the clear removing of a piece of the insert due to the formation and subsequent breakage of the BUE. For the coated samples, some adherent material can be observed on the worn flank crater (see zone I EDS in Figure VII-2) particularly for the inserts coated with TiSiN (Figure VII-2b), but not contributing for changing the cutting geometry. Take note that the only way to distinguish between the signals from

the coating and from the workpiece is through the presence of the aluminium signal since titanium is common to both and the vanadium signal is overlapped with the titanium signal. No signals of breakage are detected which can be attributed to the much harder coatings applied on the inserts which will support the stress and protect the insert. As the tool degradation is due to an abrasion mechanism, the highest tool life of all the samples is directly related to the hardest one.

Figure VII-3 SEM micrographs of the cutting edges in the inserts tested at a cutting speed of 80 m/min: a) Uncoated, b) TiSiN, c) TiSiNAg6 and d) TiSiNAg10

Figure VII-3 displays the post-mortem SEM micrographs of all the inserts tested at 80 m/min. With the exception of the uncoated tool, the worn zones do not show significant changes when compared to those of the 70 m/min tests. Adhered material can be observed in all samples although vestiges of BUEs are only visible in TiSiN (Figure VII-3b) and TiSiNAg6 (Figure VII-3c) coated ones, with predominance in the former. The main wear mechanism it's still abrasion. The uncoated tool (Figure VII-3a) does not show BUE formation and signs of breakage. The abrasion type of wear associated with the lowest hardness of this sample justify the worst tool life of all the tools (see Figure VII-1b). The reference TiSiN (Figure VII-3b) and the TiSiNAg6 (Figure VII-3c) coated inserts display similar tool life curves (see Figure VII-1b). In both cases, the presence of BUE's are visible. Although this would suggest an accelerated wear, Kümmel et al. [1] demonstrated that, depending on the BUE coverage, the BUE can be used as a protective layer

against tool wear. This, combined with the higher hardness of both these coatings helps to explain their higher tool lives. The comparative positive evolution of sample TiSiNAg6 against TiSiN when compared to the 70 m/min tests, TiSiNAg6 now shows the best tool life (see Figure VII-1b), suggesting that, besides the abrasion mechanism, the higher temperature offered by the higher cutting speed starts to make some difference, showing the benefits of the silver. This effect is still not the most relevant in the wear behaviour since the TiSiNAg10 coated insert (Figure VII-3d) does not perform as well as the other coated samples. Its lower hardness combined with the harsher abrasion leads to the premature tool failure and lower tool life.
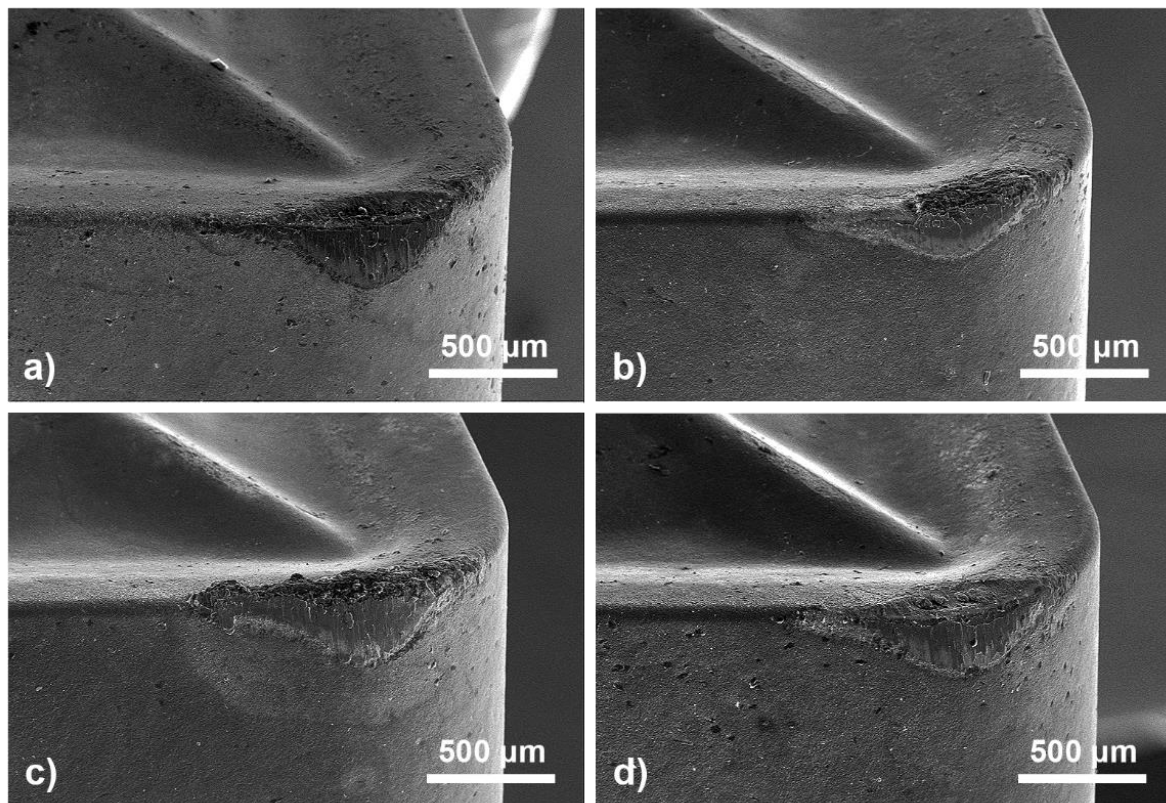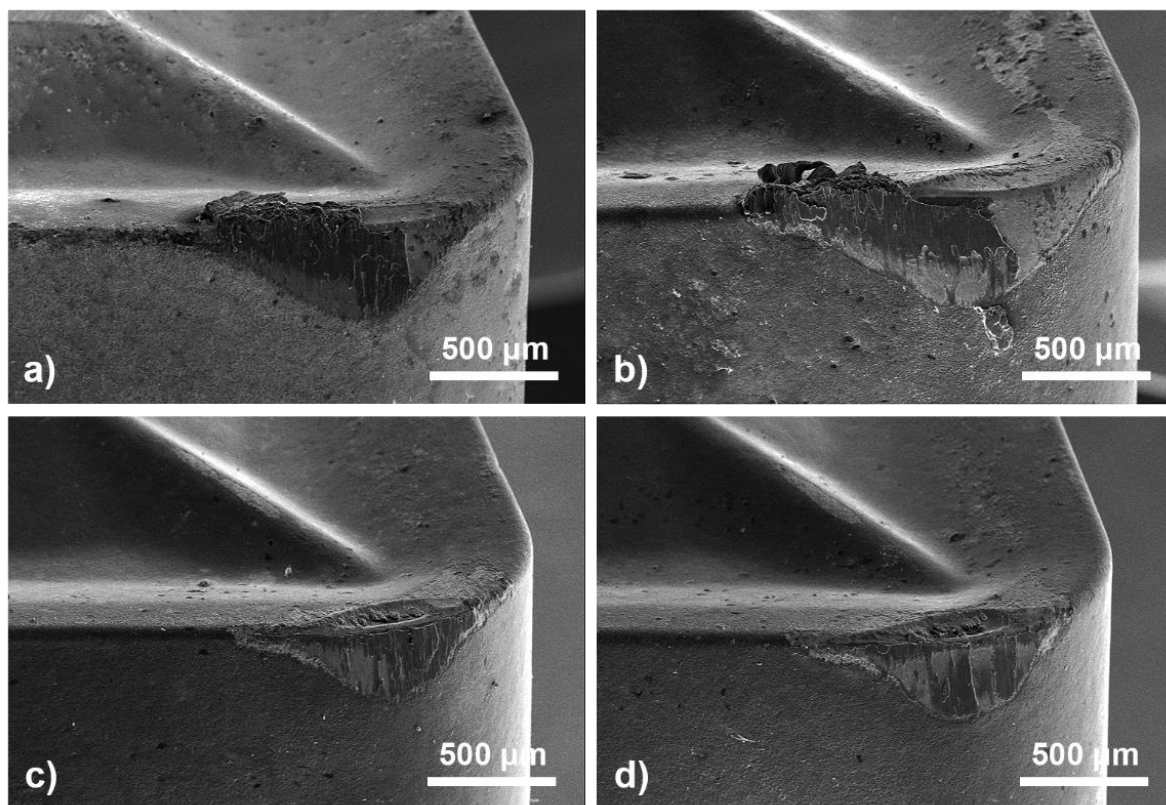

Figure VII-4 SEM micrographs of the cutting edges in the inserts tested at a cutting speed of 100 m/min: a) Uncoated, b) TiSiN, c) TiSiNAg6 and d) TiSiNAg10

The correspondent post-mortem SEM micrographs of the inserts for the cutting speed of 100 m/min are shown in Figure VII-4. Generally, the same wear mechanisms are shown as for the other tested cutting speeds, with abrasion marks still present. The strong formation of BUE is observed for the uncoated and TiSiN coated samples (Figure VII-4a and 4b, respectively). The uncoated insert shows the typical abrasion marks and the formation of BUE which combined with the higher cutting speed, and consequent higher temperature, promotes the fast degradation of the insert (see Figure VII-1c). With the temperature reaching higher levels, the hardness starts to lose its importance, as seen for the reference TiSiN inserts

(Figure VII-4b) where the combined effect of the big BUE formation and the abrasion at high temperature lead to the quick flank wear, as well as a visible coating flaking, with strong impact on its tool life (almost as low as the uncoated insert). Notwithstanding, with higher cutting speeds the addition of silver to the coatings, shows the ability to hinder or at least diminish, the formation of BUE's as seen for the inserts coated with TiSiNAg6 (Figure VII-4c) and TiSiNAg10 (Figure VII-4d). Furthermore, the silver can act as a solid lubricant, at higher temperature (higher cutting speed), reducing the friction and wear and contributing for a decrease in the coating flaking. As a consequence, a considerable increase in the tool life of these inserts are achieved in relation to the other two (see Figure VII-1c).

These results, clearly show that silver shows its potential as solid lubricant, at the higher temperatures achieved by increasing the cutting speed. Therefore, a higher productivity can be expected even without the use of liquid lubricants. Again, these results are in accordance with the previous tribological findings of Chapter VI, where it was found that only for the higher tested temperature, the silver was able to show its potential in avoiding the adhesion of material to the wear tracks and, consequently, decreasing the wear rate.

7.1.2 Industrial comparison of Ti-Si-(Ag)-N coatings with a commercial tool (CCGT 09T304-LN inserts)

Figure VII-5 shows the tool´s life curves for all the tested inserts, considering the designated end-of-life criteria of 0.3 mm flank wear. Primarily, and as a side note, it is important to refer that in all of the performed tests, no BUE formation was detected, most likely due to the sharper geometry of the insert in comparison with the laboratorial ones. Starting with the main point of comparison of this section, the commercial AlTiN coating showed, for all the tested inserts, a poor performance with the systematic breakage of the tip (see Figure VII-6a) after 4 min. By this result it is feasible to assume that the commercial coating does not withstand the stresses and heat involved in the process requiring, for better performance, the appliance of liquid lubricant.
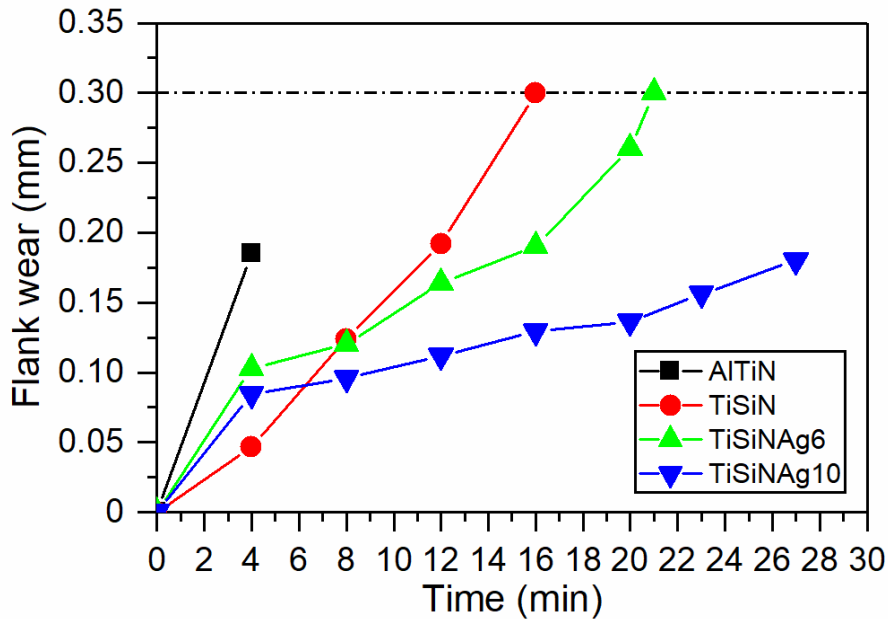
Figure VII-5 Tool life curves for all the inserts tested in an industrial environment

For the reference TiSiN coating, the tool life was significantly increased, comparing with the commercial AlTiN tested. The analysis of the post-mortem tip for the TiSiN (Figure VII-6b) shows the typical abrasion marks just as denoted for the laboratorial tests. In this case, the relatively high hardness enables the coating to withstand the stresses, increasing the tool life. When small amounts of silver are introduced (TiSiNAg6), the tool life is further increased. The wear mechanism does not differ significantly from the reference TiSiN, as the harsh abrasion marks are still clearly visible (Figure VII-6c) although the improvement in the tool life might be explained by the silver adding its lubricant effect by reducing the friction, the temperature and, consequently, the wear. Lastly, the big improvement is achieved for the TiSiNAg10 coating (see Figure VII-5), almost doubling the tool life in relation to the TiSiN coated insert even reaching only less than 2/3 of the designated criterion failure for the flank wear. By looking at the post-mortem micrograph of the TiSiNAg10 insert in the end of the test (Figure VII-6d), it is easily confirmed its much lower wear. This suggests that the silver contributes with its solid lubricant effect, leading to a tremendous increase in the tool life, independently of the lower hardness of this film.

All in all, these results go in accordance to the ones obtained in laboratorial environment: the silver addition makes a positive difference in the tool life of the inserts, especially when the cutting speed is increased, which shows the promising outcome for these coatings to be used in industrial environment while increasing the material removal rate and the consequent machining efficiency, even without the use of liquid lubricants/coolants.
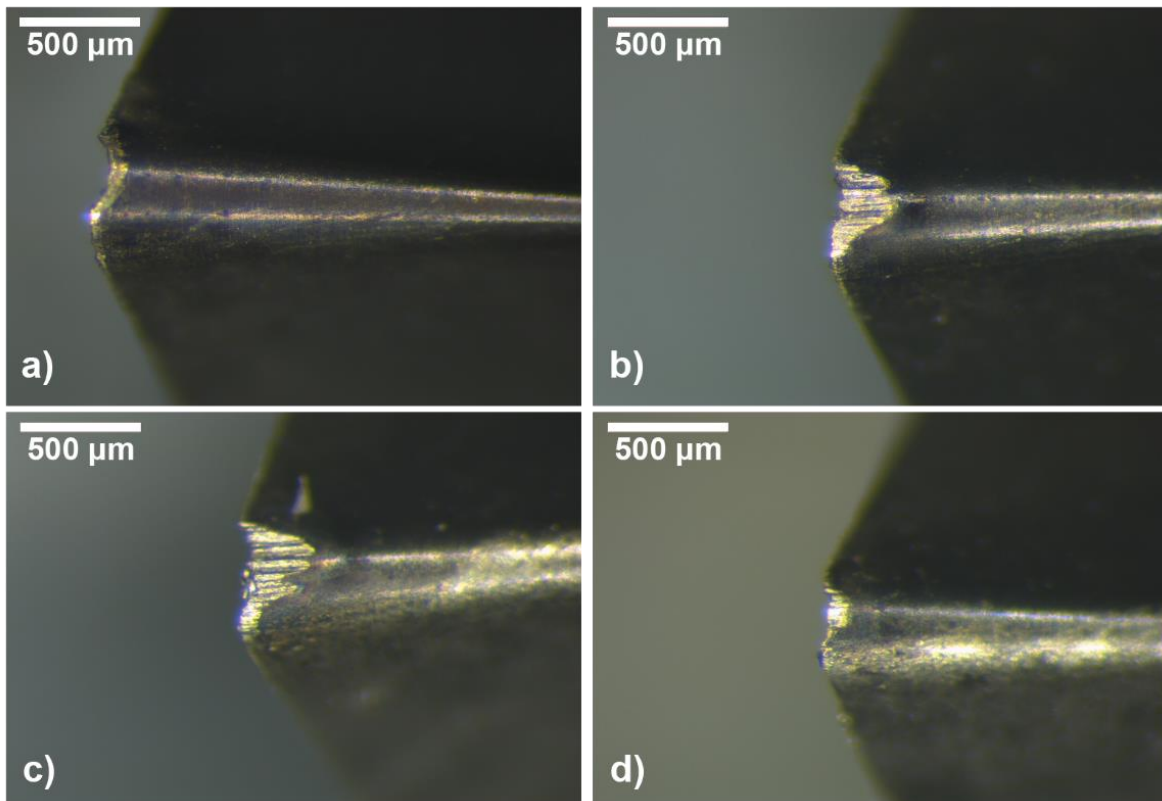
Figure VII-6 Post-mortem optical photographs of all the inserts tested in the CNC machine: a) commercial AlTiN, b) TiSiN, c) TiSiNAg6 and d) TiSiNAg10

7.2 Conclusions

The influence of silver in the machining behaviour of TiSiN(Ag) coated inserts deposited by HiPIMS working in DOMS mode, during the dry turning of the TiAl6V4 aerospace alloy was reported in this chapter. One type of cutting inserts was tested in laboratorial environment using a conventional lathe, whilst, a second type of inserts was tested in a CNC machine. Tests in the CNC machine were performed at only one cutting speed and the performance of the coated inserts benchmarked in relation to a commercial insert coated with an AlTiN film.

For the tests with the conventional lathe, it was found that the addition of silver only starts showing its beneficial effects when the cutting speed is increased. For lower cutting speeds, TiSiN showed the best tool life. However, for the highest cutting speed of 100 m/min, the improvement in the tool life with the addition of silver is obviously noticeable. Detailed analysis of the wear mechanisms corroborated the aforementioned which showed that, the higher cutting speeds combined with the addition of silver, visibly delays the flaking of the coatings and clearly reduces the formation of the BUE.

Despite of the difference in the inserts geometry used in the CNC tests, a compliance between the results obtained in both tests was sound. It was observed that the addition of silver had a tremendous effect in increasing the tool life of the inserts. All the coated inserts showed an increase in the tool life in relation to the commercial AlTiN coated insert. Among the coated ones, TiSiNAg10 showed a more than double better performance than TiSiN.

Summarily, both the distinct environment tests conducted showed that adding silver to the TiSiN system has the desired solid lubricant effect. Both TiSiNAg6 and TiSiNAg10 coatings displayed a clear improvement in the inserts lives by reducing friction, wear and the formation of BUE for high cutting speeds. This is remarkably more visible the higher the cutting speed is, which boasts the promising use of these coatings in the industry, as they allow to work with higher cutting speeds leading to the increase in the material removal rates and inferable machining efficiency.

7.3 References

[1] J. Kümmel, J. Gibmeier, E. Müller, R. Schneider, V. Schulze, A. Wanner, Detailed analysis of microstructure of intentionally formed built-up edges for improving wear behaviour in dry metal cutting process of steel, Wear, 311 (2014) 21-30.

CHAPTER VIII - Conclusions and Future Developments

The importance of Ag content for optimizing the machining

performance of Ti-Si-(Ag)-N coatings

8 Conclusions and future developments

8.1 Conclusions

TiSiN coatings alloyed with silver were successfully deposited by high power impulse magnetron sputtering (HiPIMS) using deep oscillation magnetron sputtering (DOMS) mode, in order to evaluate the influence of Ag and study their performance during the dry machining of the hard-to-cut titanium TiAl6V4 aerospace alloy. All the characterization of these coatings was conducted including, the chemical, structural, morphological, mechanical and tribological properties as well as their behaviour at high temperatures (thermal stability and oxidation resistance). Following this, the machining performance was then assessed and benchmarked in relation to a commercial coating.

Ensuing the deposition of the coatings, a combination of SEM, EDS and XRD was used to analyse and interpret the chemical and structural characteristics of the coatings as well as find the amount of silver present on the coatings. Chemical composition results showed that, as expected, when the number of Ag rods on the target was increased, the amount of silver on the coatings also progressively increased to percentages of up to 29 at.%. Additionally, the increase in the number of Ag rods was accompanied by an increase in the peak power which was found to have a direct influence on the deposition rate, the structure and the morphology of the coatings.

The deposition rate of the coatings, as expected, gradually increased with the increasing silver content on the films since the sputtering yield of the silver is considerably higher than any of the other elements or compounds being formed during film growth. However, a decrease in the deposition rate was found for the coating containing 6 at.%, which as referred before, was found to be due to the verified increase in the peak power during the deposition of this coating, that increases the metallic ion back-attraction to the target, reducing the deposition rate. SEM analysis of the cross-section morphology showed the typical columnar morphology for the coatings with silver coatings up to 3 at.%. Nonetheless, the coating with 6 at.% of Ag (TiSiNAg6) showed yet again, a complete different behaviour by transitioning into a more compact morphology rather than columnar. Recurrently, this abrupt change was explained based on the previously mentioned increase in the peak power. The increase of peak power can lead, through the peak current, to a boost in the fraction of the ionized species, increasing adatom mobility and combating the shadowing effect, effectively leading to the raise of a spontaneous compact morphology. The continuous gradual increase in the silver after this, leads to the formation of an increasingly higher porous morphology

due to the increase in the number of nucleation sites where silver, due to its much higher mobility, segregates and coalesces into bigger particles.

XRD analysis showed that all the coatings presented an fcc NaCl-type structure, assigned to the crystalline TiN phase without any presence of peaks associated with the SiN phase, suggesting its amorphous character. It was also possible observe the shift of all the TiN peaks to lower angles which corroborated the high level of residual stresses measured on the films. The addition of silver to the coatings led to the broadening of the TiN diffraction peaks which suggests a lower degree of structural order and the formation of a nanocrystalline structure. This was confirmed by the calculation of the grain size where for small amounts of silver, the grain size abruptly decreases, due to the competitive growth between the Ag, the TiN grains and the SiN phases. After this, further increase in the Ag content seems to have no influence on the grain size. Calculation of the lattice parameters corroborate the high level of residual stresses found as the lattice parameter is higher than that of the unstrained TiN, although it is not the case for the TiSiNAg3 coating which despite still showing a relatively high level of residual stresses, its lattice parameter is the same as the unstrained TiN. This might be associated with the presence of silicon in solid solution in the TiN lattice. However, yet again, the TiSiNAg6 coating presents an opposite behaviour by showing a really high lattice parameter which can be tentatively explained again by the increase in the peak power observed during the deposition of this film. The higher peak power promotes the mobility of the species, facilitating the segregation of the silicon from the TiN lattice, effectively counteracting the effect imposed by the solid substitution. This all suggests that, the nanocomposite structure able to be developed by HiPIMS still presents some silicon in solid solution in the TiN lattice.

The thermal stability of the coatings was assessed by submitting the coatings to annealing in protective atmosphere at 800 $^\circ$C. Nanoindentation, XRD and SEM-EDS were used to analyse the eventual changes in the hardness or phase distribution and to observe the silver diffusion in this ceramic matrix. Reference TiSiN coating displayed the higher hardness ($\sim$32 GPa) and Young's modulus ($\sim$290 GPa) among all the coatings. Incremental additions of silver, expectedly showed a decrease in the hardness of the coatings, as the amount of the soft phase also increased. The hardness of the coatings didn't significantly change with the annealing treatment, independently of the coatings chemical composition. Nonetheless, some small structural changes were observed as there were an increase in the intensity of the Ag peaks after annealing treatment that was explained by the segregation of silver from the topmost surface of the coatings, observed in the SEM. Another small difference observed was the shift of the peaks to higher angles which can be easily explained by the release of the stresses due to the thermal annealing

treatment. Of the most importance though, was the observation of the chemical distribution in the coatings in cross section which showed that the silver continued to be homogeneously distributed, suggesting that the SiN matrix is serving as an efficient diffusion barrier to the Ag.

TGA, XRD and SEM-EDS analysis allowed to study the oxidation behaviour of the coatings and the silver whereabouts after annealing treatment in oxidizing atmosphere. In-situ oxidation XRD allowed to perceive the phase evolution with increasing temperature by showing the first signs of oxidation appearing with the TiO2 rutile peaks at a temperature of 850 °C. Further increase in the temperature, showed the increase in the intensity of these same peaks, suggesting the thickening of the oxide scale. At 950 °C a recurrent phenomenon starts to be seen, as the Ag peaks start "disappearing". This phenomenon was then explained based on a competitive process happening between the silver aggregation and the silver evaporation/sublimation. Cross-section elemental map distribution of this coating show that there's still a part of the film left to oxidize and more importantly, in that part, the Ag signal continues to be clearly visible and homogeneously distributed suggesting that, when in the ceramic matrix, the silver still does not diffuse showing again that the SiN matrix can serve as an efficient barrier to the Ag diffusion.

Dynamic TGA results corroborated the In-situ oxidation XRD findings, confirming the on-set point of oxidation of 850 °C for all the coatings (Ag addition did not influence this characteristic). Nonetheless, Ag alloying did deteriorate the rate at which the oxidation occurred by visibly accelerating it. Another corroboration between the previously mentioned XRD results and the TG curves was found when a mass loss was perceived for the TiSiNAg6 and TiSiNAg10 coatings just as the Ag peaks on the XRD started to disappear. This was explained based on the competitive process occurring between silver aggregation and silver evaporation/sublimation, i.e. if the size of the Ag particles is small enough, their sublimation/melting point is considerably reduced which can lead to their sublimation and consequent "disappearance" and mass loss observed. When silver content is further increased (as is the case of the TiSiNAg17), this mass loss is not observed due to the fact that the higher silver content leads to the aggregation into bigger sized Ag particles which then hinders their sublimation. Isothermal TGA curves confirm the same as the dynamic curves, i.e., the addition of silver visibly deteriorated the oxidation resistance of the coatings, although in the initial part of the process it seems to be independent of the Ag content. Despite this, cross-section elemental map observation allows to perceive again that, in the un-oxidized parts of the film, the silver signal continues to be visible and homogenously distributed, suggesting the efficient barrier for Ag that the SiN matrix can provide.

The tribological performance of coatings was then assessed on a high temperature tribometer using two different types of counterbodies (alumina and TiAl6V4 balls). For the tests against alumina balls, the hardness decrease with the increments of silver allowed to perceive the detrimental effect it has on the wear resistance of the coatings, especially for room temperature. As the temperature was increased to 600 °C, the deterioration in the wear resistance with the silver content is still observable although, a general increase in the wear resistance for all the coatings was found, when compared to their equivalent counterparts at room temperature.

As for the tests conducted against the TiAl6V4 balls, the friction was found to decrease with the Ag additions for room temperature, although no measurable wear was able to be achieved for any of the coatings save for the TiSiNAg17, which suggests that the wear resistance is still deteriorating with silver addition. When the temperature was increased to 600°C, the ability of silver to hinder the adhesion of material to the wear tracks starts to become visible with the amount of adhered material from the ball becoming increasingly lower with the higher amounts of silver (especially for the TiSiNAg17 coating). This effect becomes even more pronounced when the testing temperature was increased to 900 °C, where the silver starts completely showing its beneficial effects by considerably increasing the wear resistance of the coatings (the TiSiN coating delaminated while the TiSiNAg6 coating didn't show any wear at all) and by completely hindering the adhesion of material from the ball to the wear track which might be of the utmost importance for avoiding the formation of built-up edges (BUE) during the following machining tests.

Taking everything into account, it all comes together to the final and main objective of this thesis regarding the testing of the more promising coatings in relation to their machining performance and by comparing them, in an industrial point of view, with a commercial coating used in the industry for the processing of the hard-to-cut titanium alloys. The turning tests conducted in the laboratorial environment allowed to perceive that the addition of silver only had benefits when the cutting speed was increased, since for the lower cutting speeds the reference TiSiN showed the best tool life of all the inserts. Then, both the Ag-containing coatings showed a clear improvement in the inserts lives when the cutting speed was increased. This improvement was due to the presence of Ag on the contact which delayed the flaking of the coatings and clearly reduced the formation of the BUE, just as observed in the tribological tests.

The tests conducted in the CNC machine were interestingly sound with those of the laboratorial tests by showing the potential of Ag in displaying a tremendous increase in the tool life of the inserts, even when compared with the commercial AlTiN coating tested. The TiSiNAg10 coating went further and above by

flashing double the performance of that of the TiSiN coating. With both the results of the different environments, it seems that the solid lubricant effect is showing up with both the TiSiNAg6 and TiSiNAg10 coatings displaying a clear improvement in the inserts lives by reducing friction, wear and the formation of BUE's. This is remarkably more visible the higher the cutting speed is, which boasts the promising use of these coatings in the industry, as they allow to work with higher cutting speeds leading to the increase in the material removal rates and inferable machining efficiency.

All in all, we could say that the main objectives of this work were fulfilled and that the Ti-Si-(Ag)-N system has potential as a coating to be used in the machining of hard-to-machine titanium alloys. Throughout this whole thesis, it was clearly shown that the TiSiN matrix can effectively hinder the diffusion of the silver, "solving" one of the main problematics introduced in Chapter II for this type of coatings that is the quick diffusion, fast depletion and consequent loss of the lubricious properties. Moreover, the tribological and machining characterization allowed to perceive the beneficial properties of the silver, especially for more extreme environments where higher temperatures are involved. Adding to this is also the fact that we showed how these coatings behaved better than the commercial one tested. This comes hand-to-hand with the increase in the cutting speed during the machining process by being the main proposal of this work which was successfully completed.

8.2 Future developments

Keeping in mind all the results and conclusions hereby shown, there's still some questions left unanswered: how is the silver diffusion process occurring?; how do this system behaves when employed during harsher machining processes (drilling or milling)?; does the achieved increase in cutting speed really brings any economic benefit for the industry?.

Just like any other deposition process, HiPIMS comes with its advantages and disadvantages. One of the most important features of this process and the reason it was used to deposit the coating system in this work, was its ability to deposit dense and smooth films and which, hopefully, would allow us to deposit the nanocomposite structure. The idea behind it was using the amorphous SiN phase as a diffusion barrier for the silver. As it was shown throughout this thesis, it seemed that the idea worked well and diffusion was effectively hindered using the TiSiN coating system. However, one can ask how exactly is the diffusion process happening and/or why is the diffusion not occurring? A project proposal regarding this same subject is being matured in CEMMPRE in the University of Coimbra where simple really thin multilayers of TiSiN (deposited by HiPIMS) and Ag are being deposited to assess the diffusion of silver

throughout this matrix. TEM, RBS and even simulation analysis are being conducted to try and understand better how silver behaves and how its diffusion is processed.

In this work, the machining process selected was the "easiest" and "simpler" turning process. Due to its simplicity, this process gives a good starting point for the analysis of the machining performance of the coatings studied in this work. Although the results found were really promising with the Ti-Si-(Ag)-N coatings showing a clear improvement in the tool life for higher cutting speeds, even when compared to a commercial coating, it would be legitimately interesting to see how these coatings would behave in the harsher and more commonly used machining processes, like drilling or milling. With this in mind, the Universities of Minho and Coimbra are participating in a huge national project involving multiple universities and companies (On-Surf project), where one of its main objectives is exactly the analysis of the machining behaviour of the coatings developed in this thesis during the drilling and milling of the TiAl6V4 aerospace alloy without the application of any liquid lubrication. In this project, the comparison with industrial coatings is also predicted which combined with the tool life curves and the analysis of the wear mechanisms will allow to assess the eventual use of the Ti-Si-(Ag)-N coatings in the industry.

Lastly but probably, the most important aspect to take into consideration when analysing the feasibility of this work to be applied in the industry, is the economic aspect. Despite the promising results showed throughout this thesis, it would be extremely curious to conduct a study related with the cost of the tool in the aerospace industry. Would the achievable increase in the cutting speed (more parts per unit of time, assuming no other time consumer) compensate the cost of the coating or of the more frequent substitution of the tool? A cost related study would eventually answer these questions and would actually perceive if the application of these coatings in the industry would be feasible at all.